Localisation of Ferredoxin-NADP$^+$ reductase

Manuela Kramer

Submitted in partial fulfillment of the requirements of the Degree of Doctor of Philosophy

Queen Mary University of London
United Kingdom
April 2019

Statement of originality

I, Manuela Kramer, confirm that the research included within this thesis is my own work or that where it has been carried out in collaboration with, or supported by others, that this is duly acknowledged below and my contribution indicated. Previously published material is also acknowledged below.

I attest that I have exercised reasonable care to ensure that the work is original, and does not to the best of my knowledge break any UK law, infringe any third party's copyright or other Intellectual Property Right, or contain any confidential material.

I accept that the College has the right to use plagiarism detection software to check the electronic version of the thesis.

I confirm that this thesis has not been previously submitted for the award of a degree by this or any other university.

Signature:

Date:

Details of collaboration and publications:

- $NADP^+$ reduction kinetics (figure 8.2) were measured in collaboration with Laura Mosebach, University of Münster
- The imaging on the lattice light sheet microscope was performed in co-operation with CellNanOs by Rainer Kurre, Osnabrück University
- The dimerisation assay of *Zm*FNR2 and *Zm*FNR3 (figure 7.4) was performed by Giulia Nebel, Osnabrück University
- Photosynthetic measurements on plants grown in stable light conditions (figures 8.3, 8.4 and 8.5), native PAGE (figure 3.2), blue native PAGE (figure 3.3) and western blot of FNR solubility (figure 3.1) were performed by Manuel Twachtmann (Dissertation, 2015)

List of Abbreviations

$^{\cdot}OH$	hydroxyl radicals
2Fe-2S	iron-sulfur cluster
ADP	Adenosine diphosphate
Ala	alanine
Amp	ampicillin
An	asparagine
ANOVA	analysis of variance
AP	alkaline phosphatase
APS	ammonium persulfate
Asn	asparagine
Asp	aspartic acid
At	Arabidopsis thaliana
ATP	Adenosine triphosphate
ATPase	adenosine triphosphatase
BCIP	5-bromo-4-chloro-3-indolyl-phosphate
beta-ME	beta-mercaptoethanol
BNP	blue native page
BSA	bovine serum albumin
$C_6H_{12}O_6$	glucose
$CaCl_2$	calcium chloride
CBB cycle	Calvin-Bensson-Basshan cycle
CET	cyclic electron transport
CO_2	carbon dioxide
Cr	Chlamydomonas reinhardtii
Cytb_6f	cytochrome b_6f complex
D1	photosystem II protein D1
Df	degrees of freedom
DEAE	diethylaminoethyl
DNA	deoxyribonucleic acid
dNTP	nucleoside triphosphate
DUAL-PAM	dual pulse-amplitude modulation
EDTA	ethylenediaminetetraacetic acid
EM	electron microscopy
ET	electron tomography
EtOH	ethanol
F_0	dark fluorescence yield

FAD ..... flavin adenine dinucleotide
Fd ..... ferredoxin
Fe ..... iron
F_m ..... maximum fluorescence yield
FNR ..... ferredoxin-NADP(+)-oxidoreductase
GAPDH glyceraldehyde-3-phosphate-dehydrogenase
GCN4 ..... general control protein
GFP ..... green fluorescent protein
Glu ..... glutamic acid
Gly ..... glycine
GSH/GSSG ..... glutathione
H_2O ..... water
H_2O_2 ..... hydrogen peroxide
HCl ..... hydrogen chloride
HL ..... high light
IG ..... immunogold
IGS ..... immunogold staining
Ile ..... isoleucine
IPTG ..... Isopropyl-beta-D-thiogalactopyranosid
KPO_4 ..... potassium phosphate
LB ..... lysogeny broth
LET ..... linear electron transport
Leu ..... leucine
LHC ..... light harvesting complex
LSFM ..... light sheet fluorescence microscopy
LSM ..... Confocal laser scanning microscopy
Lys ..... lysine
MeanSq ..... mean squares
Met ..... methionine
MetOH ..... methanol
$MnCl_2$ ..... manganese(II) chloride
MOPS ..... 3-(N-morpholino)propanesulfonic acid
NaCl ..... sodium chloride
NADP(H) ..... Nicotinamide adenine dinucleotide phosphate
$NaHCO_3$ ..... sodium bicarbonate
NDH ..... NADP(H) dehydrogenase
NBT ..... nitro blue tetrazolium
NPQ ..... non-photochemical quenching

O_2 ..... oxygen
O_2^- ..... superoxide
OD_{600} ..... optical density at 600 nm
Os ..... Oryza sativa
Ot ..... Ostreococcus taurii
P_{680} ..... photosystem II primary donor
PC ..... plastocyanin
PCC ..... Pearson's Correlation Coefficient
PCR ..... polymerase chain reaction
PET ..... Photosynthetic electron transport
PGR5 ..... proton gradient regulation
PGRL1 ..... proton gradient regulation-like protein
Phe ..... phenylalanine
P_m ..... maximum change in P700
Pp ..... Physcomitrella patens
PQ ..... plastoquinone
PQH2 ..... plastoquinol
Pro ..... proline
Ps ..... Pisum sativum
PsaD ..... photosystem I reaction center subunit II
PsbA ..... photosystem II protein D1
PSF ..... point spread function
PSI ..... photosystem I
PSII ..... photosystem II
PVDF ..... polyvinylidene difluoride
qL ..... coefficient of photochemical quenching
$RbCl_2$ ..... rubidium chloride
ROS ..... reactive oxygen species
scFv ..... single-chain antibody
SCLIM ..... super-resolution confocal live imaging microscopy
SDS-PAGE ..... sodium dodecyl sulfate–polyacrylamide gel electrophoresis
Ser ..... serine
SIM ..... structured illumination microscopy
SOD ..... superoxide dismutase
SumSq ..... sum of squares
TEM ..... transmission electron microscopy
TEMED ..... tetramethylethylenediamine
Thr ..... threonine

Tic62 ..... Translocon at the inner envelope membrane of chloroplasts 62
TRIS ..... Tris(hydroxymethyl)-aminomethan
TRO ..... L thylakoid rhodanese-like protein
Ty ..... r tyrosine
Val ..... valine
WT ..... wild-type
Y(I) ..... photochemical quantum yield of PS I
Y(II) ..... effective PS II quantum yield
Y(NA) ..... Nonphotochemical quantum yield of PS I, acceptor limitation
Y(ND) ..... Nonphotochemical quantum yield of PS I, donor limitation
Zm ..... *Zea mays*

Abstract

The principle research goal in this thesis is to investigate the effects of ferredoxin-$NADP^+$ reductase (FNR) sub-chloroplast location on its function and proposed role in regulation of electron transport. It was found before that FNR in *Arabidopsis thaliana* can either be soluble in the stroma or tethered to the thylakoid membrane by two identified tethers. Its primary function is to deliver electrons from ferredoxin to $NADP^+$. Its primary location therefore should be at the thylakoid membrane and the function of stroma soluble FNR is debatable. Hence, to facilitate localization studies and functional investigations, previously generated *A. thaliana* plants expressing isoforms of FNR that mainly bind to one specific tether were used as models. I explored several imaging approaches in the scope of this thesis and found that only electron microscopy delivers a sufficient resolution for conclusive assumptions about the absolute location of FNR. Hence, I developed a method to quantify the FNR labelling density on immunogold labelled chloroplasts for the defined regions of grana, margins of grana, lamellae and stroma in each genotype. The striking result is that FNR is not found soluble in the stroma in the wild-type but mainly tightly associated to the lamellae and margin regions of the grana. My work supports the hypothesis that linear electron transport takes place at the margin regions, whereas cyclic electron transport happens at the lamellae. A functional analysis of photosynthetic electron transport in these plants reveals that FNR location/differential tether binding impacts the electron transport mainly during adaptation to light or a change in light intensity

and not so much in steady-state conditions. These findings support the idea that FNR plays a regulatory role in electron transport.

Acknowledgements

I am so grateful for all the people who have guided me along the way to the completion of this thesis and would like to say a special thank you to everyone who was directly involved in this process:

First and most of all, Dr. Guy T. Hanke for a supervision style based on mutual trust, compassion and curiosity, creating the freedom for me to become an intrinsically motivated researcher. I wholeheartedly appreciate the shared knowledge not only in this field of science but beyond, the anecdotes along the way and the genuine and solid support I received.

My panel members Dr. Viji Draviam, Prof. Dr. Alexander Ruban, Dr. Rainer Kurre and Prof. Dr. Sabine Zachgo for valuable input and feedback on my progress and my research project.

Dr. Giulia Mastroianni for teaching me the art of thin sectioning and immunogold labelling with a steady hand, pointy eyelashes and a lot of patience.

Dr. Steven Le Comber for making statistics as close to enjoyable as possible. His presence was priceless when organising the numbers.

Dr. Rainer Kurre for invaluable technical support on all light microscopy applications.

Dr. Petra Ungerer for professional advice, for making everybody's life safer and easier, for friendship and compassion, soapmaking and hiking. You are a blessing.

Dr. Michael Schorsch for the friendship throughout the years, for reliably lending his sharp mind for rich scientific and personal discussions and ultimately for the scepticism in the validity of imaging

techniques, pushing me to prove the significance of my experiments to the highest level.

Hauke Winkelmann for the persistent trust in my abilities to conquer biophysics, R and LaTeX and for chasing down the errors that escaped my eye. Und fürs ewige Fachsimpeln.

Giulia Nebel for easing my growing pains by joining me on the journey, inspiring me with enthusiasm and curiosity.

Laura Mosebach for making conferences fun and for that one group experiment that worked like a clockwork.

Dr. Manuel Twachtmann for giving me a great starting position with his work on FNR.

Everyone who lent me an ear during the two most confusing and frustrating weeks of my PhD when on my journey to semi-automatic area recognition, creating space for me to emerge with a solid plan that worked out in the end. (I express my explicit ungratefulness for the printers in Fogg and JP building for teaching me nothing but frustration.)

Everybody on 4^{th} floor Fogg building, especially Irene, Wan Ling, Maddie, Ambika, Charlotte and Duccio for a supportive, fun and non-judgmental work environment and extracurricular activities.

I would also like to acknowledge the different sources of funding by the Deutsche Forschungsgemeinschaft, Bayer Foundations and of course Queen Mary, University of London for making this research possible.

Contents

List of Figures

List of Tables

1. Introduction

1.1 Photosynthesis

The foundation of the trophic energy pyramid is composed of primary producers, autotrophic organisms on which all life on this planet relies for the fixation of inorganic compounds and the creation of an aerobic atmosphere. The greatest contribution by far is made by photoautotrophic organisms who derive chemical energy equivalents from sunlight, of which the key protagonists are vascular plants on land and cyanobacteria and algae in the water. The chloroplasts of all plants and algae share a common cyanobacterial ancestor (Whatley [1993]) and are the organelles in which photosynthesis takes place. The net equation of converting carbon dioxide and water into carbohydrate and molecular oxygen in oxygenic photosynthesis (described by van Niel [1932]) is presented in eq. 1.1.

$$CO_2 + H_2O \xrightarrow{\text{photons}} [CH_2O] + O_2 \tag{1.1}$$

This process occurs in two different steps that are described as the light reactions and the dark reactions. The former describes charge separation and water splitting with subsequent linear electron flow. Simultaneously, a proton gradient is generated across

the thylakoid membrane, which in turn facilitates the production of adenosine triphosphate (ATP) and reducing equivalents in the form of nicotinamide adenine dinucleotide phosphate (NADP(H)). This requires energy in the form of sunlight and is therefore called the light reaction. The latter consumes these compounds to drive carbon assimilation into carbohydrate in the Calvin-Bensson-Bassham cycle (CBB cycle) (Calvin [1962]) and is misleadingly called the dark reaction, because it does not directly require light energy, despite being effectively dependent on the light reaction. Carbon assimilation takes place in the stroma in three enzymatic steps, and the resulting assimilated triosephosphate is then used to produce glucose. The net consumption of ATP and NADP(H) per molecule of glucose is presented in equation 1.2.

$$\begin{aligned} &6\,CO_2 + 18\,ATP + 12\,NADP(H) + 12\,H^+ \longrightarrow \\ &\quad C_6H_{12}O_6 + 18\,ADP + 18\,P_i + 12\,NADP^+ + 6\,H_2O \end{aligned} \tag{1.2}$$

In this introduction to my research project, I will be focussing on the light reactions, the photosynthetic electron transport steps that provide ATP and NADP(H) for this process. I will describe the well-defined function of my study subject ferredoxin-$NADP^+$ reductase (FNR) in linear electron transport (LET), with reference to its proposed role in cyclic electron transport (CET) for a possible function in stress response mechanisms of plants. Then, I will explain my interest in the location of this protein and how I designed my methodology to deliver answers to the key question of how the location of FNR impacts its function.

1.2 Role of Ferredoxin:NADP$^+$ oxidoreductase in electron transport

1.2.1 A defined role for FNR in linear electron transport

Linear electron transport Photosynthetic electron transport (PET) describes the process of transferring electrons from water at photosystem II (PSII) across the thylakoid membrane to ferredoxin (Fd) at photosystem I (PSI). The photosystems are large, pigment containing multi-protein complexes in the thylakoid membrane that are composed of the reaction centre with chlorophyll a and the light harvesting complexes (LHC) containing chlorophyll b and carotenoids. PET is driven by two light reactions, one at each photosystem, that negatively shift the redox potential of their primary donors P_{680} (PSII) and P_{700} (PSI), which are named after the wavelength of their peak absorbance. PSII is also called water-plastoquinone oxidoreductase and delivers the electrons that are gained from H_2O splitting in the oxygen evolving complex onto plastoquinone (PQ), which is a two-electron carrier, forming plastoquinol (PQH_2). The third big protein complex in PET is plastoquinol-plastocyanin reductase, or the cytochrome b_6f complex (Cytb_6f)which catalyses the electron transfer from PQH_2 onto the one-electron carrier plastocyanin (PC). Simultaneously, this process is coupled to the transfer of protons across the thylakoid membrane into the lumen and therefore the Cytb_6f significantly contributes to the build-up of a proton gradient. This electrochemical gradient then drives ATP production by the ATPase in a process which was first described by Mitchell [1961] in his chemiosmotic theory. The Cytb_6f is a balancing element in electron transfer, not only because it connects the two photosystems, but also because it has a key role in maintaining the

ratio of ATP/NADP(H) generation. This special function will be discussed later on in the section on cyclic electron flow. PSI, also called plastocyanin-ferredoxin oxidoreductase, receives electrons from PC and reduces the soluble [2Fe-2S] protein ferredoxin (Fd), which is the first stromal electron acceptor. Oxidising Fd_{red} in turn is the site of action of FNR, my protein of interest (review Arakaki et al. [1997]). In the LET chain, it mediates electron transport from Fd_{red} to $NADP^+$, generating NADP(H) as a reduction equivalent which can then be used in the CBB cycle.

Ferredoxin-NADP$^+$ oxidoreductase The protein ferredoxin-$NADP^+$ oxidoreductase (EC 1.18.1.2) was first isolated from spinach leaf chloroplasts by Avron and Jagendorf [1956] who were able to measure its NADPH-diaphorase activity. A year later, they showed that the 35 kDa enzyme binds one molecule of flavin adenine dinucleotide (FAD) as an active cofactor facilitating electron transport (Avron and Jagendorf [1957]). Although FNR was also found to be capable of reducing Cytochrome *f* (Zanetti and Forti [1966]), a component of the Cytb_6f, and a variety of other electron acceptors, Shin and Arnon [1965] described its major function in the catalysis of electron transfer from two molecules of Fd to one molecule of the two-electron carrier $NADP^+$, generating NADPH (equation 1.3).

$$2\,Fd_{ox} + NADP^+ + H^+ \xrightarrow{FNR} 2\,Fd_{red} + NADP(H) \qquad (1.3)$$

The catalytic ability of FNR to transfer electrons between one and two electron carriers relies on the properties of the prosthetic group FAD, which can exist in three redox states: fully oxidised, semiquinone (single electron) and hydroquinone (fully reduced) (Dud-

ley et al. [1964]). Batie and Kamin [1984] have elegantly unravelled the order of co-factor binding and electron transfer, which requires the formation of a binary complex between FNR and $NADP^+$ followed by formation of a ternary complex with Fd. The binding of $NADP^+$ is necessary to facilitate the binding of Fd_{ox} to FNR and subsequent electron transfer. Reduction of $NADP^+$ to NADP(H) on the other hand promotes the release of Fd_{red} from the complex, which is the rate limiting step in the reaction.

1.2.2 A proposed role for FNR in cyclic electron transport

Cyclic electron transport It has been discussed that the required stoichiometry of ATP/NADP(H) that is needed for the CBB cycle (3 ATP per 2 NADP(H)) cannot be met solely by LET (Kramer and Evans [2011], 2.57 ATP per 2 NADP(H)) and this ratio also has to offer flexibility during periods of increased demand for ATP (Walker et al. [2014]). In this section I will discuss one main pathway to achieve this, the cyclic photosynthetic electron flow, the controversially discussed involvement of FNR and the impact of its location.

CET was first discovered by Arnon et al. [1954], who showed ATP generation (and therefore the existence of a proton gradient) in isolated chloroplasts when PSII is not excited, indicating that electrons not originating from PSII are flowing into the system. It has been proposed, that these electrons are diverted from NADP(H) or the Fd reduced at PSI via plastoquinone and the Cytb_6f (Joliot and Joliot [2002]) back to PSI. Such a cyclic flow would be capable of boosting the amount of ATP produced in photosynthetic electron flow relative to the $NADP^+$ reduced, by uncoupling the build up of a proton gradient from NADP(H) production at PSI. There are two proposed pathways of CET around PSI that involve different plasto-

quinone reductases, but which are partly redundant: the NADP(H) dehydrogenase (NDH) pathway where electrons were originally proposed to come from NADP(H) or NAD(H) (Teicher H and Scheller [1998]) and the ferredoxin-plastoquinone reductase (FQR) pathway taking electrons from reduced Fd (Bendall and Manasse [1995], Yamamoto and Shikanai [2013], Schuller et al. [2019]). Munekage et al. [2002] identified mutants in proton gradient regulation (PGR5) with an impaired response to high light and found the thylakoid membrane PGR5 protein to be involved in electron transfer from Fd to plastoquinone. DalCorso et al. [2008] identified another transmembrane protein, proton gradient regulation-like protein (PGRL1) that forms a complex with PGR5 and associates with PSI. This pathway is regarded as the main cyclic electron transport pathway in the model plant Arabidopsis, although both are able to compensate one another (Munekage et al. [2004]). In C4-plants such as maize, the requirement for ATP is increased in specific cells and therefore both CET pathways are reported to be upregulated in these cells (Ishikawa et al. [2016], Nakamura et al. [2013], Munekage et al. [2010] and Takabayashi et al. [2005]).

FNR in cyclic electron transport There is circumstantial evidence that FNR plays a role in CET in addition to its crucial function in LET (Joliot and Johnson [2011], Ooyabu et al. [2008], Shahak et al. [1981]). CET requires the transfer of two electrons from a single electron carrier (Fd) to a two electron carrier (PQ), and it has been suggested that the FAD co-factor of FNR would be well suited for this function. In fact, it has been reported that FNR is capable of directly reducing PQ using electrons from NADP(H)(Bojko et al. [2003]). The interaction of FNR with CET conducting protein super-

complexes has been reported, and there have been various proposals of what function it fulfils, as discussed below.

FNR has been co-purified along with the Cytb_6f from maize (Okutani et al. [2005]) and spinach (Zhang et al. [2001]) and it has been suggested that a complex of these proteins could be the missing FQR. However, although quinone dependent NADP(H) oxidation has been shown for such a supercomplex (Szymańska et al. [2011]), understanding of the functional mechanism is so far lacking, and it is therefore not known whether this association might be an artifact of the Cytb_6f purification process. A supercomplex of PSI and both light harvesting complexes (LHC), Cytb_6f, PGRL1 and FNR has also been isolated from *C. reinhardtii* (Iwai et al. [2010]) and found to conduct both Fd oxidation and quinone reduction, while Mosebach et al. [2017] found that the stability of this complex is crucially dependent on the expression of PGRL1 and PGR5. Arguing against a role for FNR, Hertle et al. [2013] have reported that PGRL1 is able to accept electrons from Fd and deliver them to PQ via a thiol exchange mechanism, and therefore suggested that PGRL1 alone is capable of acting as the catalytic component of the FQR pathway. To complicate matters further, FNR has previously been co-purified with the NDH-complex from barley (Jose Quiles M and Cuello [1998]), suggesting a putative role in both pathways.

There may also be a connection between FNR location and CET. Membrane bound FNR is reported to be essential for salt stress induced CET in cyanobacteria, where van Thor et al. [2000] have shown that increased FNR bound to the thylakoid membrane via its N-terminus resulted in increased capacity for CET as tested via re-reduction kinetics of $P_{700}{}^{+}$ and photoacoustic energy determination. Moreover, in the bundle sheath cells of maize (which perform

a high rate of CET), all FNR is tightly bound to the membrane (Twachtmann et al. [2012]). This raises the question of whether the dynamics of FNR membrane binding influence its role in photosynthetic electron transport and might act as a switch between the two pathways (Joliot and Johnson [2011]).

FNR thylakoid-tethering Cyanobacterial FNR is recruited to the thylakoid via a phycobilisome binding domain on the N-terminus, although translation of another soluble FNR isoprotein lacking this domain occurs through an alternative translation initiation start site (Thomas et al. [2006]). Both of these FNR isoforms have also been reported to directly bind to model membranes (Grzyb et al. [2018]). The authors suggested that at least part of the protein is incorporated into the lipid bilayer. The same group previously observed this behaviour in both wheat and spinach FNR (Grzyb et al. [2008]). Unlike in cyanobacteria, chloroplastidial FNR is a soluble protein that does not feature a domain with membrane binding capacity. It has been the consensus that FNR can be divided into different pools depending on binding to the thylakoid membrane (Matthijs et al. [1986], Shin et al. [1985]): either soluble, loosely or tightly bound to the membrane as evaluated by biochemical procedures. It has also been shown that the proportions of these pools of FNR change in response to environmental changes, such as transition from dark to light (Benz et al. [2009]) or oxidative stress inflicted by methyl viologen (Palatnik et al. [1997]), which both result in the solubilisation of FNR. *Arabidopsis thaliana* has two isoforms of leaf-type FNR, *At*FNR1 and *At*FNR2 (Hanke et al. [2005]), of which both can be found soluble and membrane bound in the wild-type. The C4-plant *Zea mays* however, contains three of these isoforms with dif-

ferent location in the chloroplast: *Zm*FNR1 being membrane bound, *Zm*FNR2 with a dual location and *Zm*FNR3 only soluble (Okutani et al. [2005]). This very differentiated pattern further emphasizes that the location of FNR might play an important role for its function and raises the question of how exactly FNR is recruited to the thylakoid membrane.

Andersen et al. [1992] first suggested that the membrane bound FNR pool is situated at PSI. Recently however, two dedicated FNR binding proteins have been identified: Tic62, which is also a component of the chloroplast inner envelope protein translocon (Benz et al. [2009]), and TROL, or thylakoid rhodanase like protein (Jurić et al. [2009]). These integral membrane proteins share a similar binding motif for FNR (Alte et al. [2010]), around which two FNR monomers are thought to dimerise - with the binding domain increasing the surface area for interaction between the FNR monomers, and creating a stable complex. As a part of the inner envelope protein translocon, Tic62 is located at the inner chloroplastidial envelope, but can be shuttled to the thylakoid membrane via the stroma according to Stengel et al. [2008], in a $NADP^+$/NADP(H) ratio dependent way. The same group proposes that Tic62 and FNR strongly associate in the light and upon oxidation of the pool, migrate back to the envelope together. Yang et al. [2016] have shown that LIGHT-INDUCED RICE1 (LIR1) increases the affinity of FNR and Tic62 and degrades in the light. Furthermore, Benz et al. [2009] were able to show that Tic62 can also be found in the lamellae fraction of the thylakoids. The authors also showed that a knock-out of Tic62 did not result in a distinct phenotype and suggested that functionally, the interaction with Tic62 stabilises FNR and protects it from degradation during inactive periods. TROL however, shares only the thylakoidial

location Jurić et al. [2009] and a knock-out of this tether has severe consequences for the size of the chloroplasts and thylakoids, indicating that this interaction is important for photosynthetic processes. In double mutants of Tic62 and TROL, FNR is found exclusively in the soluble fraction (Lintala et al. [2014]). However, these findings rely on the interpretation of biochemical experiments: fractionating cells or chloroplasts followed by centrifugation to separate supernatant (interpreted as soluble proteins), and pellet (interpreted as membrane bound proteins).

The knock-out of individual isoforms of FNR from *A. thaliana* has shown that a knock-out of *At*FNR1 solubilises the remaining *At*FNR2 (Lintala et al. [2007]). This is not true for the remaining *At*FNR1 in the reciprocal experiment with *fnr2* plants, which retain a dual location (Lintala et al. [2009]). This might indicate a cooperative binding behaviour of the two FNR isoforms, requiring the formation of a heterodimer, with *At*FNR1 essential for membrane binding of *At*FNR2. Furthermore, this group has measured slower $P_{700}{}^{+}$ re-reduction kinetics in the dark in *fnr1* mutant compared to wild-type plants and therefore proposed that *At*FNR1 might play a role in cyclic electron flow (Lintala et al. [2007]). Both FNR mutants show a similar phenotype in standard growth conditions, with a lower rate of carbon fixation. Three different measurements to investigate cyclic electron flow were performed: thermoluminescence AG, $P_{700}{}^{+}$ re-reduction, and post-illumination fluorescence F0'rise' (which is a measurement for NDH dependent CET) of which all indicated a downregulation of CET in both mutant plants. Therefore, Lintala et al. [2007] suggest that neither isoform specifically directly channels electrons into CET. However, in plants that were low temperature adapted, both mutants show a more active CET and the

fnr2 mutant was better acclimated (Lintala et al. [2007]), raising the question of whether FNR location and binding might be important in stress response mechanisms.

In brief, there are still many open questions on this topic, but the main three points that require clarification are evident as the exact location of FNR, how environmental changes influence the location of FNR, and what function FNR fulfils in each location. The most attractive suggestion so far comes from Joliot and Johnson [2011], who suggest that FNR might act as a switch between the two electron transport ways, LET and CET.

1.3 Structural organisation of the thylakoids

Photosynthetic membranes are, with the exception of Tic62-FNR at the inner envelope, the main proposed location for membrane bound FNR. In the following section I will describe these highly structured membrane entities and their different domains in regard to their form and function. Photosynthetic membranes need to offer a large surface area to house all the required membrane complexes and therefore exhibit a layered organisation to increase the ratio of area to volume. Simultaneously, the total enclosed volume needs to be comparatively small so that diffusion of soluble electron carriers is not compromised. Photosynthetic organisms have evolved an intricate thylakoid membrane network with sheets of membranes enclosing a flat but continuous cisterna, the lumen. In cyanobacteria, they are evenly spaced out and located at the peripheral cytoplasm of the cell (e.g. in *Anabaena variabilis* (Peschek and Sleytr [1983]) and *Synechocystis* sp. PCC6803 (van de Meene et al. [2006])). However, these membranes are usually not densely packed to allow space for the stroma-protruding light harvesting phycobilisomes (Mullineaux

[2005]).

The thylakoids of higher plants, which were firstly described by Menke [1962], show a more organised ultrastructure within the chloroplast, and can be divided into highly appressed grana stacks and unappressed stromal lamellae. The grana stacks have a diameter between 300 to 600 nm and contain up to 20 layers of appressed membranes, which are interconnected by unstacked stromal lamellae to form a continuous network with a connected lumen. Different models have been proposed of how this network is organised in a three-dimensional space. The helical model, first developed by Paolillo [1970], proposes that each cylindrical granum is connected by multiple stromal lamellae that are wound around the stack in a helical fashion. Advances in electron tomography (ET) lead to a different interpretation by Shimoni et al. [2005] who have suggested that grana stacks in *Lactuca sativa* are composed of repeating units of paired layers that are formed out of the bifurcated stromal lamellae. However, new ET studies broadly support the helical model in Arabidopsis, spinach, pea and tobacco plants (Mustárdy et al. [2008], Daum and Kühlbrandt [2011], Austin and Staehelin [2011]).

Lateral heterogeneity In addition to the division of the thylakoid domains into appressed and non-appressed membranes, these domains also show differences in their protein composition. Andersson and Anderson [1980] first discovered a lateral heterogeneity of protein complexes in the domains of isolated spinach chloroplasts with PSII enriched in the grana stacks and stroma lamellae enriched in PSI. This principle extends to other proteins as well e.g. the ATPase and PSI, which protrude too far into the stroma to enter the grana stacks and are therefore exclusively found in the lamellae or in the

stroma facing outer membranes of the grana (Daum et al. [2010]). Likewise, the main proportion of LHCII can be found in the grana (Koochak et al. [2019]). With both photosystems spatially divided, long-distance electron transport has to be facilitated between the two. The PQ pool was found to be restricted in its diffusion (Joliot et al. [1992]), so only the Cytb_6f and the soluble plastocyanin putatively remain for this role. The Cytb_6f was found evenly distributed between the grana and the lamellae, as confirmed by membrane fractionation and immunogold (IG) labelling experiments (Allred and Staehelin [1986]), and is dynamically relocated in response to light (Vallon et al. [1991]). Johnson et al. [2014] albeit have recently proven by affinity mapping atomic force microscopy (AFM) that in native conditions PSII and the Cytb_6f are evenly dispersed throughout the grana stack. This even distribution has been a subject of debate to some extent as discussed by Dekker and Boekema [2005], who suggest that the Cytb_6f might get pushed to the periphery or excluded from the grana stacks under conditions where severe stacking occurs and PSII-LHCII form mega complexes or semi-crystalline lattices (Nosek et al. [2017]). This suggests that the grana membranes themselves are not thoroughly homogenous in their protein composition in certain conditions, which demonstrates the need to define the very outer regions of the stack as a functionally differentiated domain. The NDH complex that facilitates one pathway of CET in the thylakoids is found in the stroma lamellae, also due to its bulky structure that sterically hinders grana location (Lennon et al. [2003]). The majority of PGR5/PGRL1 heterodimers are localised in the stromal lamellae, to a lesser extent in the grana margins, and little amount of PGRL1 monomer in the grana stacks (Hertle et al. [2013]).

Irrespective of the definition of a distinct margin protein domain, the lateral protein heterogeneity of the thylakoid membranes suggest that the LET takes place in areas where all required components - from the PSII, plastoquinone pool over Cytb_6f to plastocyanin and PSI are located within reasonable distance from each other (grana margins). On the other hand the process of CET can only occur efficiently in domains where Cytb_6f and PSI are present along with the NDH or PGR5/PGRL1 (stromal lamellae, Pribil et al. [2014]).

The term grana margins is presented in the literature in an ambivalent way and it is very important to distinguish between the structural and the functional definitions of grana margins. Dekker and Boekema [2005] describe the margins as the strongly curved membrane that connects two stacked membranes that enclose the lumen. With this definition they argue that neither the photosystems, nor the Cytb_6f can be located in the margins due to steric hindrance of the curvature, that light harvesting is not happening in this region and that there is no evidence that the ATPase is located in this fraction of the membranes either. The authors conclude that the bent membranes are essentially protein-free and argue that any proteins that have been assigned to the margins are not directly located within these areas but immediately adjacent. Preparations of isolated membranes using detergents would therefore not reflect the composition of the structural margins but rather functional margins containing all components neccessary for LET. An extensive study by Koochak et al. [2019] shows that isolated curved membranes and connecting periphal regions of the stacks that were isolated by detergent treatment contained both photosystems, the cytochrome b_6f complex and ATPase, suggesting that this is the domain where LET takes place. The authors found the margin regions also enriched in

monomeric, reaction centre free PSII cores domains, suggesting this is the place where PSII repair, disassembly and degradation might take place.

The conserved nature of lateral heterogeneity in thylakoid membranes suggests that this has a functional importance for the light reactions, and there are different suggestions as to why grana have evolved in the first place. Trissl and Wilhelm [1993] argue that a separation of the two photosystems can prevent the spillover of excitation energy between the antenna complexes which would favour the excitation of PSI, which is a rapid energy trap, rather than PSII. Joliot et al. [2004] have proposed that the lateral heterogeneity enables CET to work efficiently directly upon illumination, which requires the electron carriers to be spatially separated in the thylakoids. Furthermore, it was proposed by Mullineaux [2005] that grana stacking is rather a way to facilitate diffusion of the membrane soluble PQ to and from the reaction site of PSII while still retaining a large three dimensional light harvesting machinery. This would mean that the light harvesting not only takes place laterally within one membrane layer, but also vertically between two adjacent membranes (Albertsson [1982]) and it implies that the grana stacks are not homogeneous, but that opposing membranes can have different compositions of PSII and LHCII (Boekema et al. [2000]). In the light of the lateral heterogeneity in protein composition and function of the thylakoid membranes, the location of FNR has been investigated insufficiently so far, especially when regarding the proposition of Joliot and Johnson [2011] that FNR might act as a key switch between CET and LET. Their hypothesis suggests that differential recruitment of FNR to either margin or lamellae regions could be fundamental to the underlying mechanism.

Dynamic reorganisation Both the stacking of the thylakoid membranes and the dynamic change in protein organisation itself have great potential for regulating light energy harvesting and electron transport processes. The thylakoid network can dynamically change at both membrane architecture level and protein complex level upon environmental triggers, mainly light intensity (Kirchhoff [2013]).

In general, low light conditions cause a high thylakoid/stroma volume ratio, broader grana stacks and a higher stacking ratio and along with that comes a higher chlorophyll content in the chloroplasts (Anderson [1986]). Khatoon et al. [2009] in turn showed that unstacking of the appressed membranes occured in high-light conditions and traced a higher PSII reaction centre protein turnover back to a more easily facilitated diffusion of proteins in the membrane, coinciding with an increase of margin area. This might enable repair processes of the damaged PSII by making it more accessible (Herbstová et al. [2012]), especially as a whole lumenal protein machinery is involved in PSII assembly (Mulo et al. [2008]). Furthermore, Khatoon et al. [2009] argue that highly stacked grana are more efficient in production of reactive oxygen species (ROS) and therefore an unstacking would redeem some of the ROS generation in high-light conditions. It has also been reported that the thylakoid lumen can undergo swelling upon the transition from dark to light (Kirchhoff et al. [2011]), increasing diffusion space for the soluble electron carrier plastocyanin, and regulatory proteins and enable PSII repair in a relatively less crowded lumen.

Changes in light conditions not only impact the structural organization, but also protein distribution in the thylakoid membrane. For example, the ratio of LHCII to PSII and LHCII to the Cytb_6f increases in low light (Anderson [1986], Kirchhoff et al. [2007]). This

size-increase of the antennae optimizes the photosynthetic yield in limiting light conditions. Another mechanism of balancing light harvesting between the two photosystems is a change in connectivity of the antenna complexes to the reaction centres, the state transitions (Allen [2003]). This reversible process describes the re-distribution of LHCII between PSI and PSI depending on the wavelength of the excitation light. The mechanism is mediated by phosphorylation of the LHCII by the state transition STN7 kinase (Bellafiore et al. [2005]) and subsequent diffusion to PSI. This in turn is dependent on the redox state of the PQ pool at the Cytb_6f, transducing unequal excitation of the two photosystems and activating the LHCII kinase (Vener et al. [1997], Zito et al. [1999]). This process would also be facilitated by dynamic re-stacking of the membranes (Kirchhoff [2013]). Other protein re-arrangements are made in the antennae in response to changing light quality, described as non-photochemical quenching (NPQ). Excess light energy that is absorbed by the antenna complexes can be dissipated as heat by quenching of the excited chlorophyll. This is facilitated by pH-activated structural changes of parts of the antenna complex in the xanthophyll cycle (Sacharz et al. [2017]). It also triggers aggregation of LHCII in the grana (Johnson et al. [2011]).

All these findings illustrate that the entire light reactions of photosynthesis are tightly regulated by thylakoid architecture and protein distribution and their dynamics in response to changing light conditions. Lateral heterogeneity is influenced by architectural changes, changes in redox state of electron carriers and changes in pH-gradient across the thylakoid membrane. Therefore, the location of FNR is also likely to be subject to dynamic changes in the membrane and the electron transport chain and this has yet to be investigated in

detail, especially in regard to its putative role as switch between LET and CET.

1.4 Correlation of FNR content with stress tolerance

Exerting control over the process of light energy conversion into chemical energy is of high interest to humanity with its ever increasing demands for food and fuel. Therefore, efforts have been made to further optimise this process by manipulating components of the electron transport in transgenic plants. Because a severe lack of FNR in transgenic tobacco plants was found to restrict the rate of photosynthesis (Hajirezaei et al. [2002a]), overexpression of FNR to increase the rate of photosynthesis and therefore biomass was a tempting approach that was proven to be unfeasible by Rodriguez et al. [2007]. However, the authors found that tobacco plants overexpressing FNR were more tolerant to photooxidative damage and postulated a role for FNR in the relief of electron pressure during excess light conditions by partitioning the reductive power into other pathways. In the following section, I will briefly outline mechanisms of stress response of higher plants with particular attention to the molecular responses to photooxidative stress in the photosynthetic electron transport chain and FNRs postulated roles.

Possible role of FNR in stress tolerance Due to their sessile lifestyle, plants are highly adapted and optimized to the biological condition of their habitat. However, when conditions change this requires a response of the plant to maintain homeostasis. We speak of stress when the environmental conditions turn adverse and inhibit the normal function of an affected organism.

This stress can occur in the form of biotic stressors (e.g. herbi-

vores, insects infestation or pathogens) or a great variety of abiotic factors (e.g. temperature, oxidative stress, water supply, radiation, salinity, wind (for review see Mahajan and Tuteja [2005]). Stress response usually requires initial sensing and response activating signalling pathway through formation of phytohormones or reactive oxygen species (ROS) which then trigger a response on many levels of organisation (Fujita et al. [2006]). A response via induction of gene expression leads to the production of two groups of proteins that dos Reis et al. [2012] have classified: enzymatic and structural proteins (e.g. detoxification enzymes, glutathion-S-transferases, heat shock proteins) or regulatory proteins (e.g. protein kinases, transcription factors).

While these response mechanisms are adequate for responses to some stress factors such as biotic factors or temperature, where changes happen comparatively slowly, this does not apply for light stress. Light induced excessive excitation of the photosynthetic transport chain can lead to severe damage by the generation of reactive oxygen species e.g. hydrogen peroxide (H_2O_2) in the Mehler reaction (Mehler [1951]) or superoxide (O_2^-) via reduced Fd (Asada et al. [1974], Misra and Fridovich [1971]) and PSI (Takagi et al. [2016]) which have the capability to damage and destroy nucleic acids, membranes and proteins. H_2O_2 can further react to create hydroxyl radicals ($^{\cdot}OH$) in the Fenton reaction (Fenton [1894]), which cannot be detoxified enzymatically and are therefore particularly dangerous. Due to this circumstance, plants give prevention of $^{\cdot}OH$ formation first priority and have evolved sophisticated, rapid response strategies to regulate the redox state of PET by a network of tight regulation which is crucial for survival.

O_2^- and H_2O_2 can be eliminated by superoxide dismutases (SODs)

and ascorbate peroxidase/catalase respectively in the water-water-cycle, in which the excess electrons are immediately scavenged (Asada [1999]). This reaction requires ascorbate which in turn needs to be re-generated by either reduced Fd or the GSH/GSSG (ascorbate-glutathione cycle, Chew et al. [2003]), supported in turn by NADPH. Hajirezaei et al. [2002a] could show that the ratio of $NADP^+$ to NADP(H) increased when FNR activity was lowered in antisense-FNR tobacco plants, which is supported by the findings of Lintala et al. [2014] and Kozuleva et al. [2016]. Kozuleva et al. [2016] revealed the close connection of FNR activity to the redox metabolism of the chloroplast by showing that (H_2O_2) evolution in FNR over-expressing Arabidopsis was lower than in wild-type plants, suggesting that this is due to the higher photoreduction rate of $NADP^+$ and a shorter lifetime of reduced Fd. They also found that a decrease in FNR enzyme content results in a higher oxidation state of the glutathione pool, whereas increased FNR contents results in an increased reduction state of glutathione and also decreased total glutathione levels. Moreover, the authors reported that in vitro, excess FNR relative to Fd resulted in a large increase in superoxide production. Their data indicates that stress resistance in FNR over-expressing plants might be due to "priming" of expression of genes involved in the oxidative stress response, activated by an increase in superoxide.

1.5 Experimental approach

The data suggests that FNR has multiple functions in the chloroplast: its crucial role in LET, its putative role as a switch to CET, and a role in regulation of oxidative stress response (Mulo [2011]). It remains unclear to what extent these functions are dependent on

the isoform, interaction partners and attachment to the membrane.

Apart from biochemical studies that showed co-purification with other complexes or fractionation of the thylakoid membrane, there is very little data on the location of FNR from imaging approaches. The biochemical methods are sufficiently accurate to assign FNR clearly to the chloroplasts and even membrane and soluble fractions, but as discussed in section 1.3 the chloroplast and especially the thylakoid network can be further divided into different sub-compartments. If the proposition of Joliot and Johnson [2011] that FNR acts like a switch between LET and CET reflects reality, then it might be expected that location of FNR at the grana margins enhances LET, while CET might be promoted when FNR is located at the lamellae, because that is how electron flow in the thylakoid is thought to be compartmentalised (see section 1.3). This possibly requires a dynamic relocation of FNR between these two sub-compartments as response to changes in conditions.

This opens up two major questions to be tested by imaging of FNR: Firstly, the unravelling of FNRs distribution between the stroma and the membrane in varying conditions and secondly co-localisation studies with its tethers TROL and Tic62 and other possible binding partners in the membrane like Cytb_6f.

The diffraction limit of light only allows a resolution of 200 nm in standard applications, which is enough to resolve the grana stacks. Reconstruction techniques such as structured illumination microscopy (SIM) can further increase the resolution to about 100 nm, but this is still not enough to resolve the sub-compartments of the thylakoids where structural changes happen in the two-digit nm scale (Kirchhoff [2013]). Furthermore, the chlorophyll autofluorescence that can usually be exploited as a convenient marker for the grana stacks is

not easily detectable in the lamellae regions (van Spronsen et al. [1989]), so only parts of the thylakoid network are visible. The development of super-resolution imaging techniques allows imaging below the diffraction limit, but most of the efforts with fluorophore-labelled targets have been restricted to non-photosynthetic tissues (Schubert [2017]), possibly because the chlorophyll autofluorescence can cause complications for the acquisition process. Iwai et al. [2016] recently resolved the grana and lamellae regions of *Physcomitrella patens* chloroplasts in a three-dimensional and time-resolved manner by super-resolution confocal live imaging microscopy (SCLIM). This was achieved by measuring two wavelengths of the chlorophyll autofluorescence, which could then be attributed to the different antenna composition in the grana and lamellae. Individual layers of thylakoids could be resolved for the first time by light microscopy imaging in non-destructive 3D-SIM (Iwai et al. [2018]). However, none of these state-of-the-art techniques - although promising - have yet been used to visualise a fluorophore-labelled sample in the thylakoid membrane.

The main research focus in my thesis is the investigation of the sub-chloroplastidial location of FNR, so I chose to employ well-established transmission electron microscopy (TEM). This technique produces images where the grana stacks and stroma lamellae are clearly distinguishable and FNR can simultaneously be visualised by immunogold (IG) labelling. The difficulty in this approach lies in the reliability of label quantification. Negi et al. [2008] have used TEM and IG-labelling in a co-localising approach and came to the conclusion that parts of the soluble FNR pool is co-localised with glyceraldehyde-3-phosphate-dehydrogenase (GAPD). However, they present no convincing controls for their experiment, so this result

remains questionable. This highlights the importance of statistical power in the design of IG experiments. Although double-labelling of different proteins is possible in principle, interpretation only makes sense in terms of absolute location and not co-location of individual proteins. For a reliable co-localisation of proteins, light microscopy is the tool of choice to detect any spatial overlap of two signals in the same pixel (Zinchuk et al. [2007], Costes et al. [2004]). I therefore investigated the co-location of FNR with its tether TROL using SIM on a light-sheet fluorescence microscope. Furthermore, I correlate the findings of these localisation studies with photosynthetic and physiological measurements to establish whether specific localisation patterns correlate with changes in electron transport and stress tolerance. With this experimental setup, I am aiming to provide new insights about the sub-organelle location of FNR and the impact this has on photosynthetic function.

2. Material and Methods

2.1 Material

All chemicals were obtained from Sigma Aldrich (Gillingham) unless otherwise stated. All enzymes and restriction endonucleases were obtained from Thermo Fisher (Dartford) unless stated otherwise.

Plant material and growth conditions *A.thaliana* seeds were soaked in H_2O for 2 days at 4°C prior to sowing to induce germination. The plants were grown in a 6:6:1 soil mix of John Innes No3, Levington Advana Pot and Bedding Compost and Sinclair Perlite Standard. The genetic plant lines are Arabidopsis, columbia ecotype wild-type, *fnr1* mutant (Lintala et al. [2007], Hanke et al. [2008]) and all three maize FNR isoforms under control of the wild-type promoter (Okutani et al. [2005]) introduced into the *fnr1* mutant background (table 2.1). For stable light conditions, plants were grown in a growth cabinet (Percival, Perry, Iowa) at a light intensity of about 120 µE and a humidity of 70% for 16 h a day with temperatures of 18 °C at night and 22 °C during the day. Fluctuating light conditions were simulated in the same conditions, but with cycles in light intensity of 5 min about 10 µE followed by 5 min of about 190 µE throughout the day to ensure that the plants are subjected to the same amount

of photons approximately.

Table 2.1: Plant lines

Genetic line	Background
A.thaliana wild-type	Columbia ecotype
A.thaliana fnr1	WT Col. ecotype
*A.thaliana Zm*FNR1	*A.thaliana fnr1* Col. ecotype
*A.thaliana Zm*FNR2	*A.thaliana fnr1* Col. ecotype
*A.thaliana Zm*FNR3	*A.thaliana fnr1* Col. ecotype

Table 2.2: Primers and peptides

Name	Sequence	Obtained from
ZmTROL2	CGSSPATTRPRPQSPYPNYPDFKPPSSPSPSAPQ	LifeTein, Somerset, USA
MK_SEQ_pQE60_Fw	CCTTTCGTCTTCACCTCGAGAAATC	Eurofins Genomics, Ebersberg, Germany
MK_SEQ_pQE60_Rv	GGTCATTACTGGATCTATCAACAGG	Eurofins Genomics, Ebersberg, Germany
MK_SEQ_GFP-Epitope_Fw	CTACCATCTGGAAAACGAAGTGG	Eurofins Genomics, Ebersberg, Germany

Table 2.3: Antibodies used in immunolabelling experiments

Antibody	Application & concentration
Primary antibodies	
Rabbit anti-Cytb_6	Western blots (1:50000)
Rabbit anti-Cyt$f$	EM(1:100)
Rabbit anti-LHCI	Western blots (1:8000)
Rabbit anti-LHCII	Western blots (1:8000)
Rabbit anti-NDH-SU	Western blots (1:10000)
Rabbit anti-PC	Western blots (1:2000)
Rabbit anti-PGRL1	Western blots (1:3000)
Rabbit anti-PsaD	Western blots (1:5000)
Rabbit anti-PsbA	Western blots (1:10000)
Chicken anti-PsbA	LSM (1:200)
Rabbit anti-Rubsico-LSU	Western blots (1:50000)
Rabbit anti-*Zm*TROL	Used for Atto-565 conjugation
Guinea pig anti-*Zm*TROL	LSM (1:200)
Rabbit anti-*Zm*FNR2	Western blots (1:20000)
	LSM (1:1000)
	EM (1:200)
Secondary antibodies	
AP-conjugated anti-rabbit	Western blots (1:30000)
HRP-conjugated anti-guinea pig	Western blots (1:30000)
IG-conjugated anti-rabbit	EM (1:200)
Alexa488-conjugated anti-chicken	LSM (1:200)
Cy2-conjugated anti-guinea pig	LSM (1:200)
Cy3-conjugated anti-rabbit	LSM (1:200)
Conjugated antibodies	
Atto565-conjugated anti-Cyt$f$	NA
Atto565-conjugated anti-*Zm*TROL	LSFM (70 mM)
Atto488-conjugated anti-*Zm*FNR2	LSFM (1 mM)

Table 2.4: Bacterial strains

Strain	Properties
E.coli XL-1 Blue	recA1 endA1 gyrA96 thi-1 hsdR17 supE44 relA1 lac [F´ proAB lacIqZ Δ M15 Tn10 (Tetr)].
E.coli BL21 Δ iscr	fhuA2 [lon] ompT gal [dcm] Δ hsdS Δ iscr

Table 2.5: Plasmid constructs

Name	Properties
pQE-60-LFNR	Amp^R
pEX-K4-ZFNR1LoopA	GFP-epitope loop-A-tagged FNR, Kan^R
pEX-K4-ZFNR1LoopB	GFP-epitope loop-B-tagged FNR, Kan^R
pEX-K4-ZFNR1LoopC	GFP-epitope loop-C-tagged FNR, Kan^R
pQE-60-ZFNR1LoopA	GFP-epitope loop-A-tagged FNR, Amp^R
pQE-60-ZFNR1LoopB	GFP-epitope loop-A-tagged FNR, Amp^R
pQE-60-ZFNR1LoopC	GFP-epitope loop-A-tagged FNR, Amp^R

Table 2.6: Restriction endonucleases

Enzyme	Restriction site
HindIII	5'...A—AGCTT...3'
	3'...TTCGA—A...5'
NcoI	5'...C—CATGG...3'
	3'...GGTAC—C...5'

2.2 Molecular techniques

2.2.1 Cloning

Production of chemically competent *Escherichia coli* 100 ml of *E. coli* cells in lag-phase were harvested by centrifugation for 10 min at 4°C and 5460 G in a Megafuge 40R (Thermo Scientific), resuspended in 30 ml of pre-cooled, sterile-filtered TFB1-buffer (table 2.7) and incubated on ice for 10 min. Another centrifugation step followed and

the pellet was resuspended in 4 ml of pre-cooled, autoclaved TFB2-buffer (table 2.7). The cells were shock frozen in liquid nitrogen and stored at -80°C until further use.

Table 2.7: Buffers for production of competent cells

TFB1-buffer	TFB2-buffer
30 mM potassium acetate	10 mM MOPS
50 mM $MnCl_2$	75 mM $CaCl_2$
100 mM $RbCl_2$	15 mM $RbCl_2$
10 mM $CaCl_2$	15% Glycerine (v/v)
15% Glycerine (v/v)	
pH 5.8 with acetic acid	pH 7.8 with NaOH

Transformation of *Escherichia coli* 100 µl of competent *Escherichia coli* were incubated on ice for 30 min with 1 µl of plasmid followed by heat-shock treatment for 90 seconds at 42°C in a Thermomixer comfort 5436 (Eppendorf, Stevenage) and a 2 min incubation on ice. The cells were added to 1 ml of Miller's LB broth and incubated on a shaker for one hour at 37°C. 150 µl of the sample was transferred to LB agar plate containing 50 µg/ml ampicillin and incubated over night at 37°C.

Plasmid isolation Plasmid DNA was selectively isolated from *E. coli* cultures grown in the respective selection LB medium with the help of Mini Preparation Kit from Qiagen (Manchester) or Machery&Nagel (Düren, Germany) following the instructions of the manufacturer.

Restriction digest Plasmid DNA and DNA fragments that were amplified via PCR were treated with type II restriction endonucleases to cut them at specific sites for further cloning (table 2.6). The re-

action mixtures were incubated for 1 h at the temperature optimum of the respective enzymes (37°C). Reaction mixtures consisted of up to 5 µg DNA, 1 µl restriction enzyme, 2 µl 10x buffer (Tango) in a total volume of 20 µl.

Colony polymerase chain reaction Transformed *E. coli* colonies were identified by colony polymerase chain reaction (PCR). Single colonies were picked from LB selection medium agar plates and introduced into the PCR mix. Then, the same colony was used to induce an over-night culture. The primers MK_SEQ_GFP-Epitope_Fw and MK_SEQ_pQE60_Rv (table 2.2) were used for the detection of the DNA fragment of the respectively right size for each loop insertion. The PCR mix and program is presented in table (2.8). Promising colonies were further cultured.

Table 2.8: Colony polymerase chain reaction

mix	program
2 µl 10x buffer	1. 2 min, 95°C
0.4 µl dNTP	2. 30 s, 95°C
1 µl primer (Fw)	3. 30 s, 60°C
1 µl primer (Rv)	4. 1 min, 72°C
0.25 µl DreamTaq	5. 10 min, 72°C
15.35 µl H_2O	30 cycles of step 2 - 4

Ligation DNA fragments can be enzymatically linked to each other using DNA ligase, that catalyses the formation of a phosphodiester bond between the 5' phosphate terminus of one DNA fragment and the 3' hydroxyl terminus of another fragment. The ligation with a volume of 20 µl contained 100 ng DNA of recipient vector, threefold molar excess of DNA insert, 1 µl T4 DNA Ligase and 2 µl T4 DNA Ligase Buffer. After 2 h incubation at room temperature, the ligated

DNA plasmid was transformed into competent *E.coli* cells.

Agarose gel electrophoresis Agarose gel electrophoresis was used to separate DNA fragments according to their size. A 1% agarose solution in TAE (50 mM TRIS, 50 mM acetic acid, 1 mM EDTA) buffer was prepared and 5 µl of SYBR Green (Thermo Fisher) was added after the solution cooled down to 60°C before pouring. The samples were mixed with DNA gel loading dye (Thermo Fisher). Gel electrophoresis was carried out with 100 V until the dye front passed through the gel for sufficient separation. The SYBR Green stained bands were detected under blue light.

Agarose gel extraction DNA fragments separated by agarose gels were extracted using Min Elute Gel Extraction Kit (Qiagen) following the instructions of the manufacturer.

2.2.2 Loop-tagged FNR

The three plasmids containing the sequence for the GFP-epitope loop-tagged FNR were obtained from Eurofins (see appendix, chapter 11). In order to test the altered FNR isoforms for enzyme activity and binding behaviour, they were cloned into an expression vector. The pQE-60-LFNR plasmid backbone and the pEX-K4-ZFNR1Loop plasmids (table 2.5) were digested with HindIII and NcoI restriction endonucleases (table 2.6) to provide the backbone and inserts respectively for the ligation of the GFP-epitope loop-tagged FNR sequences into the pQE-60 plasmid. Promising transformed colonies were identified via colony PCR, cultured over-night in 5 ml LB medium, the plasmid isolated and sequenced (Eurofins) using the primers MK_SEQ_pQE60_Fw and MK_SEQ_pQE60_Rv (table 2.2).

2.2.3 SDS-PAGE and western blotting

Sodium-dodecyl-sulfate polyacrylamide gel electrophoresis SDS-PAGE was performed after Laemmli, 1970 to separate proteins based on their apparent molecular weight.

Table 2.9: SDS-PAGE gel buffer

4 x upper gel buffer (UGB)	4 x lower gel buffer (LGB)
0.5 M TRIS-HCl pH 6.8 0.4% (w/v) SDS	1.5 M TRIS-HCl pH 8.8 0.4% (w/v)
upper gel concentration 4.5%	lower gel concentration 12%
1 ml 4 x UGB 0.5 ml 40% acryl./bisacrylamide 2.42 ml H_2O 5 µL TEMED 150 µL 10%APS	2.5 ml 4x LGB 3 ml 40% acryl./bisacrylamide 4.4 ml H_2O 4 µL TEMED 50 µL 10%APS

Table 2.10: SDS electrophoresis buffer

10 x electrophoresis buffer	Solution A	2 x loading dye
25% UGB	1% (w/v) SDS	0.5% beta-ME
40% glycerol	250 mM TRIS	0.4% (w/v) SDS
55% H2O	1.92 M gylcine	55% Solution A
		bromphenolblue

The samples were denaturated in loading dye (Table 2.10) at 95°C for 5 min (Thermomixer Comfort 5436, Eppendorf) and loaded to an acrylamide gel (table 2.9) with Prestained PageRuler Plus (Thermo Fisher, Dartford). A current of 25 mA per gel was applied to the MiniProtean III System (BioRad, Watford) chamber filled with electrophoresis buffer (see Table 2.10) until desired separation occured.

Western blotting Following separation, the proteins were transferred onto a polyvinylidene difluoride (PVDF) membrane (0.2 µm, Bio-Rad) for immunodetection.

Table 2.11: Western blot and immunodetection buffer composition

Transfer buffer	Alkaline phosphatase buffer	Tris buffered saline
25 mM TRIS	100 mM TRIS-HCl	50 mM TRIS-HCl
200 mM glycine	100 mM NaCl	150 mM NaCl
	5 mM $MgCl_2$	
	pH 9.5	pH 7.5

The membrane was equilibrated in 100% MetOH and placed into a blot sandwich on the anode side of the gel and immersed in transfer buffer (Table 2.11). Transfer took place at 4°C and 70 V for one hour.

Immunolabelling The free binding sites on the membrane were blocked in 1% BSA in Tris buffered saline (TBS, table 2.11) for one hour during gentle agitation. The first antibody was applied in 0.5% BSA in TBS (for respective antibody concentration, see table 2.3) and incubated for at least one hour. Three 5 min washing steps with TBS followed and the secondary antibody alkaline phosphatase conjugate was applied in 0.5% BSA in TBS for another hour. The membrane was washed again three times for 5 min in TBS, before the membrane was equilibrated in alkaline phosphatase buffer (see table 2.11) containing 0.125% (v/v) 5-bromo-4-chloro-3-indolyl-phosphate (BCIP) and 0.125% (v/v) nitro blue tetrazolium (NBT) for detection. The reaction was allowed to take place in the dark, until the signal reached the desired intensity.

2.2.4 Protein expression and purification

Expression Over-night cultures of BL21 *E.coli* transformed with the different FNR plasmids (table 2.5) were used to inoculate 2 l of lysogeny broth containing 100 µg/ml ampicillin. The cultures were grown at 37°C until they reached an OD_{600} of 0.5 and expression was then induced by adding isopropyl-beta-D-thiogalactopyranosid (IPTG) to an end concentration of 1 mM. The cultures were incubated at 37°C for 12 hours.

Purification The cells were harvested by centrifugation at 2000 G in a centrifuge (Megafuge 40R, Thermo Scientific) for 10 min and the pellets were resuspended in a solution of 50 mM TRIS and 200 mM NaCl and protease inhibitor pefabloc (Roche, Welwyn Garden City) at pH 7.5. The sample was kept on ice at all times. Cell lysis was achieved by sonication in 3 s intervals at 70% power in a sonicator (VCX130 VibraCell by Sonics, Newtown, CT) and the lysate was centrifuged at 12000 G for 15 min to separate and discard the resulting pellet. The supernatant was added to equal volumes of diethylaminoethyl-cellulose (DEAE-cellulose), which does not bind to FNR at this salt concentration, and stirred thoroughly. The mixture was filtered through a miracloth in a ceramic funnel and ammonium sulfate was slowly added while stirring the flow-through to achieve a concentration of 40% saturation. Another centrifugation step followed and the pellet was discarded. Again, ammonium sulfate was stirred in slowly until a concentration of 70% saturation. The sample was centrifuged and this time, the supernatant was discarded, while the pellet was resuspended in 1 ml of 50 mM TRIS, pH 7.5. The solution was dialysed in 4 l of the same buffer for 1 h. After an exchange of buffer, the sample was dialysed over night. A

still cloudy solution was centrifuged once again and the sample was applied to an anion exchange column. A salt gradient from 0 to 300 mM NaCl in 50 mM TRIS, pH 7.5 was applied to gradually elute the proteins from the column. The FNR fraction was collected in the second peak, characterized in its yellow colour. For desalting, the elution was cenctrifuged in a concentration column at 5000 G for 20 min followed by dilution and further concentration. The mixture was loaded onto a ferredoxin conjugated sepharose column (self-made) and again eluted with NaCl gradient from 0 to 300 mM. The yellow elution fractions were collected and concentrated as before and the loop-tagged FNR proteins were ready to test in binding, dimerization and activity assays.

2.2.5 FNR functionality tests

Dimerization *Zm*FNR2, *Zm*FNR3 (Okutani et al. [2005]) and the loop-tagged FNR-L isoforms were tested for their ability to form dimers. 50 µl of 20 µM of purified protein were loaded onto a Superdex 75 10/300 GL (GE Healthcare, Chicago, USA) size exclusion column and eluted with 50 mM TRIS, 20 mM NaCl (pH 7.5) On this column the FNR dimer elutes at around 9 ml flow-through and the monomer at 15 ml.

Binding to TROL FNR binding to the TROL protein was tested on the same Superdex 75 10/300 GL column. This time, a mixture of 200 µl of 5 µM TROL FNR-binding peptide (table 2.2) and 50 µl of 8 - 10 µM FNR was applied to the column. A single peak indicates no binding of FNR to TROL, whereas a double peak represents TROL-FNR complex and non-bound FNR.

Activity The FNR activity tests were carried out in three experimental replicates for FNR-LA and FNR-LC in a buffer of 50 mM TRIS, 100 mM NaCl (pH 7.5).

Table 2.12: FNR activity assay. Total assay volume 100 µl.

Reagent	Concentration
ferredoxin	20 µM
FNR	20 nM
NADP(H)	50 µM
Glucose-6-Phosphate dehydrogenase	0.33 units/assay
Cytochrome *C* (oxidized)	200 µM
Glucose-6-Phosphate	3 mM

The reaction mixture was composed as indicated in Table 2.12. The glucose-6-phosphate and its dehydrogenase were added to regenerate NADP(H) in the course of the reaction so it could not serve as a limiting factor. Five readings were conducted on each experimental replicate in a microplate reader (FluorstarOmega, BMG Labtech, Ortenberg, Germany).

$$\mathrm{Cyt_{ox}} + \mathrm{Fd{-}NADP(H)} \xrightarrow{\mathrm{FNR}} \mathrm{Cyt_{red}} + \mathrm{Fd{-}NADP^{+}} \qquad (2.1)$$

The reduction of oxidized Cyt *C* by ferredoxin, reduced in turn by FNRs activity as NADP(H) diaphorase as described in Shin, 1971 (see Eq. 2.1) can be measured in an increase of absorption at 550 nm wavelength in a spectrophotometer.

2.2.6 Immunolabelling for microscopy

Immunfluorescence labelling of isolated chloroplasts

***A.thaliana* chloroplast isolation** Chloroplasts of *A.thaliana* wild-type, *fnr1*, *fnr1*ZmFNR1, *fnr1*ZmFNR2 and *fnr1*ZmFNR3 plants were

isolated from whole plants harvested at the end of the dark period and kept in the dark until the fixation was finished.

Table 2.13: Buffer composition for chloroplast isolation.

Homogenization buffer (HB)	Resuspending buffer (RB)
0.45 M sorbitol	0.3 M sorbitol
20 mM tricine	20 mM tricine
10 mM EDTA	2.5 mM EDTA
10 mM $NaHCO_3$	
0.1% BSA	
pH 8.4	pH 7.6

Homogenizing of the plants took place in 100 ml frozen HB (see Table Table 2.13) in a pre-cooled laboratory blender (Waring, Stamford, CT) in 3 pulses of 2 seconds. and the homogenate was filtered through four layers of muslin into an erlenmeyer flask on ice. The plant material was discarded and the flow-through was filtered again through 4 layers of muslin plus one additional layer of buffer-soaked cotton wool. The flow-through was centrifuged for 2 min at 3500 G in a Megafuge 40R (Thermo Scientific) at 4°C. The supernatant was discarded and the chloroplasts were gently resuspended in a drop of RB (see Table 2.13) using a natural paint brush. 50 ml of RB were added and the centrifugation step repeated. The washed chloroplasts were resuspended again in a drop of RB and kept in the dark on ice until further use.

Immunfluorescence labelling A drop of isolated chloroplasts were applied directly to 0.5 mm objective round glass slides and settled for 30 min in the dark.

Table 2.14: Immunfluorescence staining of isolated chloroplasts. The solutions are prepared in resuspension buffer (RB) from the recipe in table 2.13

Reagent	Incubation time [min]
3% formaldehyde	30
3 x RB	2
0.1% TritonX-100	7
3 x RB	2
2% BSA	30
1st antibody	60
3 x RB	2
rothiblock	60
2nd antibody	90
3 x RB	2

Then, the chloroplasts were immunolabelled with antibodies (table 2.3) according to the protocol in table 2.14, while kept in the dark until fixation was completed. The chloroplasts were then ready to be visualised in LSFM or mounted with Fluoroshield mounting medium (Sigma-Aldrich) for use in LSM.

Immunogold labelling of leaf sections

Embedding The first fully unfolded leaves of wild-type, *fnr1*, and *Zm*FNR expressor *A.thaliana* plants were sampled for immunogold labelling to ensure consitency in developmental stage and kept in the dark until the end of the fixation step. The leaves were harvested at the end of the dark period and cut into 1 mm strips with a sharp razor. The strips were transferred to a 3% paraformaldehyde/0.125 M phosphate buffered saline (PBS) in a syringe, creating an underpressure with the plunger to ensure full penetration of the tissue and removing any air from the parenchyma which would interfere with thin-sectioning later on.

Embedding into LR White resin (Agar Scientific, Stansted) re-

Table 2.15: LR White embedding procedure

Reagent	Incubation time [min]
70% EtOH	30
90% EtOH	30
100%EtOH	30
100% EtOH	30
50% EtOH/50% LR White	60
100% LR White	60
100% LR White	over night

quires replacement of the water in the tissue first (see protocol in table 2.15). The strips were transferred to gelatine capsules, filled to the top with LR White resin and covered with a piece of wax. Hardening of the resin took place in an oven at 60˚for 2.5 h. The capsule was removed and the resin block cleaned from the wax. These blocks were now subsequently used for thin-sectioning.

Labelling procedure After cutting the blocks on a Reichert-Jung ultramicrotome (Leica, Nussloch, Germany) into 70 nm thin-sections, they were transferred onto EM nickel grids and consecutively immunogold labelled. Following the procedure in Table 2.16, the grids were air dried in a dust free container and ready to use in transmission electron microscopy.

Table 2.16: Immunogold labelling procedure in a covered wet chamber. PBS was used in a concentration of 0.125 M.

Reagent	Incubation time [min]
50 µL PBS	2
20 µL 5% H_2O_2	5
50 µL PBS / 50 mM glycine	3 x 3
5% BSA in PBS	10
10 µL 1^{st} antibody in 1% BSA in PBS	30
50 µL 1% BSA in PBS	3 x 6
10 µL 2^{nd} antibody in 1% BSA in PBS	30
100 µL PBS	8 x 2
50 µL 1% glutaraldehyde	5
100 µL H_2O	8 x 2
20 µL 4% uranyl acetate	4
100 mL H_2O	3 x 20 dips

2.3 Biophysical techniques

2.3.1 Dual-pulse amplitude measurements

Fluorescence measurements The chlorophyll fluorescence and the P_{700} absorption were monitored simultaneously in a DUAL-PAM-100 measuring system (Walz GmbH [2009], Pfullingen, Germany) in whole leaves of 30 min dark incubated plants. The dark fluorescence yield (F_0) was detected immediately after dark incubation. The maximum change in P_{700} signal (P_m) was determined after 30 s far-red light and application of a saturation pulse. During illumination (140 µE m^{-2} s^{-1}), the maximum fluorescence yield (F_m') and the maximum change in P_{700} (P_m') signal were determined by applying a new saturation pulse at each indicated time point. All parameters were calculated as described in the Walz GmbH [2009] handbook.

P_{700} reduction state measurement The P_{700} reduction state before and after 15 min of high light illumination (900 mmol m^{-2} s^{-1}) was determined as described previously by Hanke et al. [2008]. P_{700} absorption was measured as a far-red light source (12 W m^{-2} s^{-1}) was switched on and off and the total capacity of P_{700} reduction was established with a saturation pulse of a 50 ms actinic light xenon flash.

$NADP^+$ reduction kinetics The $NADP^+$ reduction kinetics were measured with the NADPH/9-AA module of the DUAL-PAM-100 measuring system according to Schreiber and Klughammer [2009]. Isolated chloroplasts of each genotype were dark incubated for 15 min. The equivalent volume between 5 and 10 µg chlorophyll was added to a volume of 1 ml 0.3 M sorbitol, 5 mM $MgCl_2$ and 20 mM KPO_4 at pH 7.6 and stirred briefly. The measurements were carried out without stirring to decrease background noise. The measuring light was set at 4 and 100 Hz during the dark. At 10 ms prior illumination with actinic red light, the frequency was set to 5000 Hz and measuring light to 14 in order to decrease background noise. 100 ms after illumination was stopped, the frequency was again decreased to 100 Hz. An average of 9 measurements was generated by cycles of 50 s dark and 30 s illumination.

2.4 Imaging techniques

2.4.1 Confocal laser scanning microscopy

Confocal laser scanning microscopy (LSM) was performed on a 510 META NLO laser scanning microscope (Zeiss, Jena, Germany) using an Argon laser (488 nm) for the excitation of Alexa488 and Cy2 conjugated antibodies for detection of the emission peak at 508 nm and He-Ne laser (543 nm) for the excitation of Cy3 con-

jugated antibody for detection of the emission peak at 570 nm. The chlorophyll autofluorescence was recorded in the range between 650 and 710 nm. The channels were sequentially imaged through an oil-immersed Plan-Apochromat 63x/NA 1.4 DIC objective to avoid cross-talk.

2.4.2 Light sheet fluorescence microscopy

The lattice light sheet fluorescence microscopy was conducted according to Chen et al. [2014] in a sample-scan with a fixed hexagonal lattice light sheet ($NA_{max} = 0.55$, $NA_{min} = 0.48$) and the sample was moved through the light sheet in 180 nm steps via a piezo stage. The imaging was performed in dithered mode with a pixel size of 103.5 in three channels (488 nm fiber laser for autofluorescence of chlorophyll and Atto488 conjugated antibody and 561 nm fiber laser for Atto565 conjugated antibody) with a shutter speed of 20 ms per frame. The autofluorescence channel was separated by a 647 LP Edge Basic (Semrock, New York) longpass filter and the Atto signal via a 523/610 HC dualband (Semrock) dual pand pass filter. 100 nm beads (TetraSpeck Microspheres, Thermo Scientific) in the respective colour were recorded in objective-scan mode for the experimental determination of the point spread function (PSF).

2.4.3 Transmission electron microscopy

The transmission electron micrsocopy was performed on a Jeol JEM-1230 microscope (Jeol, Peabody, MA) equipped with a Morada CCD camera and iTEM Olympus software at 80.00 kV.

2.5 Bioinformatics

2.5.1 Software

Table 2.17: Software and databanks that were used in this thesis.

Software	Version/Distribution	Plugin
ImageJ	1.52e	Versatile Wand
		Coloc2
R	1.1.456	ggplot2
Zotero	5.0.64	Better BibTex
TeXstudio	2.12.10/MikTex	Texshade
SnapGene	3.3.4	

2.5.2 Image deconvolution

The LSFM dataset was corrected for chromatic shift, deskewed to equalise the Z-stack and deconvolved with the help of the experimental PSF with the Richardson-Lucy algorithm (Chen et al. [2014]).

2.5.3 Correlation coefficient calculation

The Pearson's Correlation Coefficient (PCC) was calculated for the whole Z-stack of a single chloroplasts after cropping to exclude as much background as possible using the Coloc2 tool in ImageJ.

2.5.4 Signal density analysis

The areas of interest on the electron micrographs of chloroplast thin-sections were defined as stroma, grana, margins and lamellae. These are composed of either just the darker stained membranes (grana), or membranes and close-by stromal area (lamellae and margins) or the lighter stroma alone. The micrographs were printed and the areas of interest were manually coloured in red (margins), blue (lamellae) and green (grana). These images were then scanned and analysed in

ImageJ with help of the Versatile Wand Tool. By substraction of the sum of grana, lamellae and margin area from the total chloroplast area, a value for the stroma was calculated. Then, the gold particles were manually counted on each micrograph and the labelling density of each sub-compartment was calculated as particles/µm^2.

2.5.5 Statistical analysis

The statistical analysis of variance (ANOVA) and post-hoc analysis Tukey's tests were performed in R [2013].

2.6 Evaluation of plant growth

The whole plants grown in different light conditions were harvested for determination of their fresh weight after 38 days. They were weighed and an SDS sample was prepared for genotype screening. For seed production and yield measurement, the plants were grown for 107 days until flowering and then dried out outside the chamber. The weight of the seeds was determined. For screening, one leaf was removed when the plants started flowering.

3. Characterisation of maize FNR expressors

The principle research goal in this thesis is to investigate the effects of FNR sub-chloroplast location on its functional role in LET and CET. Okutani et al. [2005] have found three different leaf-type FNRs in maize plants that are either soluble (*Zm*FNR3), membrane-bound (*Zm*FNR1) or in both locations (*Zm*FNR2) based on biochemical fractionation methods. Twachtmann et al. [2012] have generated *A.thaliana* mutant plants expressing the respective maize FNR under control of the native *At*FNR1 promoter. However, the total FNR content in these plants is higher than in the wild-type and therefore crossed with *fnr1* knock-out mutants to generate a background in which the plants have an amount of FNR that is comparable to wild-type levels (unpublished data). In this chapter, a thorough study of tether binding behaviour and characterization of growth and seed yield of these mutant plants will be presented. This was done to confirm their suitability for further studies of the relationship between FNR location and its function in electron distribution. In order to be used as tools for the investigation of how FNR location can regulate PET, it should first be established that the other major components of PET are unaffected by the introduction of these

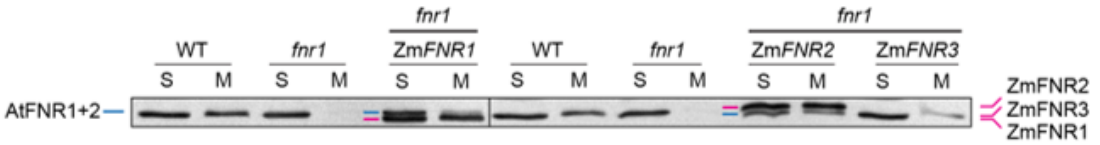

Figure 3.1: **Western blot of FNR solubility in Arabidopsis wild-type, *fnr1*, *fnr1* ZmFNR1, *fnr1* ZmFNR2 and *fnr1* ZmFNR3.** Wild type, *fnr1* and *Zm*FNR1, *Zm*FNR2 and *Zm*FNR3 expressors in the *fnr1* background were grown in 12h light/12h dark cycles. Extracts were made from mature leaves and separated into soluble (S) and membrane (M) fractions. Samples were subjected to SDS-PAGE before immunoblotting and detection of FNR with primary antisera against *At*FNR2 and alkaline phosphatase conjugated secondary antisera. Equal amount of protein was loaded. Migration of different FNR iso-proteins is indicated to the right and left of the gel.

Table 3.1: **Ability of FNR monomers to dimerize in vivo.** "D" indicates ability to form a dimer, "X" indicates that no dimerization is possible and dashes indicate there is no data currently available.

	*At*FNR1	*At*FNR2	*Zm*FNR1	*Zm*FNR2	*Zm*FNR3
*At*FNR1	D				
*At*FNR2	D	X			
*Zm*FNR1	-	X	D		
*Zm*FNR2	-	D	-	D	
*Zm*FNR3	-	X	-	-	X

genes.

3.1 FNR membrane tethers

Leaf extracts from the previously described *fnr1* mutant plants with expression of *Zm*FNR isoforms were biochemically separated into a soluble and a membrane fraction to investigate whether maize FNR in Arabidopsis shows the same behaviour in localization as they do in *Z.mays* plants.

Figure 3.1 shows western blots immunolabelled with antibody raised against *Zm*FNR2 (which recognizes all FNR isoforms from both plants). Presented are soluble and membrane fractions for the wild-type and all mutant plants. In the wild-type, there is slightly more FNR detectable in the soluble than in the membrane fraction.

Twachtmann et al. [2012] have reported that the maize FNR isoforms crystallize as homodimers and Alte et al. [2010] describe a structure of two FNR subunits with its binding peptide from the Tic62 protein. This suggests a tendency of FNR to dimerize *in vitro*. Upon knock-out of *At*FNR1 the remaining membrane bound *At*FNR2 disappears completely which indicates a binding-cooperativity of the two Arabidopsis FNR *in vivo*. *At*FNR2 is recruited back to the membrane by introduction of *Zm*FNR2, but not by *Zm*FNR1 and *Zm*FNR3. If we assume that the membrane binding in chloroplasts that we see on the western blots is dependent on the formation of FNR dimers we can deduce from this which FNR isoforms are able to form a dimer in Arabidopsis. The dimerization behaviour of the different FNR isoform monomers is described in table 3.1. *fnr2* knock-out mutants in Arabidopsis have shown to be able to recruit FNR to the thylakoids as described by Lintala et al. [2009], so if dimerization is required for binding, the remaining *At*FNR1 must be able to form a homodimer on its own. They also show that in the wild-type, both Arabidopsis FNR isoforms can be partially found at the membrane, indicating that *At*FNR1 and *At*FNR2 can form a heterodimer, whereas *At*FNR2 alone does not bind/dimerize.

A native PAGE was performed to confirm this experiment, especially because *Zm*FNR3 and *At*FNR2 migrate to a similar place in SDS-PAGE, and to address the question of whether introduction of the different maize FNRs recruits *At*FNR2 back to the membrane. The milder sample treatment of a native PAGE also leaves some protein complexes intact, so this method also addresses the question of whether FNR is part of higher weight complexes in a native environment.

In the western blot of a native PAGE in figure 3.2, FNR con-

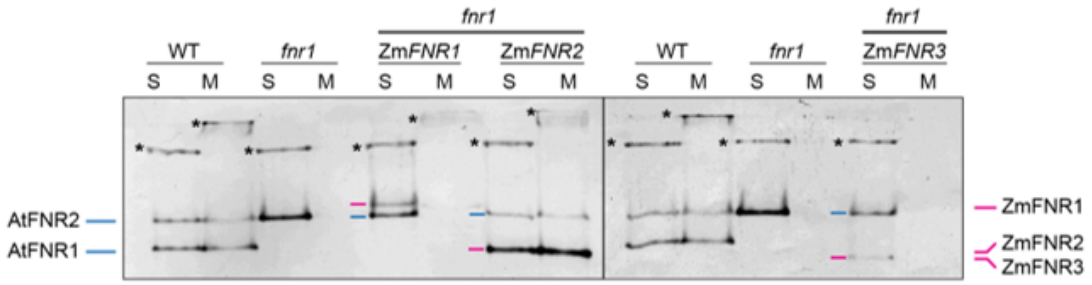

Figure 3.2: **Native PAGE to determine sub-chloroplast location of FNR.** Wild type, *fnr1* and *Zm*FNR1, *Zm*FNR2 and *Zm*FNR3 expressors in the *fnr1* background were grown under long day conditions in moderate light. Protein extracts were diluted to 2 µg/µl before separation into soluble (S) and membrane (M) fractions and loading the equivalent of 20 µg protein in each lane on a native PAGE. Following immunoblotting proteins were challenged with antisera against *Zm*FNR2 and secondary antisera conjugated to alkaline phosphatase. Migration positions of Arabidopsis FNR (blue) and maize FNR (magenta) are indicated to the left and right, respectively and where both proteins can be separated on the blot. High molecular weight complexes are indicated by asterisks.

taining high-molecular weight complexes (indicated by asterisks) are visible additionally to the different FNR monomers. A comparison of *fnr1Zm*FNR1 and *fnr1Zm*FNR2 membrane fractions reveals that the entire membrane bound FNR in *fnr1Zm*FNR1 plants is found in high-molecular weight complexes and *At*FNR2 is not recovered to the membrane, whereas introduction of *Zm*FNR2 will rescue *fnr1* phenotype by recruiting *At*FNR2 to the membrane. *fnr1*ZmFNR3 plants show a similar distribution to *fnr1*, but with one additional *Zm*FNR3 band indicating that the soluble *Zm*FNR3 is not capable of recruiting *At*FNR2 back into membrane complexes.

FNR itself does not contain a membrane binding domain and any loose interaction to the membrane is likely to be disrupted by the biochemical fractionation treatment. Therefore, the membrane-bound FNR visible on these blots requires tethering to the membrane via other proteins. So far, two different membrane tethers are known for FNR (see introductory chapter 1.2.2 for extensive information):

Tic62 and TROL. The three maize FNR isoforms were tested for their binding behaviour to these tethers via western blotting of blue native page (BNP).

Figure 3.3 shows a BNP of isolated thylakoid membranes of the five different genotypes, loading controls on the left and western blots decorated with antibodies against TROL and *Zm*FNR2 (which recognises all FNR isoforms) on the right. TROL protein can be detected either as monomer or bound in complexes mainly with FNR. The signal at around 145 kDa (the size of the FNR-TROL complex) is especially strong in *fnr1*ZmFNR1 thylakoids, indicating that *Zm*FNR1 and TROL interact strongly. The wild-type also shows some FNR-TROL complex, however most of the FNR in the thylakoids of these plants is found in higher-weight complexes. In the other genotypes, TROL is primarily present in its monomeric form, showing little or no interaction of FNR and TROL. Most of the FNR in the wild-type thylakoids is found in a complex running between 230 and 440 kDa corresponding to Tic62-FNR complexes as described by Benz et al. [2009]. *fnr1*ZmFNR2 thylakoids show bands at the same molecular weight, indicating that *Zm*FNR2 and Tic62 interact. *fnr1* and *fnr1*ZmFNR3 preparations show no bands, presumably because their FNR is soluble and therefore not present in the thylakoids.

Our model organism *A.thaliana* has two FNR isoforms (*At*FNR1 and *At*FNR2) that are both membrane bound or soluble and dynamically change location. This flexibility makes interpretation of differences between wild-type and knock-out plants complicated. On the basis of the findings in this section, the newly created maize FNR expressors in the *fnr1* background are much better tools to study FNR function in relation to its location. Each genotype contains FNR in

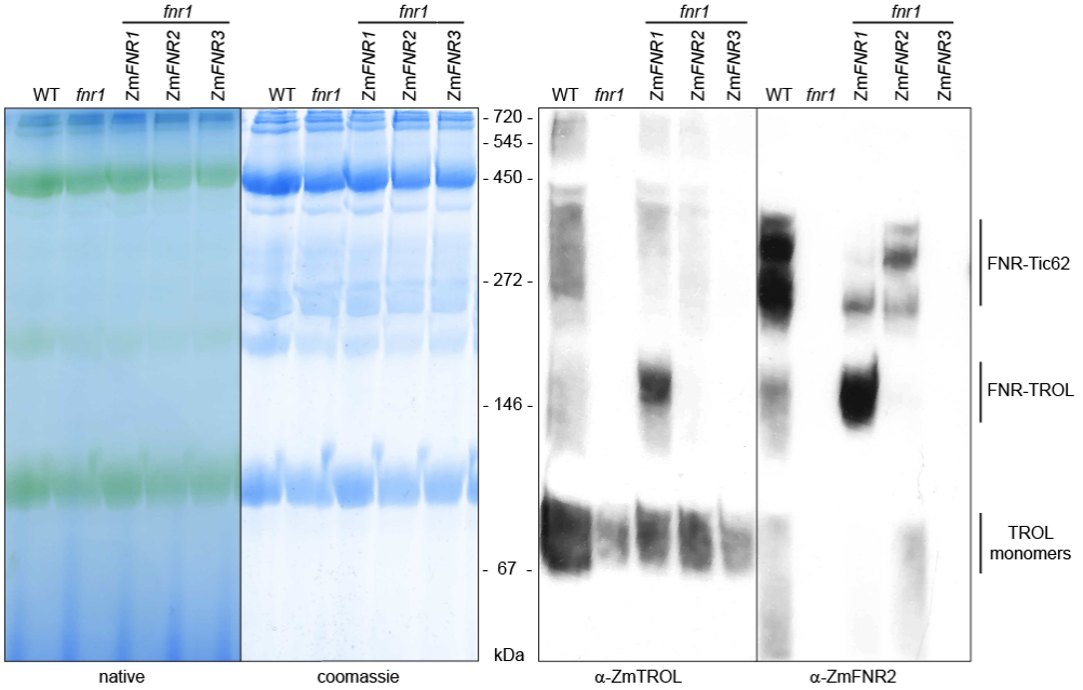

Figure 3.3: **Recruitment of maize FNR isoforms into specific Arabidopsis thylakoid membrane complexes in Arabidopsis wild-type, *fnr1*, *fnr1*ZmFNR1, *fnr1*ZmFNR2 and *fnr1*ZmFNR3.** Chloroplasts were isolated from wild type, *fnr1* and lines expressing the maize FNR genes in the *fnr1* background. Thylakoid membranes were solubilized with n-Dodecyl-maltoside and subjected to blue native-PAGE (BNP). Samples were loaded on an equal chlorophyll basis. Immunoblotting and detection of FNR and TROL containing complexes was performed with antisera raised in rabbit and guinea pig respectively, with secondary antisera conjugated to horseradish peroxidase (chemiluminescence) and alkaline phosphatase respectively. Left panel shows the blue native-PAGE gel before and after staining with coomassie. Right panel shows immunoblots to detect FNR and TROL. FNR- and TROL-containing complexes are indicated to the right of the figure. Positions of molecular mass markers are indicated between the gels and the blots in kDa.

a unique location: in *fnr1*ZmFNR1 plants, FNR is TROL-bound, *fnr1*ZmFNR2 plants contain FNR that forms a complex with Tic62 and *fnr1*ZmFNR3 only has soluble FNR.

3.2 Abundance of LET and CET components

I propose that trapping FNR into distinct complexes might decrease the flexibility of FNR to quickly divert electrons to different sinks as a response to stress. There is a possibility that long term upstream adaptation of the components of the photosynthetic apparatus to compensate for this: a shift in antennae or photosystem abundance, changes in plastocyanin or Cyt b_6f complex content and expression of components of CET (NDH and PGRL1) could occur and complicate the interpretation of any measurements.

In order to establish whether there is an effect in our genotypes, this was tested by western blotting plant extract of each genotype and immunolabelling of the respective compounds (see Figure 3.4).

Compared to the wild-type, *fnr1* mutant plants show visibly less FNR in total, which is increased by the respective maize FNR when expressed, distinguishable by their different size, with *Zm*FNR1 being slightly smaller than *At*FNR1,while *Zm*FNR2 is slightly bigger and *Zm*FNR3 with a size between those two. Photosystem II protein D1 (PsbA) and light harvesting complex II (LHCII) do not show any differences in abundance and neither do the electron carriers plastocyanin (PC) and the Cyt b_6 as part of the Cyt b_6f. This indicates that under these conditions a decreased FNR content or inhibition of FNR binding capacity does not have an upstream effect on protein expression of early components in the electron transport chain. However, photosystem I reaction center subunit II (PsaD) and light harvesting complex I (LHCI) abundance seems to be slightly enhanced

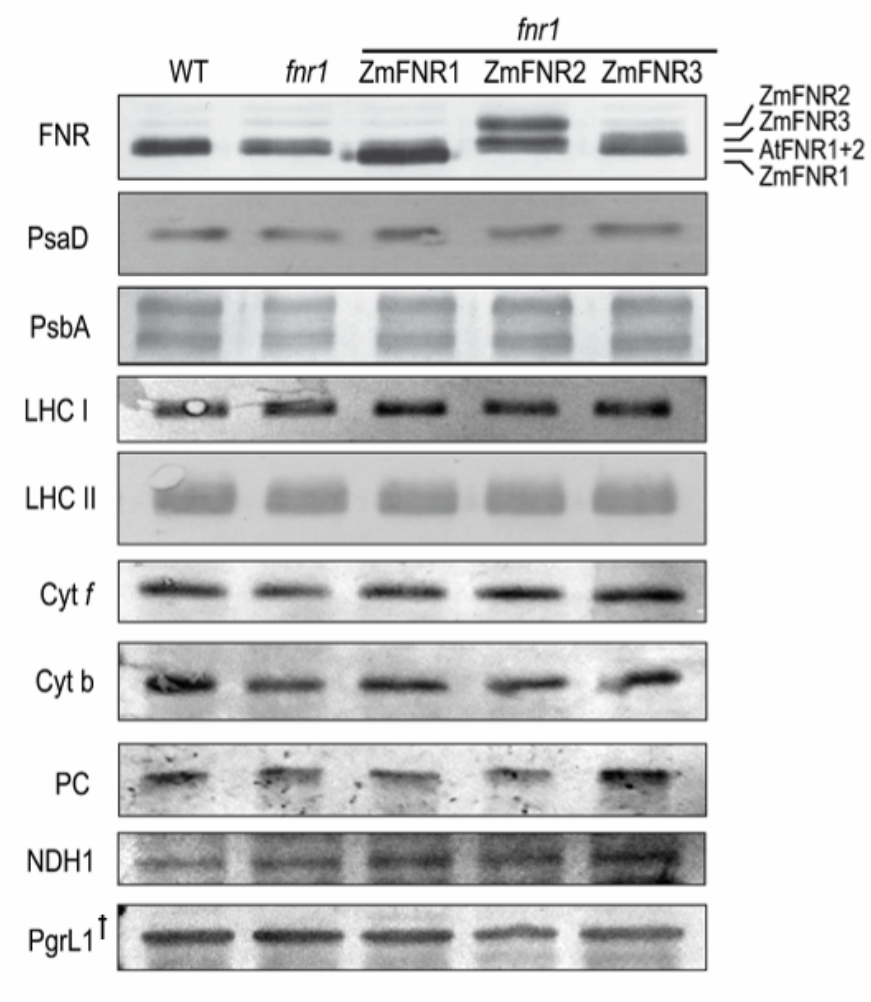

Figure 3.4: **Western blot of FNR solubility in Arabidopsis wild-type, *fnr1*, *fnr1*ZmFNR1, *fnr1*ZmFNR2 and *fnr1*ZmFNR3.** Leaf extracts or isolated chloroplasts (indicated by cross) were normalised for equal protein content and separated by SDS-PAGE and transferred to a PVDF membrane via western blotting. The membranes were immunodecorated with indicated antisera and the protein was detected via colorimetric changes caused by secondary antibody-conjugated alkaline phosphatase.

in *fnr1* ZmFNR1 plants, where FNR is bound to the TROL protein. This suggests that, to some degree, there may be higher abundance of PS I and in particular its antennae complexes in this genotype. Two components of the independent cyclic electron transport routes (as described by Shikanai [2014]), the ferredoxin-plastoquinone reductase PGRL1 and the NADH dehydrogenase NDH show no marked changes among the genotypes. On the basis of these findings, I can be confident that if any further (photosynthetic) measurements detect differences between genotypes, then these differences will predominantly be due to a direct effect of FNR location to the respective site and not due to large secondary effects on the abundance of other photosynthetic complexes.

3.3 Growth and yield

Electrons from the light reaction are diverted to different electron sinks in the plant. Plant fitness is directly dependent on survival of the plant until it reaches the age of reproduction and the production of seeds (Gnan et al. [2017]). In order to test whether FNR interactions really are important for plant growth and fitness, I assessed the performance of the genotypes described in this chapter regarding biomass and seed yield.

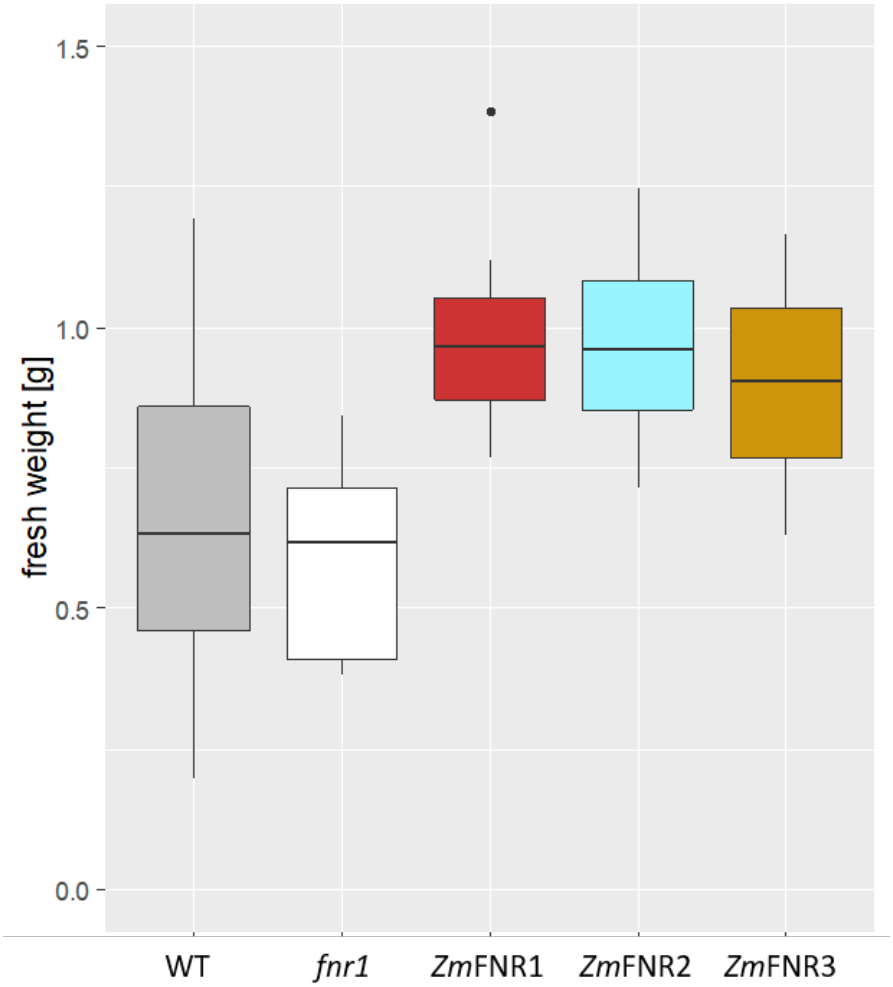

Figure 3.5: **Boxplot of the fresh weight of Arabidopsis wild-type, *fnr1* and maize FNR expressor plants in stable light conditions.** Three to eleven individuals were measured after 38 days of growth in 16 h a day, 120 µE. Statistical analysis is presented in table 3.2

Table 3.2: **Statistical analysis of the fresh weight of Arabidopsis wild-type, *fnr1* and maize FNR expressor plants grown in stable light conditions.** Descriptive statistics, analysis of variance (ANOVA) and Tukey post hoc test. Boxplot is presented in figure 3.5

Descriptive statistics				Tukey post hoc p adj			
				fnr1	*fnr1* ZmFNR1	*fnr 1* ZmFNR2	*fnr1* ZmFNR3
	n	mean	sd				
fnr1	9	0.57	0.06				
fnr1 ZmFNR1	8	0.99	0.2	0.007			
fnr1 ZmFNR2	4	0.97	0.22	0.057	0.999		
fnr1 ZmFNR3	3	0.9	0.27	0.243	0.978	0.994	
WT	11	0.65	0.29	0.941	0.03	0.158	0.488
ANOVA							
	Df	SumSq	MeanSq	F-value	Pr(>F)		
genotype	4	1.123	0.28086	5.08	0.003	**	
Residuals	30	1.659	0.05529				

In figure 3.5, plant fresh weight after 38 days of 16 h light, 8 h dark illumination of 120 µE is presented. The according descriptive statistics, analysis of variance (ANOVA) and post-hoc Tukey test results are depicted in table 3.2. The ANOVA is a test to compare the variance within each group to the variance between groups. The conducted ANOVA on the genotypes was significant ($F(4,30)=5.08$, p=0.003), indicating that the variance between genotypes differs from the variance within genotypes, so a Tukey post hoc analysis was performed to evaluate which genotypes would differ statistically significantly at $p < .05$. Strikingly, the wild-type and *fnr1* knock-out plants do not exhibit a statistically significant difference in biomass production (p=0.941). Replacing *At*FNR1 by *Zm*FNR1 caused a statistically relevant increase in biomass compared to the wild-type and *fnr1* knock-out plants (p=0.03 and p=0.007, respectively). The

other two maize FNR expressors do not exhibit statistically relevant p-values, but also show the tendency of increased growth compared to wild-type and *fnr1* plants. Remarkably, reducing the flexibility of FNR to dynamically change location is not only not disadvantageous, but even might benefit the plant growth in these stable light conditions.

More than biomass production, differences in seed yield will provide information on the reproductive fitness of the respective plant.

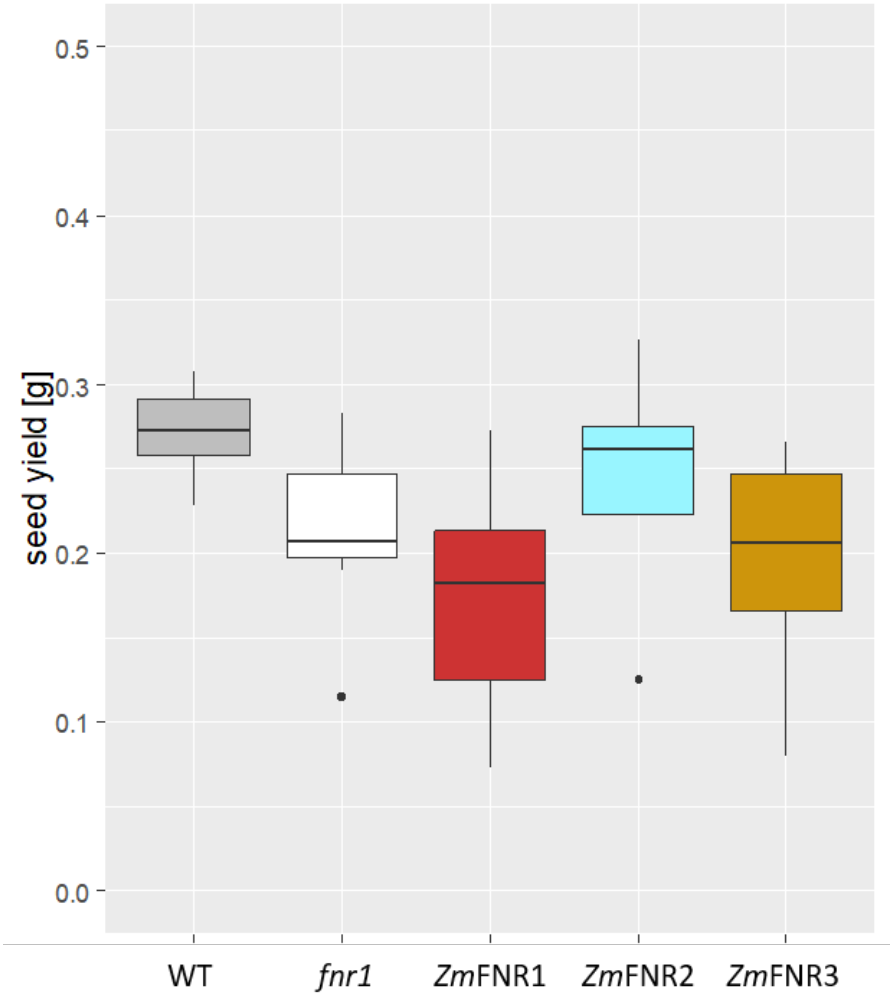

Figure 3.6: **Boxplot of the seed weight of Arabidopsis wild-type, *fnr1* and maize FNR expressor plants in stable light conditions.** Five to ten individuals were measured after 107 days of growth in 16 h a day, 120 µE and then dried. The seeds were harvested and the seed weight per individual was measured. Statistical analysis is presented in table 3.3

Table 3.3: **Statistical analysis of the seed weight of Arabidopsis wild-type, *fnr1* and maize FNR expressor plants grown in stable light conditions.** Descriptive statistics, analysis of variance (ANOVA) and Tukey post hoc test. Boxplot is presented in figure 3.6

Descriptive statistics				Tukey post hoc p adj			
				fnr1	*fnr1* Zm1	*fnr1* Zm2	*fnr1* Zm3
	n	mean	sd				
fnr1	10	0.21	0.05				
fnr1 Zm1	9	0.18	0.07	0.65			
fnr1 Zm2	5	0.24	0.08	0.88	0.26		
fnr1 Zm3	10	0.2	0.06	0.97	0.94	0.61	
WT	10	0.27	0.03	0.16	0.006	0.87	0.04
ANOVA							
	Df	SumSq	MeanSq	F-value	Pr(>F)		
genotype	4	0.050	0.01257	4.018	0.008	**	
Residuals	39	0.122	0.00312				

The ANOVA on the genotypes showed a statistically relevant difference in seed yield (F(4,39)=4.018, p=0.008, see figure 3.6 and table 3.3 for the according statistics). The seed yield in *fnr1* mutant plants has a tendency to be lower than that in the wild-type, but this effect is not statistically significant (p=0.16). However, plants expressing either *Zm*FNR1 or *Zm*FNR3 show a statistically significant decrease in seed weight, compared to the wild-type plants (p=0.006 and p=0.04) but not compared to *fnr1* mutants. The fnr1ZmFNR2 plants do not exhibit this difference compared to the wild-type (p=0.87). This raises the question whether FNR in a dual location is required to ensure optimal seed production in plants growing in stable light conditions.

3.4 Growth and yield in fluctuating light

It has been proposed that FNR plays a part in electron distribution between LET and CET (Joliot and Johnson [2011]). In the conditions of stable light intensity, the plants are likely to maintain a steady state of ideal adaptation for optimal use of electrons in carbon fixation. Although necessary at low levels to increase proton motive force and meet the ATP demands of the Calvin cycle, CET as a valve for excess electrons is a minor pathway under these conditions. Therefore, plants were grown in fluctuating low to medium light conditions (cycles of 5 min 10 µE and 5 min 190 µE), providing a similar total amount of photon exposure as the stable light conditions in figure 3.5 and figure 3.6, to provoke CET upon each increase of light intensity. Plants do this to protect PSI from damage by excess light (Suorsa et al. [2012]). It has been shown by Alte et al. [2010], that tether binding does not affect the enzyme activity of FNR and among the three different isoforms, only *Zm*FNR1 shows a slightly decreased activity *in vitro* (Okutani et al. [2005]). If the location of FNR has an impact on the plants ability to perfom CET this should be reflected in growth and seed production differences between plants with FNR fixed at a specific chloroplast location, when grown under fluctuating light.

Figure 3.7 shows the fresh weight data of plants grown for the same period of time as before, but this time the light intensities were fluctuating between 10 and 190 µE every 5 minutes during daytime. The total amount of photons was kept equal to the plants grown in constant illumination intensity. The according statistical values are depicted in 3.4. Overall, the production of biomass in all genotypes was reduced to about 10% of the biomass in stable illumination, in-

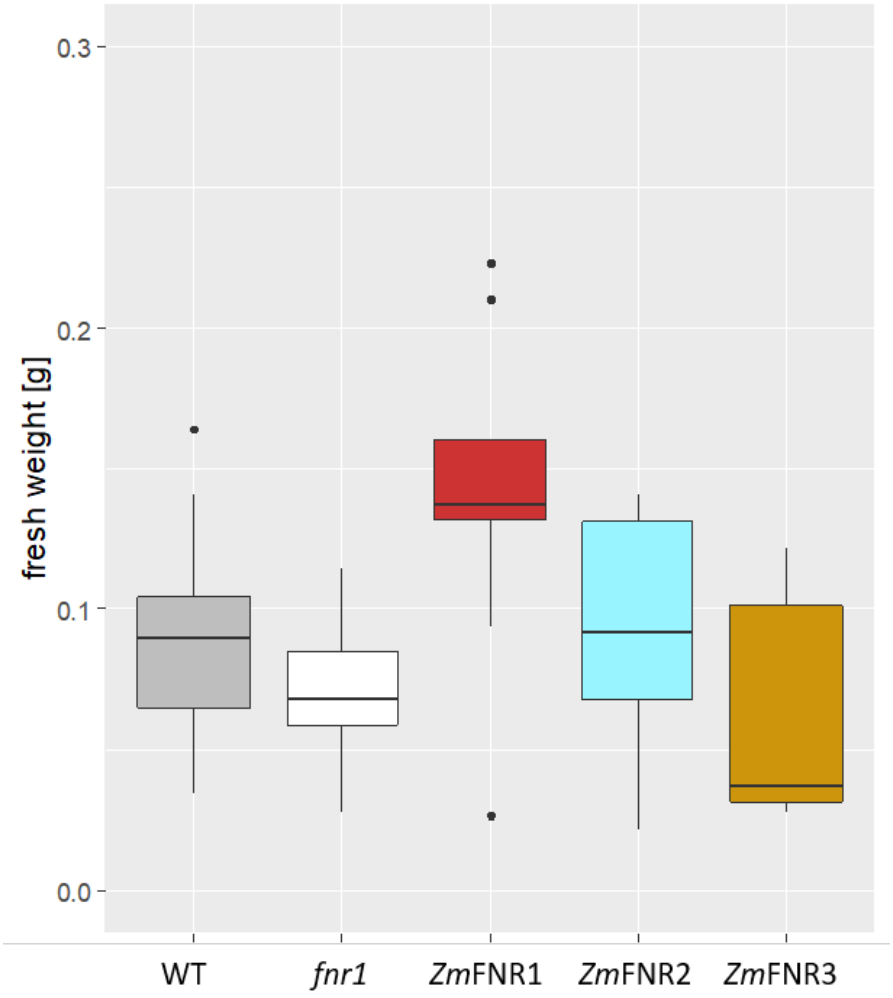

Figure 3.7: **Boxplot of the fresh weight of Arabidopsis wild-type, *fnr1* and maize FNR expressor plants in 16 h a day, with 5 minutes cycles of 190 µE and 10 µE.** Six to ten individuals were measured after 38 days of growth in long-day fluctuating light. Statistical analysis is presented in table 3.4.

Table 3.4: **Statistical analysis of the fresh weight of Arabidopsis wild-type, *fnr1* and maize FNR expressor plants grown in fluctuating light conditions.** Descriptive statistics, analysis of variance (ANOVA) and Tukey post hoc test. Boxplot is presented in figure 3.7.

Descriptive statistics				Tukey post hoc p adj			
				fnr 1	*fnr1* ZmFNR1	*fnr 1* ZmFNR2	*fnr1* ZmFNR3
	n	mean	sd				
fnr1	9	0.07	0.03				
*fnr1*ZmFNR1	9	0.14	0.06	0.02			
*fnr1*ZmFNR2	9	0.09	0.04	0.87	0.15		
*fnr1*ZmFNR3	6	0.06	0.05	0.99	0.01	0.70	
WT	10	0.09	0.04	0.87	0.12	0.99	0.70
ANOVA							
	Df	SumSq	MeanSq	F-value	Pr(>F)		
genotype	4	0.029	0.00721	3.942	0.009	**	
Residuals	38	0.069	0.00183				

dicating that in these conditions less electrons are used for carbon fixation. It is still interesting to compare if the tendency of improved growth in maize FNR expressors was retained. The ANOVA showed a statistical difference between the genotypes again ($F(4,38)=3.942$, $p=0.009$) and a Tukey test was performed. Statistically, none of the genotypes could maintain its advantage in biomass production compared to wild-type, although *fnr1*ZmFNR1 does show a tendency ($p=0.12$) of improved growth. However, *fnr1*ZmFNR1 statistically exceeds the fresh weight of the *fnr1* mutant plants ($p=0.02$) and *fnr1*ZmFNR3 ($p=0.01$). The other maize FNR expressor lines did not exceed the wild-type statistically significantly, indicating a relatively more severe effect of the fluctuating light on growth in these genotypes. Although plant growth overall suffers from fluctuating light intensities, plants with TROL-bound FNR appear to compensate best.

Similarly to biomass production, the yield in seed weight signifi-

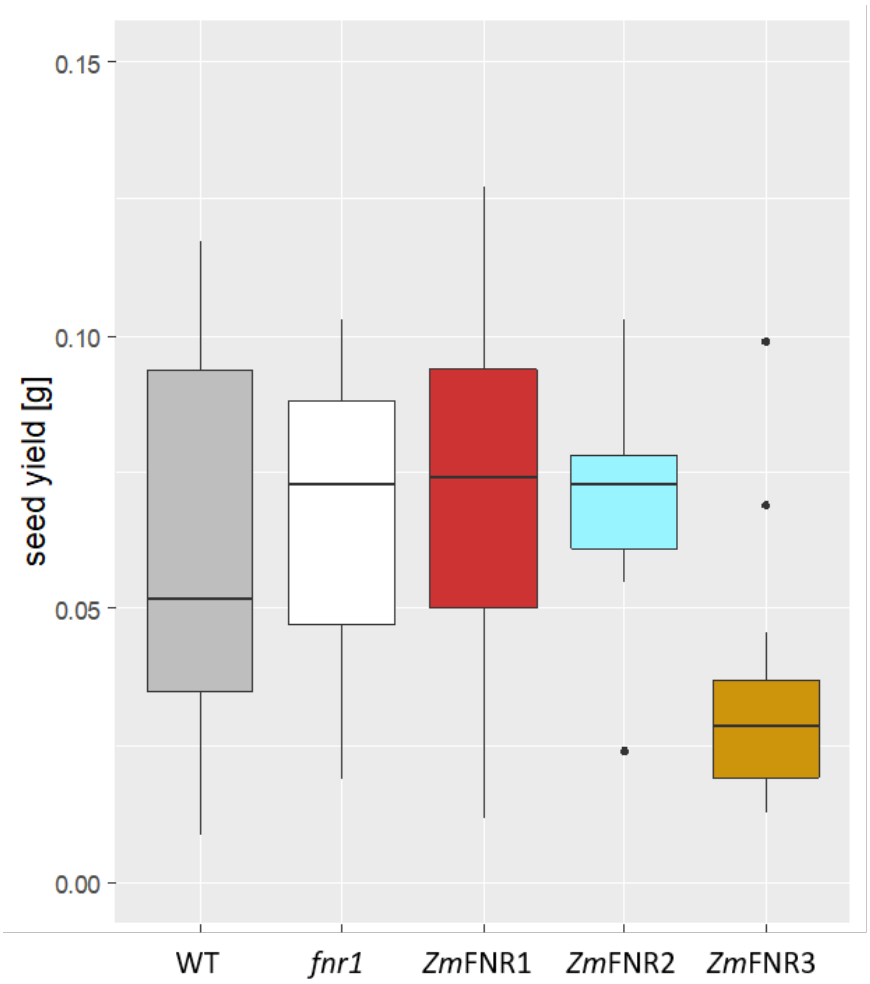

Figure 3.8: **Boxplot of the seed weight of Arabidopsis wild-type, *fnr1* and maize FNR expressor plants in fluctuating light conditions.** Nine to nineteen individuals were measured after 107 days of growth in 16 h a day, with 5 minutes cycles of 190 µE and 10 µE and then dried. The seeds were harvested and the seed weight per individual was measured. Statistical analysis is presented in table 3.5

Table 3.5: **Statistical analysis of the seed weight of Arabidopsis wild-type, *fnr1* and maize FNR expressor plants grown in fluctuating light conditions.** Descriptive statistics, analysis of variance (ANOVA) and Tukey post hoc test.

Descriptive statistics				Tukey post hoc p adj			
				fnr 1	*fnr1* ZmFNR1	*fnr1* ZmFNR2	*fnr1* ZmFNR3
	n	mean	sd				
fnr1	19	0.07	0.02				
fnr1 ZmFNR1	18	0.07	0.03	0.99			
fnr1 ZmFNR2	9	0.07	0.02	0.99	0.99		
fnr1 ZmFNR3	12	0.04	0.03	0.03	0.02	0.06	
WT	11	0.06	0.04	0.99	0.98	0.98	0.15
ANOVA							
	Df	SumSq	MeanSq	F-value	Pr(>F)		
genotype	4	0.011	0.00278	3.282	0.0165	*	
Residuals	64	0.054	0.00085				

cantly decreases in fluctuating light by more than half of the harvest in constant light. The ANOVA still reveals a statistically significant difference between genotypes ($F(4,64)=3.282$, $p=0.0165$), so a post hoc Tukey test was performed. The differences between the genotypes that could be observed in constant illumination disappear largely. The one exeption to this is in *fnr1* ZmFNR3 plants, where seed production is almost completely disrupted (statistically significant compared to *fnr1* with $p=0.03$ and *fnr1* ZmFNR1 with $p=0.02$ and showing a tendency aswell for *fnr1* ZmFNR2 with $p=0.06$ and wild-type with $p=0.15$). This effect is not observable in the *fnr1* mutants, in which FNR is also unable to bind to the thylakoid membrane. This might indicate that a disturbed seed production is not caused by missing membrane bound FNR, but rather too much soluble FNR. It remains elusive what causes this breakdown, because little is yet known about the function of *Zm*FNR3 yet.

4. FNR spatial distribution

Different isoforms of FNR are reported to be supposedly located either soluble in the stroma (Okutani et al. [2005]) or associated to the thylakoid network. As a 35 kDa protein cannot penetrate the 2 nm stromal gap in the grana stacks, the available membranes that FNR can bind to are either the border regions of the grana stacks or the protruding stromal lamellae. Of the FNR binding complexes, Jurić et al. [2009] report TROL to be located at the stroma lamellae - grana stack interface. The Cyt b_6f is universally distributed through the thylakoid network, although others have reported that under specific light conditions it also concentrates at the margin (Vallon et al. [1991]). According to Benz et al. [2009], Tic62 is found both soluble, evenly distributed on the lamellae and bound to the chloroplast inner envelope membrane where it is suggested to facilitate redox regulation of protein import involving FNR (Stengel et al. [2008]). For a more detailed discussion of the thylakoid protein composition, please see introduction, section 1.3.

Protein distribution between different regions of the thylakoids and especially lamellae is difficult to visualize using conventional light microscopy without the application of super-resolution techniques due to diffraction limits. In addition, the strong autofluorescence of the chlorophyll that accumulates in the disks of the

grana stacks covers a wide range of wavelengths (600 nm to 800 nm, García-Plazaola et al. [2015]), limiting the probes available for use in super-resolution microscopy, especially in the red range.

In this chapter of the thesis, I will present an imaging technique for FNR localization: transmission electron microscopy (TEM), semi-automatic area recognition and statistical analysis to localize FNR at the thylakoid membranes.

4.1 Electron microscopy method development

TEM generates images of a thin-section of the whole plant tissue. In many of the chloroplasts, the intricate system of thylakoid membranes is very well preserved and can be visualised by contrasting with uranyl acetate resulting in images where the lamellae can be clearly differentiated from the grana stacks. This is dependent on the quality of fixation and sectioning, but also the spatial orientation of the chloroplast within the section: only if the cut is vertical to the grana stacks a reasonable differentiability is obtained. Following imaging, only chloroplasts with clear internal membrane structures were selected for this analysis. A specific antibody against *Zm*FNR2 (which will recognize all 5 isoforms of FNR) as described in chapter 3.1, was used for immunogold staining (IGS). We have produced genotypes with isoforms of FNR bound to specific tethers (3.1) and those tethers have been localized in different compartments as previously discussed: *Zm*FNR1 predominantly binds to TROL which was found in the margin and lamellae regions (Jurić et al. [2009]), *Zm*FNR2 mainly binds to Tic62 (Benz et al. [2009]) that is located in either the lamellae, the inner envelope membrane or soluble and *Zm*FNR3 does not specifically bind to any membrane tether (Twachtmann et al. [2012]). Therefore, the subcompartments

of interest were predefined as 1) grana, 2) margins of grana and appressed membranes, 3) lamellae and 4) stroma. This study focusses specifically on FNR that is involved in electron flow at photosynthetically active membranes and staining of this compartment was negligible, so no initial analysis of the inner envelope was carried out.

TEM results in a two-dimensional nature of the sample: the labelled sections are only about 70 nm in thickness and on top of that the antibody does not penetrate the sample but only attaches to epitopes that are freely present at the surface. This leads to a relatively low labelling efficiency being visible on the final image, which requires careful statistical evaluation to draw conclusions about the location of proteins in specific subcompartments of interest. This requires calculation based on signal density per area on a sufficient number of images for a statistically relevant analysis.

The thylakoid membrane network is highly dynamic (Anderson et al. [2012]) and the grana diameter can change as an adaptation in response to light (Herbstová et al. [2012]). On top of this, it is not evident whether trapping FNR at a certain tether might have any downstream effects on the thylakoid architecture. Furthermore, the individual chloroplasts selected for analysis exhibit not only different sizes, but also variation in the fraction of stroma, depending on the section that is recorded. Based on this variety, it is important to quantify the area of each predefined subcompartment of interest per individual chloroplast and to determine the amount of respective label in these subcompartments.

Mayhew [2011] reviewed different methods to assign non-random distribution for signal density in organelles or on membranes: A raster or line probes respectively are randomly superimposed on the

image and the distribution of crossing points that can be assigned to the organelle or to membrane sections represent the expected proportions of these within the analysed subcompartments. These methods pose two inherent problems: firstly, a high accuracy of the estimation of proportions would require the use of a very fine raster/line probes with exponentially more crossing points to analyze and secondly, areas can only be compared to other areas and membranes can also only be compared to other membranes by this technique. Although initially considered, this renders the discussed methods useless for my approach to compare grana stacks, margin, lamellae and stroma. Moreover, the nature of IGS means that the distance between target protein and the gold label can increase to up to 30 nm (Hermann et al. [1996]) by adding up the size of the first and the second antibodies. Therefore, the IG signal of membrane tethered FNR might not appear exactly on the border of membrane/stroma, but more or less in the adjacent zone in any direction around the membrane and thus can be treated as a narrow area surrounding any membrane. Treating all subcompartments of interests as areas opens the question of how to measure each of these subcompartments on every single micrograph.

Automatic area recognition I initially considered the use of automated area recognition to define subcompartments. High-level contrast that could be achieved by osmium tetroxide treatment is not applicable for IG-labelling techniques because the high density of osmium tetroxide compromises the visibility of the small gold label. As an alternative, the sections were stained by uranyl acetate and so the membranes usually appear slightly paler than the grainy stromal background on a micrograph (see figure 4.1(A)). This contrast is still

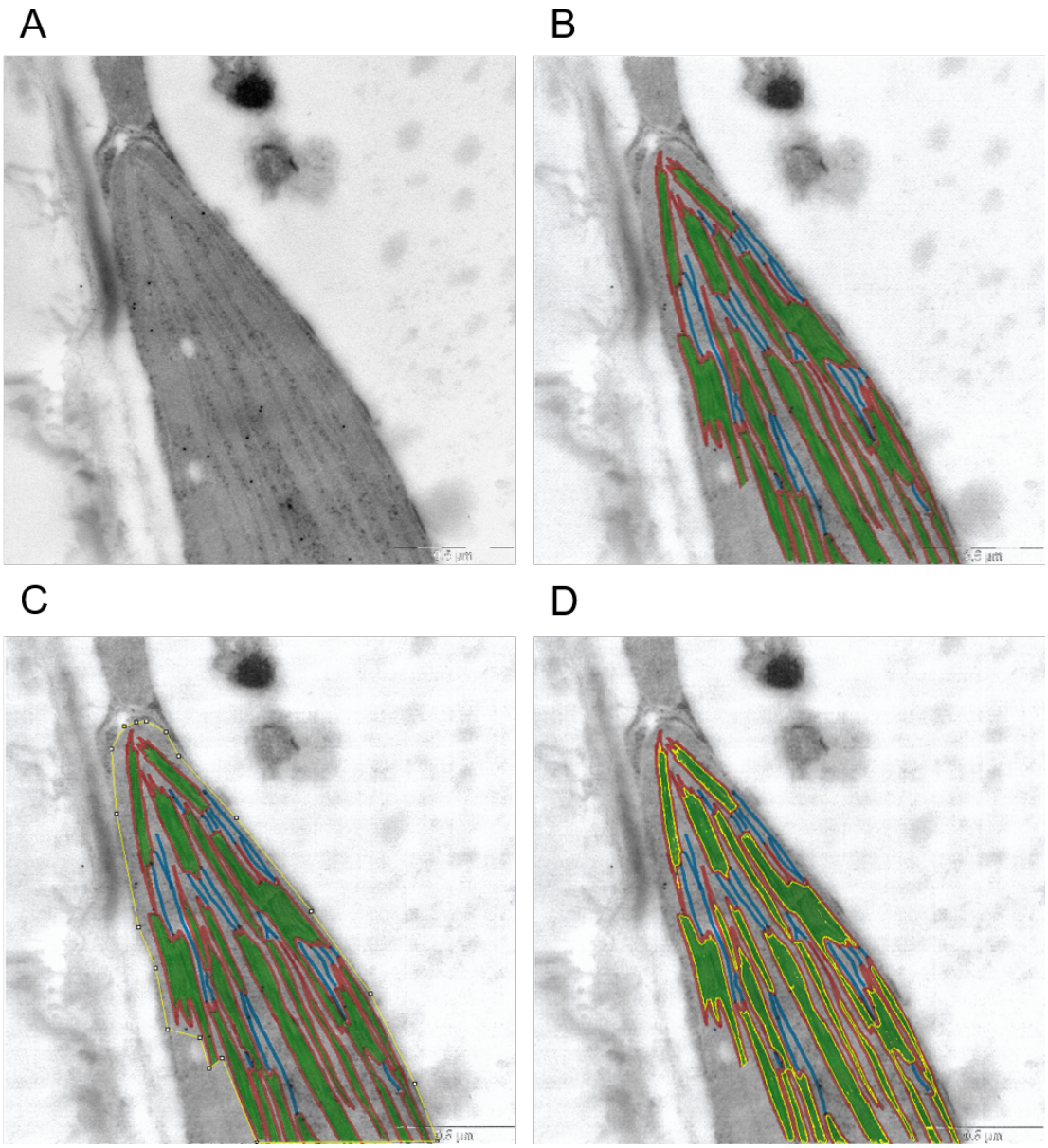

Figure 4.1: **Method of semi-automatic subcompartment definition and measurement of area on micrographs of Arabidopsis chloroplasts.** (A) Original micrograph of a thin-sectioned Arabidopsis chloroplast embedded in LR-White resin. The section was contrasted with 4 % uranyl-acetate and FNR was IG-labelled with gold beads of 10 nm diameter (1^{st} and 2^{nd} antibody concentration 1:200). (B) The areas of interest were coloured in by hand: green = grana, red = margins of grana or other appressed membranes, blue = lamellae. (C) Selection of total analyzed area in ImageJ. (D) Automatic area selection by colour recognition in ImageJ.

rather low compared to the various artefacts that can be expected. The TEM-camera that was installed with the microscope used in this study employs automatic contrasting, which sometimes makes it possible to increase the contrast by shifting the electron beam slightly away from the sample. This trick improves the visibility of the membranes by increasing the contrast, but creates micrographs with irregular illumination. Both of these problems make an automated area recognition increasingly difficult. There are a few analysis programs available that are designed for histological analysis of tissues like the freeware QuPath (Bankhead et al. [2017]) or the Fiji plug-in "Trainable Weka Segmentation", but none of them delivered desirable results. Even if the membranes were automatically selectable, two problems would still remain: how to distinguish grana stacks from the lamellae and how to accurately frame the grana stacks and define the resulting area as margin. Although theoretically this could be solvable by machine-learning and computer vision algorithms, a dataset functioning as sample input in which these subcompartments can be recognized by predefined parameters would need to be generated first. Depending on how accurate the result needs to be and how difficult the initial automated pattern recognition is, these sample inputs still require large numbers. Consequently, I abandoned the approach of a fully automated area recognition.

Semi-automatic area recognition ImageJ and many other image processing tools provide a function to select pixels by their colour/shade. The overall pale appearance of the micrographs make it ideal to manually add colour on a printout that can then be re-scanned (see figure 4.1 (B)) and selected by the magic wand tool in ImageJ. The width of the colouring stroke was set to approximately twice the size of the

gold particle which equals 20 nm, but is still a conservative estimate because of the previously discussed distance of the label from the actual epitome. The scale bar in each image provides the program with spacial information so the overall area of the total sum of selected pixels can be calculated by the program. Hence, in order to calculate the area of the stroma, I subtracted the individually measured areas of grana, margin and lamellae from the overall analyzed area. Occasionally, it was not possible to accurately distinguish the membranes from the background in the whole chloroplast, so instead of measuring the whole chloroplast area, I manually selected the total area analyzed (see figure 4.1 (C)). This also gave me the opportunity to exclude larger artifacts from the analysis. An example of the subcompartment selection in ImageJ by colour is presented in 4.1 (D) for the grana stacks in green.

I initially tested one individual of the wild-type Arabidopsis to verify if this general proceedure would give feasible results: in other words, a non-random distribution in at least one of the compartments. A good internal control is first of all the cytosol, where there should be no FNR detectable and any signal from this compartment can be regarded as unspecific labelling. Furthermore, we know that FNR cannot penetrate into the grana stacks as described above and this provides a second control to test the sensitivity of the subcompartment selection method.

For this trial, the subcompartments of grana margin and lamellae were combined to simplify the protocol (red and blue respectively in figure 4.1 (B) to (D)). Figure 4.2 shows boxplots of the absolute signal density of defined subcompartments in label per μm^2 for 22 chloroplasts. An ANOVA was performed and the results are presented in table 4.1, showing a statistically highly significant dif-

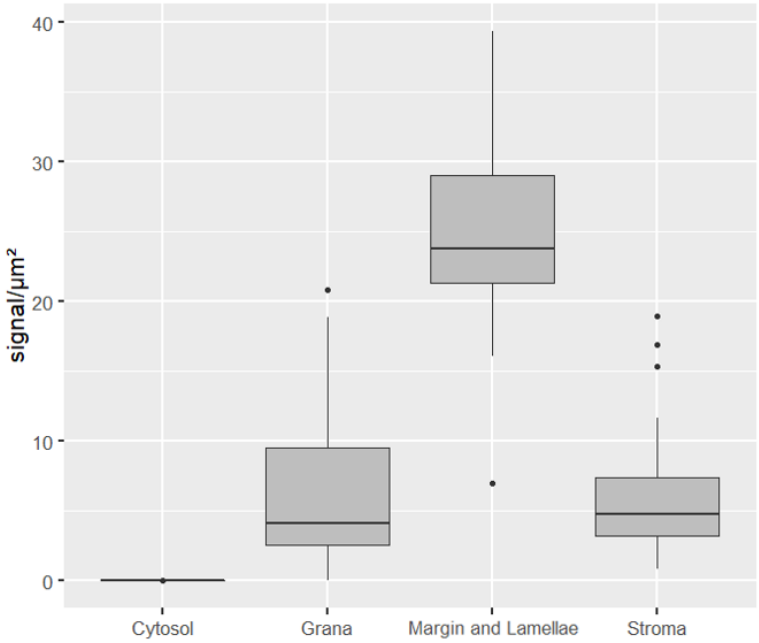

Figure 4.2: **Boxplot of IG-labelled FNR signal density in subcompartments of Arabidopsis wild-type plants.** One dark-incubated leaf of a wild-type A.thaliana plant was embedded in LR-White resin and thin-sectioned, followed by IG-labelling against FNR (1^{st} and 2^{nd} antibody concentration 1:200). The specified areas were measured and the gold-label counted for 22 chloroplasts in total. Statistical analysis is presented in table 4.1.

ference in the FNR signal density of the different subcompartments ($F(3,84)=84.36$, $p=2 \times 10^{-16}$) and a post hoc Tukey test revealed that only the areas of stroma and grana show no difference ($p=0.999$). In the cytosol there is no signal detectable with the exception of a few outliers, indicating a negligible low background signal of unspecific antibody binding. Remarkably, the medians of grana and also stroma range close to 5 signals per µm^2, while the median of margin and lamellae signal lies significantly higher at 24 signals per µm^2. We know for a fact that any signal from the grana must be an artefact resulting from the analysis. Colouring the subcompartments manually will possibly introduce inaccuracies by misinterpretation of the membrane structures or slight changes in stroke width. In the execution of this method it was necessary to be strictly consistent, so this might be the reason for a set amount of false-positive counts in the grana. There was rarely any label right in the middle of a grana stack so the gold particles counted for this subcompartment were usually located more ambiguously in the outer rims and could have possibly been mis-assigned from the margin due to the stringent assignment of a 20 nm limit defined around membranes. The non-existent background noise from the cytosol supports this argument because it has no direct contact surface to a subcompartment where we would expect FNR. There was no label found at the inner envelope in this experiment indicating that it is highly unlikely for a significant fraction of FNR to bind to that part of Tic62 that is found in the inner envelope membrane. The labelling density in the stroma of the 22 chloroplasts shows no difference to that of the grana. If we assume that the same inaccuracies of the analysis method that apply for the grana also apply for the stroma, it can safely be said that no significant fraction of FNR is located

in the stroma of the wild-type chloroplasts. It is instead always associated to the membranes of the thylakoid that are adjacent to the stroma (margin and lamellae) with a five times higher labelling density. This finding contradicts earlier studies on FNR-GAPDH co-localization in the chloroplast (Negi et al. [2008]). In this paper however, the overall label density was higher due to over-night antibody incubation times in contrast to the 30 min incubation times in this experiment, potentially leading to higher unspecific binding. Furthermore, no appropriate controls for background noise are presented which suggests that a misinterpretation of the data by Negi et al. [2008] is possible. An exclusively membrane bound location of FNR also does not reflect the current dogma that FNR exists in soluble and membrane bound pools, and does not match any of the findings from biochemical methods presented earlier. A reason for this might be the disruptive sample treatment used in biomechanical separation of "soluble" and "membrane bound" proteins, that will - no matter how gentle - break weak attachments between FNR and the membrane and therefore might lead to false assignment of FNR as soluble.

This set of chloroplasts was then used to determine a guideline for the appropriate number of samples for the following studies to ensure optimal numbers for a sufficiently high statistical power in turn for the time invested.

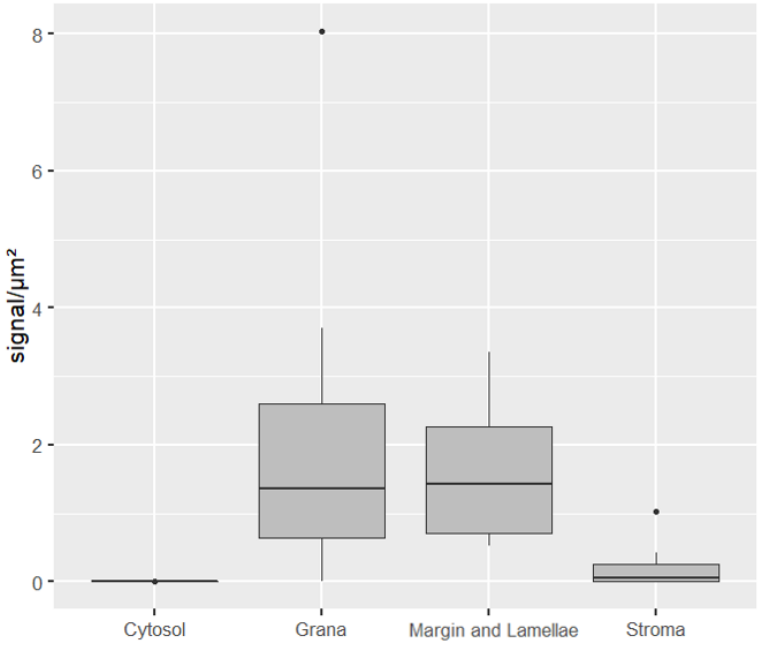

Figure 4.3: **Boxplot of IG-labelled Cyt *f* signal density in subcompartments of Arabidopsis wild-type plants.** One dark-incubated leaf of a wild-type A.thaliana plant was embedded in LR-White resin and thin-sectioned, followed by IG-labelling against Cyt *f* (1^{st} antibody concentration 1:100, 2^{nd} antibody concentration 1:200). The specified areas were measured and the gold-label counted for 14 chloroplasts in total. Statistical analysis is presented in table 4.1.

Table 4.1: **Statistical analysis of signal densities of FNR and Cyt *f* in subcompartments (s.comp) of Arabidopsis wild-type plants to confirm the validity of this method on two different proteins.** Analysis of variance (ANOVA) between the genotypes and Tukey post hoc test. m/l = margin/lamellae. According boxplots of the analysed dataset are presented in figures 4.2 (for FNR) and 4.3 (for Cyt *f*).

ANOVA						
	Df	SumSq	MeanSq	F-value	Pr(>F)	
FNR						
s.comp	3	7695	2565.1	84.36	2×10^{-16}	***
Residuals	84	2554	30.4			
Cyt *f*						
s.comp	3	38.63	12.878	9.674	3.54×10^{-05}	***
Residuals	52	69.22	1.331			

Tukey post hoc p adj			
	cytosol	grana	m/l
FNR			
grana	0.001		
m/l	0	0	
stroma	0.001	0.999	0
Cyt *f*			
grana	0.001		
m/l	0.004	0.830	
stroma	0.975	0.001	0.015

As an additional control, I chose to label a protein exclusively located in the thylakoid membranes where a specific antibody was available and previous studies have shown a dual location of the protein as well, but this time an equal distribution throughout the whole thylakoid network of grana stacks, margin regions and lamellae (presented by Allred and Staehelin [1986]). A sample of the same wild-type plant was thin-sectioned and immunostained for Cyt *f* with the same nanogold-conjugated secondary antibody as before. The calculated signal densities for this are presented in fig-

ure 4.3 and the respective statistical analysis is presented in figure 4.1. An ANOVA which again showed a statistically highly significant difference in signal density between the different subcompartments ($F(3,52)=6.543$, p=3.54 x 10^{-05}) and a post hoc Tukey test revealed that margin/lamellae and grana signal density shows no difference (p=0.830). Although the densities are overall lower than for FNR which is probably on account of the antibody used, we see little to no label in the stroma area and equal density of gold particles (around 1.5 signals per µm^2 in both grana stacks and margin/lamellae regions. This is in line with the results of the Cyt b_6f immunogold-labelling experiment by Allred and Staehelin [1986] and is another confirmation that this study design delivers accurate results even with a low overall labelling density.

4.2 FNR location in the wild-type and *fnr1* mutant

The preliminary study gave a promising result, but still only accounts for just one individual, so I repeated the experiment with three biological replicates. Four exemplary micrographs of wild-type Arabidopsis with immunogold labelled FNR are presented in figure 4.4. As the exclusive membrane location of FNR in wild-type Arabidopsis was an unexpected result, I also analysed a plant where all FNR is reported to be soluble. With the *fnr1* knock out plants, we have a genotype available where all of the remaining AtFNR2 should be soluble according to biochemical analysis (Lintala et al. [2009], Lintala et al. [2007] and Hanke et al. [2008]). Four example micrographs of *fnr1* leaf sections with immunogold labelled FNR are presented in figure 4.5. An analysis of variance (ANOVA) was performed on each genotype to check if there is a statistically significant difference within individuals (results depicted in table 4.2). This

analysis revealed a big statistically significant effect of the subcompartment ($N(3,122)=12.025$, p=5.97 x 10^{-07} for the wild-type and $N(3,186)=13.035$, p= 9.16 x 10^{-08} for the *fnr1* mutant), but no effect of individuals within the group of each genotype indicating that the number of individuals (3) was adequate to deliver statistically relevant results.

Table 4.2: **Statistical analysis of signal densities of FNR in three individuals of wild type and *fnr1* plants to confirm adequate sample size.** Analysis of variance (ANOVA) on the signal densities in each subcompartment (s.comp) on a group of three individuals per genotype.

ANOVA						
	Df	SumSq	MeanSq	F-value	Pr(>F)	
wild-type						
s.comp	3	1205	401.6	12.025	5.97 x 10^{-07}	**
individual	2	144	71.8	2.149	0.121	
s.comp:individual	6	13	2.2	0.066	0.999	
Residuals	122	4074	33.4			
fnr1						
s.comp	3	422.9	140.96	13.035	9.16 x 10^{-08}	**
individual	2	5.5	2.77	0.256	0.774	
s.comp:individual	5	78.8	15.77	1.458	0.206	
Residuals	186	2011.4	10.81			

Having confirmed this, I proceeded to compare both genotypes with each other, which is presented in figure 4.6 and the statistical analysis depicted in table 4.3, which shows a statistically significant difference of signal densities between the subcompartments ($F(2,243)=118.787$, p=2 x 10^{-16}). The post hoc Tukey test shows a p-value of 0 for any combination with margin/lamellae areas, but no statistically significant difference between stroma and grana (p=0.993). The ANOVA showed no difference between the genotypes. This indicates that even though there is less FNR in total, the distribution across the areas does not change. Though there is visibly less FNR present in the combined margin and lamellae region there still sig-

nificantly more than in the grana or the stroma. Again, this result is surprising because the knock-out of *At*FNR1 which supposedly represents the membrane bound fraction and facilitates membrane binding of *At*FNR2 via dimer formation does not lead to a solubilization of the remaining *At*FNR2, which is still located at the membrane. This implies that *At*FNR2 must have its own mechanism for membrane binding either to a tether that is yet unknown or direct interactions to one of the protein complexes in the thylakoid membrane. It also raises the question, whether the formation of a dimer as discussed earlier in chapter 3.1 is at all required for membrane binding. However, we do not know whether the *At*FNR2 signal from the thylakoid margins and lamellae in *fnr1* mutant plants results from monomers or dimers, therefore this question cannot be fully addressed at this stage.

Table 4.3: **Statistical analysis of signal densities of FNR in subcompartments of wild-type and *fnr1* plants to compare signal distribution between the two genotypes.** Analysis of variance (ANOVA) on the signal densities of each subcompartment (s.comp) in three individuals per genotype. Tukey post hoc test shows only the results for the comparison of corresponding areas in each genotype. m/l = margin/lamellae. A corresponding boxplot on the analysed dataset is presented in figure 4.6.

ANOVA						
	Df	SumSq	MeanSq	F-value	Pr(>F)	
s.comp	2	3710	1855.0	118.787	2×10^{-16}	***
genotype	1	12	11.5	0.738	0.3911	
individual	4	892	223.1	14.284	1.74×10^{-10}	***
s.comp:genotype	2	136	68.2	4.367	0.0137	*
s.comp:individual	8	723	90.4	5.786	9.24×10^{-07}	***
Residuals	243	3795	15.6			

Tukey post hoc p adj		
s.comp	m/l	stroma
grana	0	0.9928023
m/l		0

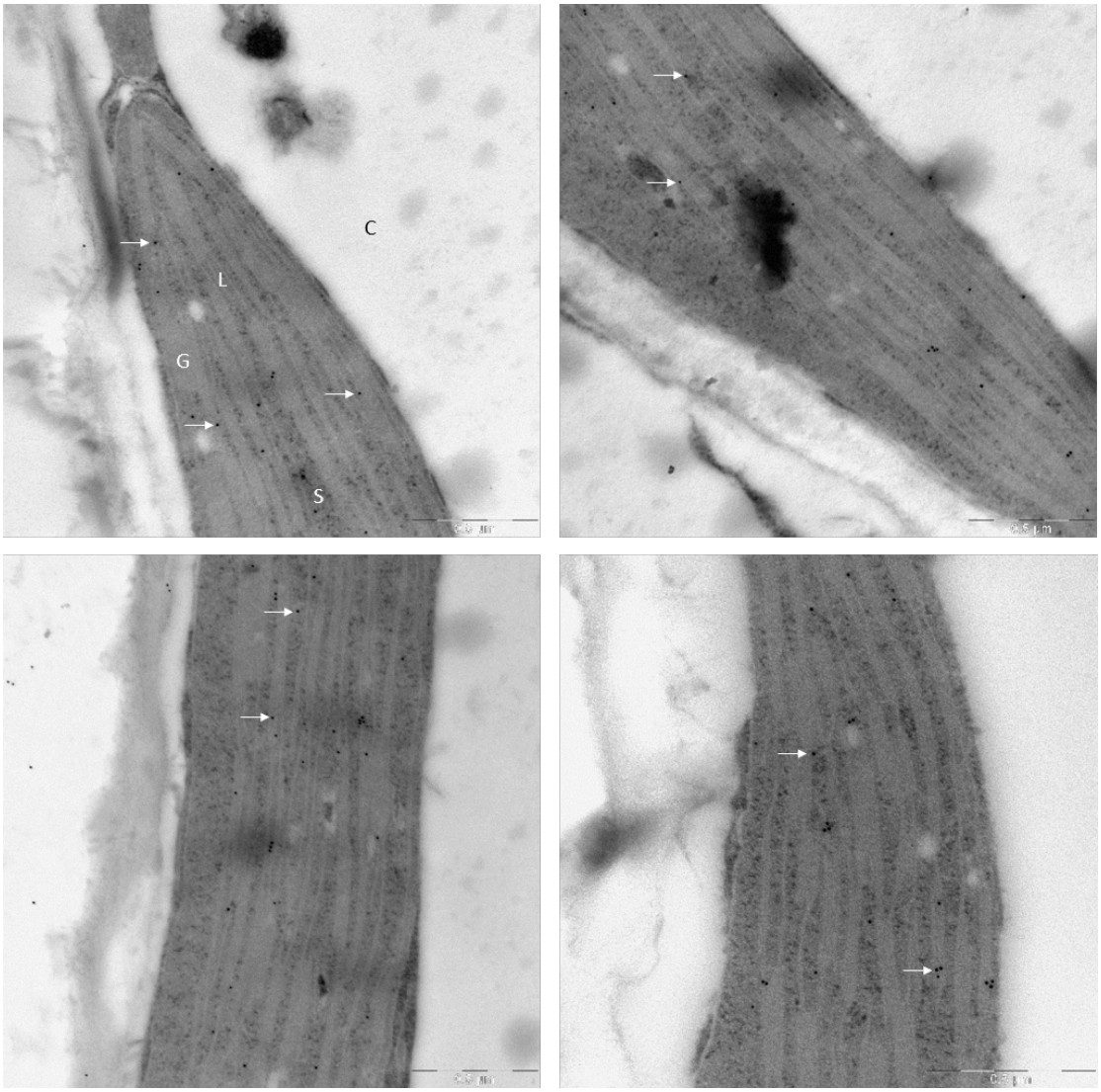

Figure 4.4: **Micrographs of wild-type Arabidopsis chloroplasts with IG-labelled FNR.** Dark-incubated leaves of *A.thaliana* wild-type plants were embedded in LR-White resin and thin-sectioned, followed by IG-labelling against FNR (1st and 2nd antibody concentration 1:200) and visualisation by transmission electron microscopy. G = grana; S = stroma; L = lamellae; C = cytosol. The white arrows highlight gold particles.

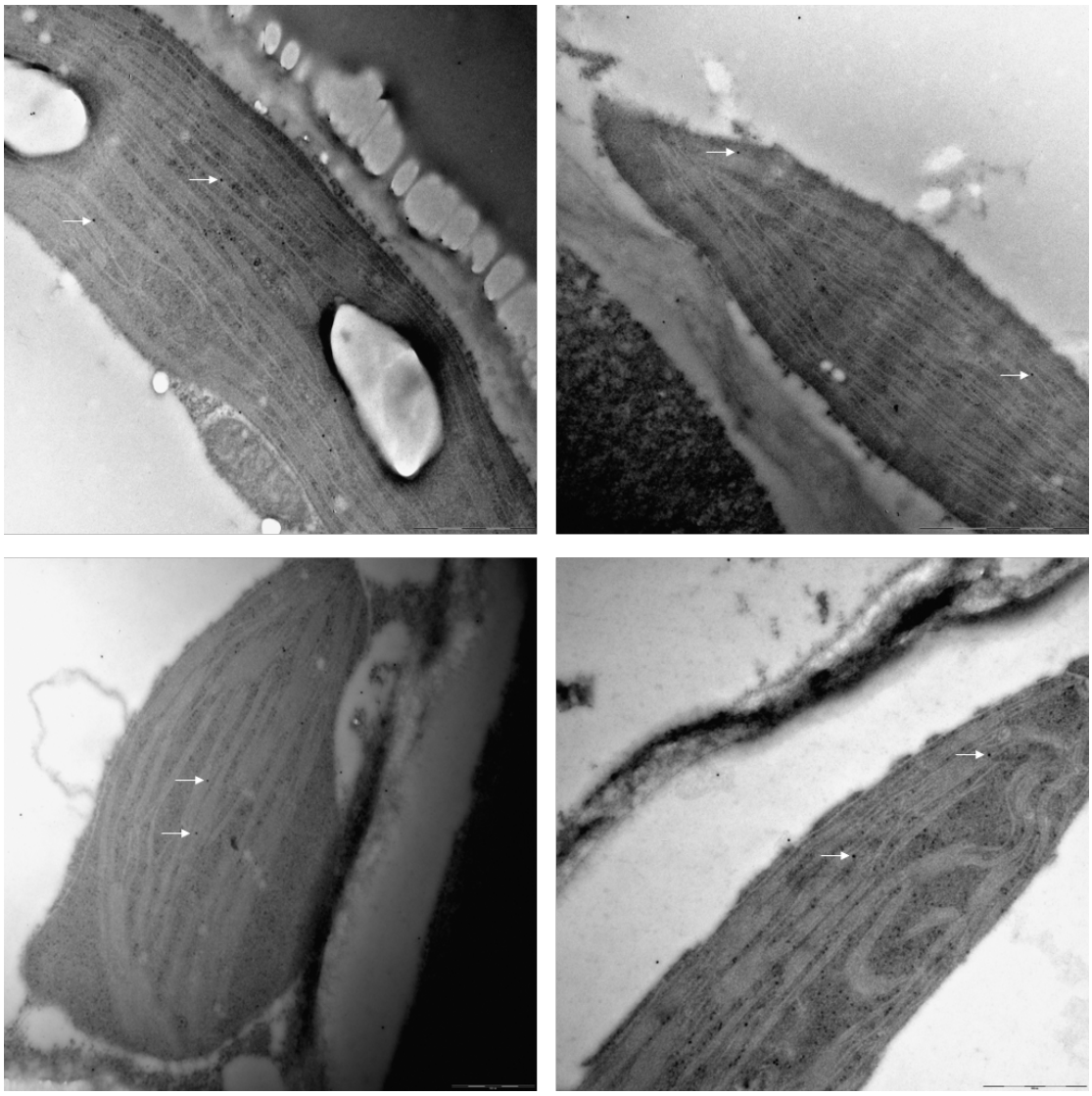

Figure 4.5: **Micrographs of *fnr1* Arabidopsis chloroplasts with IG-labelled FNR.** Dark-incubated leaves of *A.thaliana fnr1* mutant plants were embedded in LR-White resin and thin-sectioned, followed by IG-labelling against FNR (1st and 2nd antibody concentration 1:200) and visualisation by transmission electron microscopy. The white arrows highlight gold particles.

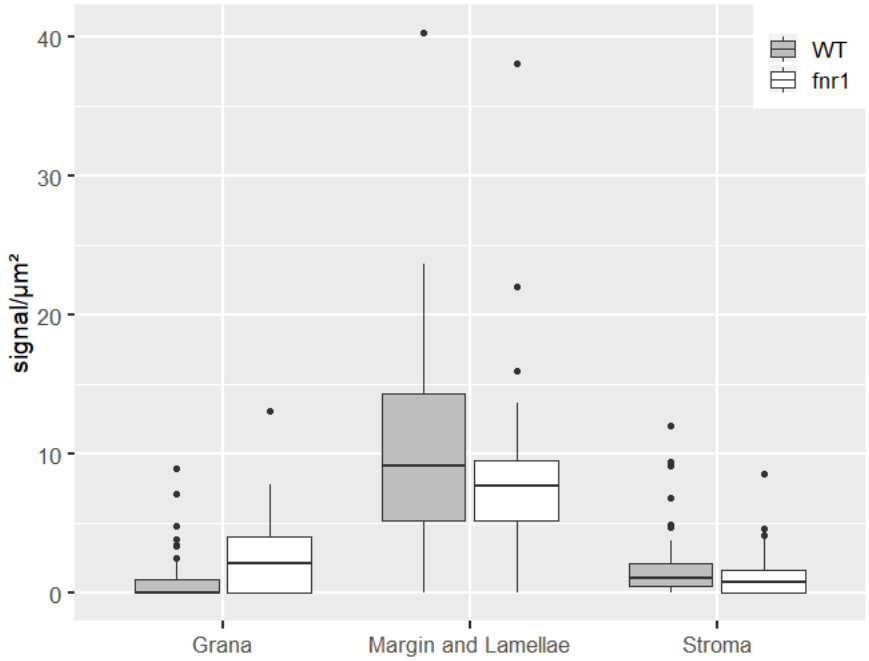

Figure 4.6: **Comparative boxplot of IG-labelled FNR signal density in subcompartments of Arabidopsis wild-type and *fnr1* plants.** Dark-incubated leaves of WT and *fnr1 A.thaliana* plants were embedded in LR-White resin and thin-sectioned, followed by IG-labelling against FNR (1^{st} and 2^{nd} antibody concentration 1:200) and visualisation by transmission electron microscopy. At least 14 chloroplasts in three different individuals per genotype were analysed. The specified areas were defined and the gold-label density calculated. Presented is the signal density per μm^2. Statistical analysis is presented in table 4.3.

5. Compartmentalization of FNR to different thylakoid domains

5.1 Area distribution

Table 5.1: **Statistical analysis of signal densities in three individuals of each genotype of the maize FNR expressor plants to confirm adequate sample size.** Analysis of variance (ANOVA) on the signal densities in each subcompartment (s.comp) on a group of three individuals per genotype.

ANOVA						
	Df	SumSq	MeanSq	F-value	Pr(>F)	
fnr1 ZmFNR1						
s.comp	3	1116	372.2	16.544	1.47 x 10^{-09}	***
individual	2	71	35.6	1.581	0.209	
s.comp:individual	6	145	24.2	1.077	0.378	
Residuals	184	4139	22.5			
fnr1 ZmFNR2						
s.comp	3	1587	529.1	13.942	3.26 x 10^{-08}	***
individual	2	48	24.0	0.633	0.532	
s.comp:individual	6	102	16.9	0.446	0.847	
Residuals	180	6832	38.0			
fnr1 ZmFNR3						
s.comp	3	2434	811.3	21.614	6.58 x 10^{-12}	***
individual	2	95	47.5	1.266	0.285	
s.comp:individual	6	127	21.2	0.564	0.759	
Residuals	170	6381	37.5			

After successfully establishing a method to deliver statistically relevant and repeatable results, I extended the experiment to the maize

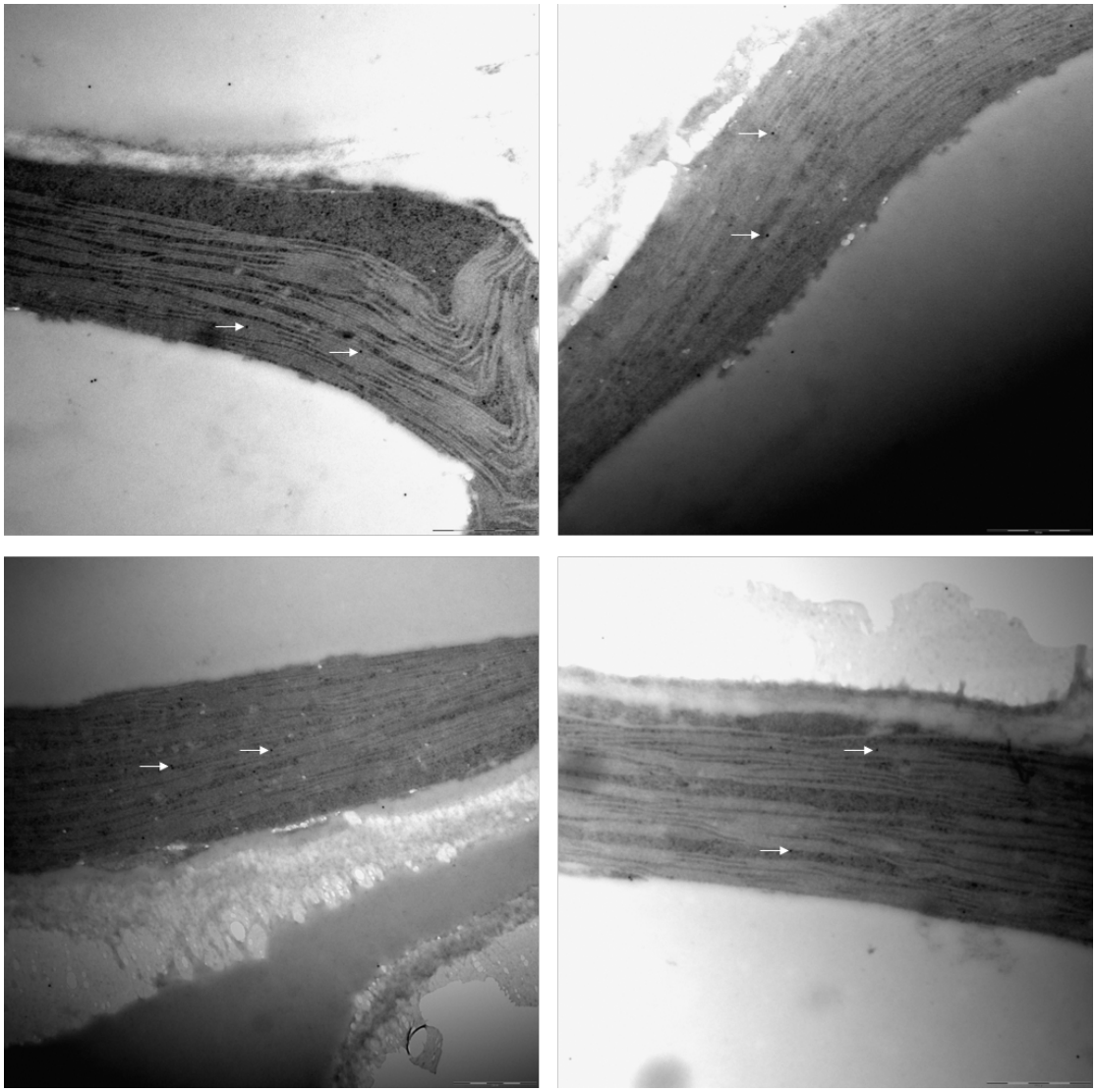

Figure 5.1: **Micrographs of *fnr1*ZmFNR1 Arabidopsis chloroplasts with IG-labelled FNR.** Dark-incubated leaves of *A.thaliana fnr1*ZmFNR1 plants were embedded in LR-White resin and thin-sectioned, followed by IG-labelling against FNR (1st and 2nd antibody concentration 1:200) and visualisation by transmission electron microscopy. The white arrows highlight gold particles.

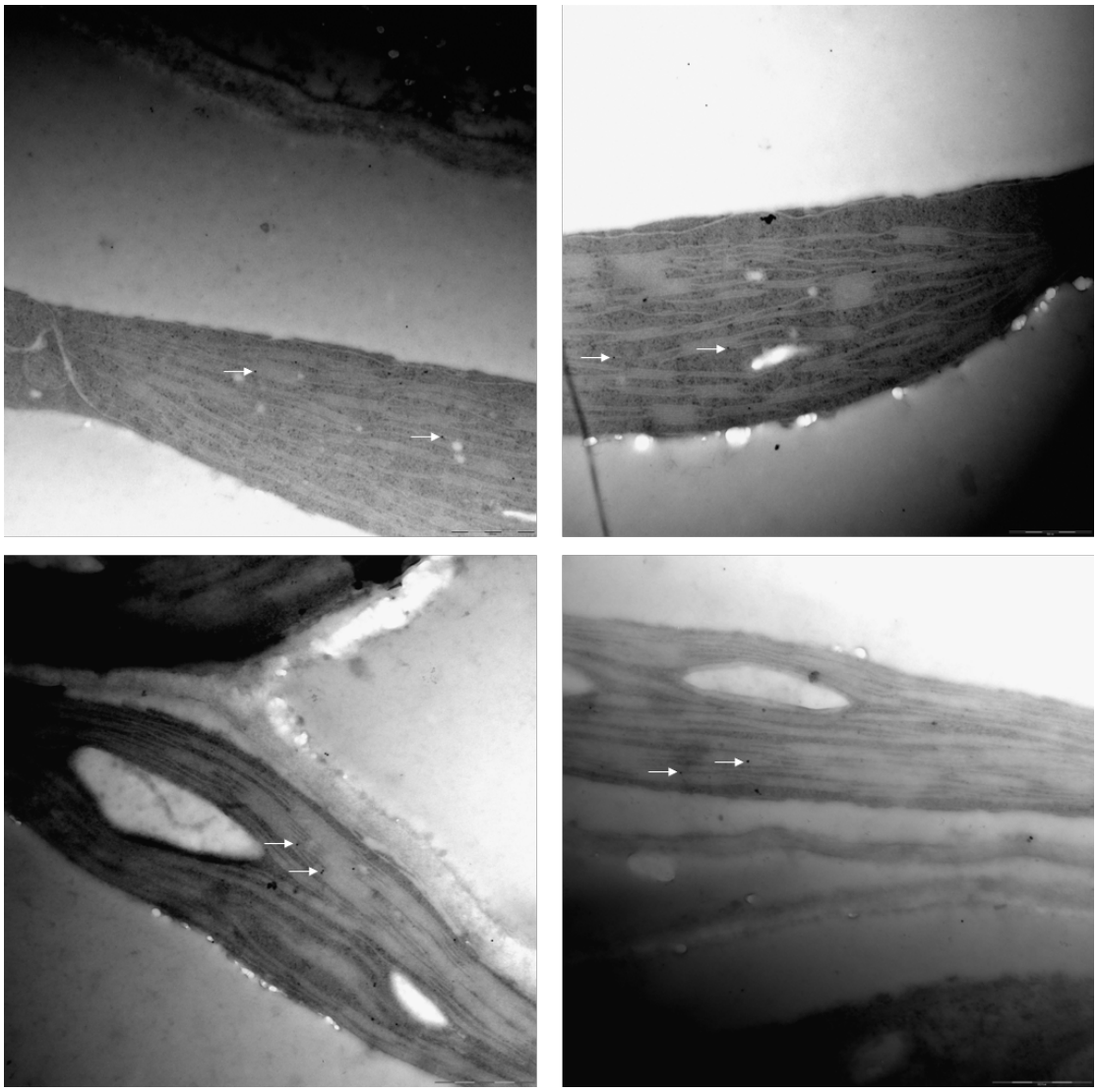

Figure 5.2: **Micrographs of *fnr1*ZmFNR2 Arabidopsis chloroplasts with IG-labelled FNR.** Dark-incubated leaves of *A.thaliana fnr1*ZmFNR2 plants were embedded in LR-White resin and thin-sectioned, followed by IG-labelling against FNR (1st and 2nd antibody concentration 1:200) and visualisation by transmission electron microscopy. The white arrows highlight gold particles.

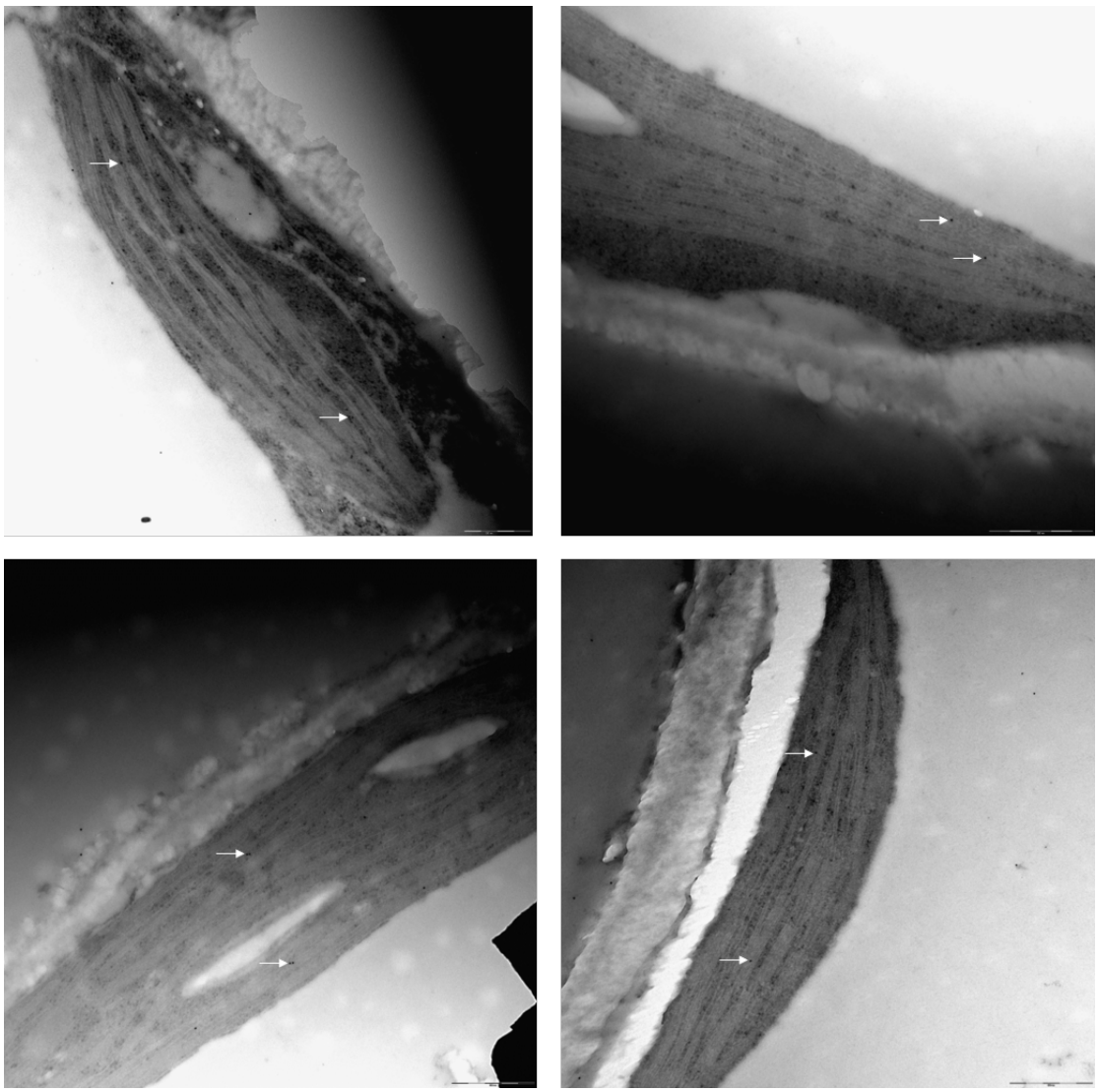

Figure 5.3: **Micrographs of *fnr1*ZmFNR3 Arabidopsis chloroplasts with IG-labelled FNR.** Dark-incubated leaves of *A.thaliana* plants *fnr1*ZmFNR3 were embedded in LR-White resin and thin-sectioned, followed by IG-labelling against FNR (1^{st} and 2^{nd} antibody concentration 1:200) and visualisation by transmission electron microscopy. The white arrows highlight gold particles.

FNR expressor plants in the *fnr1* mutant background described in chapter I 3. The aim of this experiment was to detect any differences in FNR location at the thylakoid membrane that might be due to variation in tether binding behaviour. Four exemplary micrographs of *fnr1*ZmFNR1 are presented in figure 5.1, of *fnr1*ZmFNR2 in figure 5.2 and figure 5.3 shows examples of *fnr1*ZmFNR3. Before comparing genotypes, I aimed to establish whether there was statistically significant difference between the individuals of each genotype, to test whether the three individuals that were measured represent an adequate sample size. The results of the analysis of variance are depicted in table 5.1 and show that there is no internal variation within the genotypes and the three individuals per genotype are sufficient for statistical rigour: all three genotypes show a strong effect of subcompartment (*fnr1*ZmFNR1: $F(3,184)=16.544$, $p=1.47 \times 10^{-09}$, *fnr1*ZmFNR2: $F(3,180)=13.942$, $p=3.26 \times 10^{-08}$, *fnr1*ZmFNR3: $F(3,170)=21.614$, $p=6.58 \times 10^{-12}$), but no statistically significant effect of the individual.

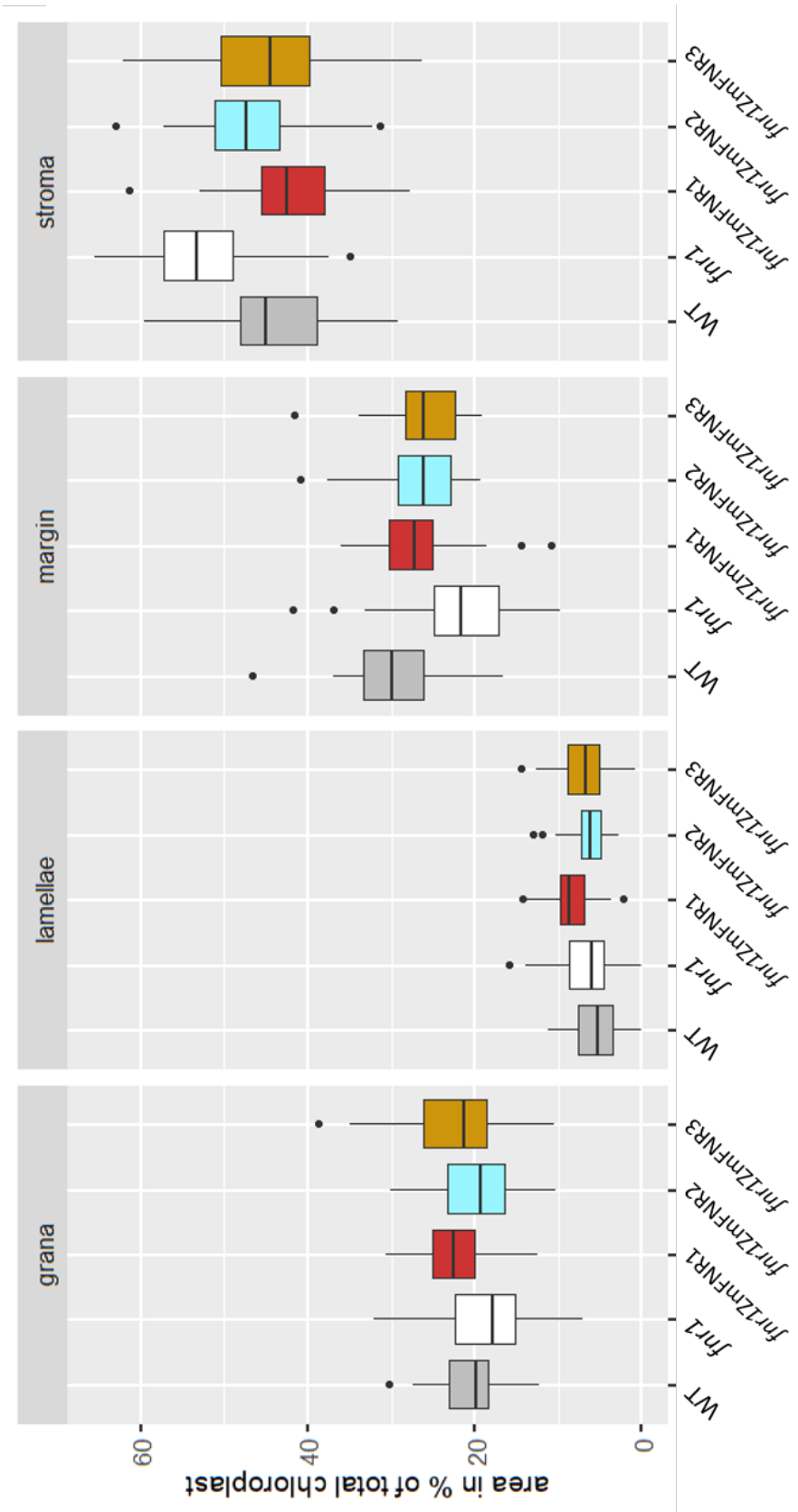

Figure 5.4: **Comparative boxplot of total area coverage in percent per subcompartment for the wild type, *fnr1* mutant plant and maize FNR expressors.** Around 15 chloroplasts in three different individuals per genotype were analyzed. The specified areas were measured and presented as a percentage of the total chloroplast area. Statistical analysis is presented in table 5.2.

Table 5.2: **Statistical analysis of the relative area size of the subcompartments (s.comp) in percent in wild-type, *fnr1* mutant and maize FNR expressor chloroplasts.** Above: Analysis of variance (ANOVA) on relative area size of each subcompartment in three individuals per genotype. Below: Tukey post hoc test for the combination area and genotype, where only values lower than the significance level of 0.05 are depicted. A corresponding boxplot on the analysed dataset is presented in figure 5.4.

ANOVA						
	Df	SumSq	MeanSq	F-value	Pr(>F)	
s.comp	3	190210	63403	2653.03	2 x 10^{-16}	***
genotype	4	0	0	0.00	1	
individual	10	0	0	0.00	1	
s.comp:genot.	12	5875	490	20.49	2 x 10^{-16}	***
s.comp:individ.	30	4553	152	6.35	2 x 10^{-16}	***
Residuals	920	21987	24			

Tukey post hoc p adj area:genotype		
	fnr1	*fnr1* ZmFNR1
margin		
WT	0	
fnr1 ZmFNR1	3 x 10^{-07}	
fnr1 ZmFNR3	0.00235	
stroma		
WT	0	
fnr1 ZmFNR1	0	
fnr1 ZmFNR2	1.1 x 10^{-06}	1.6 x 10^{-05}
fnr1 ZmFNR3	0	

As described at the beginning of chapter 4, there is a functional differentiation of the non-grana thylakoid membrane domains: the margin region, where LET takes place and lamellae for CET. Therefore the signal densities for these domains were treated as separate subcompartments in the following. There is a possibility that knock-out of FNR might have some downstream effect on the stacking of membranes and also relative amounts of different membrane do-

mains. If the coverage of the defined areas changes, but not the amount of FNR tethers and if they are restricted to particular membrane domains, this might lead to an increased or decreased density of tethers in this subcompartment which could be reflected in the overall signal density. To test this, I plotted the estimated percentage of the chloroplast area that is covered by each subcompartment in the hope of revealing any drastic differences between the genotypes in figure 5.4. The corresponding analysis of variance is depicted in 5.2 and shows a strong effect of the subcompartment ($F(3,920)=2653.03$, $p=2 \times 10^{-16}$), meaning that the defined domains within the chloroplast differ from each other, but no statistically significant changes in percentage of covered area when genotypes or individuals are compared. As expected, the total lamellae area is the smallest with medians below 10 % coverage. Remarkably, grana and margin cover a very similar percentage of the chloroplast (20% and 25%, respectively). In contrast, almost half of the measured area is assigned to the stroma. Only the *fnr1* mutant plants show a small shift in area coverage with a slightly higher area of stroma and a decreased margin area. This is reflected in the result of a post hoc Tukey test on s.comp:genotype. Compared to all other genotypes a statistically significant increase of *fnr1* stroma percentage was measured ($p<1.6 \times 10^{-05}$). Accordingly, the margin area of *fnr1* plants was statistically significantly decreased compared to all genotypes but *fnr1*ZmFNR2 ($p<0.00235$). Therefore this result might suggest a decrease in total thylakoids in comparison to the stroma in *fnr1* mutants which is in line with the findings of Lintala et al. [2007] that *fnr1* plants show a slightly paler phenotype and a lower chlorophyll content. The test also showed a statistically significant difference in stromal area between *fnr1*ZmFNR1 and *fnr1*ZmFNR2

plants, but not for any other subcompartment. The total coverage area of the subcompartments are not dramatically different when comparing all genotypes, with only slight aberrations for the *fnr1* mutant plants. This suggests, that the overall tether density should not change dramatically between the different thylakoid domains. Therefore, any large changes in FNR staining density are unlikely to be caused by variation in membrane subcompartment area coverage between genotypes but rather as a result of binding behaviour of the respective FNR isoform.

5.2 FNR distribution at the thylakoid membrane

To answer the question of whether the distribution of different FNR-tether associations varies in the thylakoid domains the signal densities that were measured for each micrograph were plotted as in the experiments before (figure 5.5). The corresponding statistical analysis is shown in table 5.3 and reveals that there is a statistically significant effect of subcompartment and genotype (for area: $F(3,844)=67.116$, $p=2 \times 10^{-16}$ and for genotype: $F(4,844)=4.990$, $p=0.000559$), meaning that distribution of FNR between thylakoid domains varies between genotypes. In all genotypes, there is a tendency for low signal density in the grana and stroma and higher signal density in the margin and lamellae. The Tukey post hoc test in table 5.3 on subcompartments shows that in fact all subcompartments differ statistically significantly ($p < 0.005$) apart from stroma and grana where there is no difference detectable ($p=0.9463$). The same test was run to compare different genotype pairs. All maize FNR expressors and the wild-type show a statistically significant difference to the *fnr1* mutant plants ($p < 0.034$). This is likely an effect of the mutant having considerably less FNR at the lamellae

fraction of the thylakoids when compared to all other genotypes.

Every boxplot presented so far represents values for at least fifteen individual measurements for each subcompartment. This grants a high statistical power, but due to the low labelling intensity there is an important downside: The smaller the measured subcompartment, the higher the likelihood that no signal can be detected. This means, that there are cumulatively more measurements of zero signals per μm^2 in the lamellae, which distorts the graph and also the statistical analysis. This effect is most pronounced in the lamellae, but applies to all other subcompartments as well. This leads to a high variance of values for each boxplot and makes a meaningful interpretation of subtle changes in distribution very difficult.

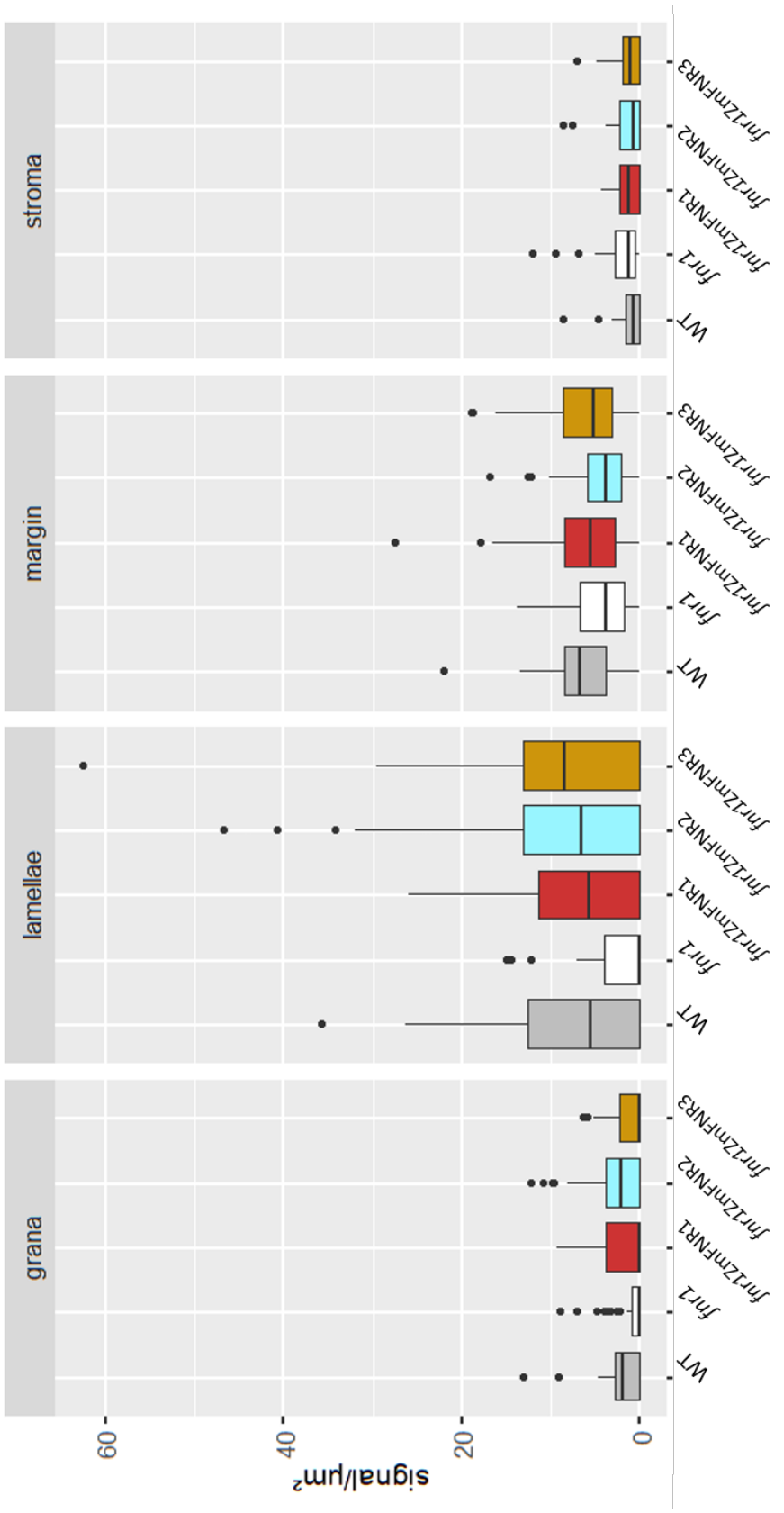

Figure 5.5: **Comparative boxplot of IG-labelled FNR signal density in subcompartments of Arabidopsis wild-type, *fnr1* mutants and maize FNR expressor plants.** Dark-incubated leaves *A.thaliana* plants were embedded in LR-White resin and thin-sectioned, followed by IG-labelling against FNR (1st and 2nd antibody concentration 1:200). Around 15 chloroplasts in three different individuals per genotype were analyzed. The specified areas were measured and the labelling intensity was calculated for each chloroplast. Outliers are indicated by dots and statistical analysis is presented in table 5.3.

Table 5.3: **Statistical analysis of signal densities of FNR in subcompartments (s.comp) of wild-type, *fnr1* mutant and maize FNR expressor plants to compare signal distribution between all genotypes.** Above: Analysis of variance (ANOVA) on the signal densities of each subcompartment in three individuals per genotype. Below: Tukey post hoc tests for the combinations of subcompartments and the combinations of genotypes are presented. A corresponding boxplot on the analysed dataset is presented in figure 5.5.

ANOVA						
	Df	SumSq	MeanSq	F-value	Pr(>F)	
s.comp	3	5539	1864.3	67.116	2×10^{-16}	***
genotype	4	554	138.6	4.990	0.000559	***
individual	10	379	37.9	1.366	0.191208	
s.comp:genotype	12	1199	99.9	3.596	2.93×10^{-05}	***
s.comp:individual	29	466	16.1	0.578	0.964106	
Residuals	844	23445	27.8			

Tukey post hoc p adj				
s.comp	grana	margin	stroma	
margin	0			
stroma	0.9463	0		
lamellae	0	0.0055	0	
genotype			*fnr1*	*fnr1*
	wild-type	*fnr1*	ZmFNR1	ZmFNR2
fnr1	0.0102			
fnr1 ZmFNR1	0.963	0.034		
fnr1 ZmFNR2	0.999	0.005	0.975	
fnr1 ZmFNR3	0.999	0.001	0.848	0.994

In order to circumvent this problem, I calculated the area densities per individual instead of per chloroplast by summing up all measured subcompartment area values and signal values first and then calculating the density. This gives a more accurate estimation of real signal number per area, because it does not shift the means towards zero or distort the values to a higher variance, but comes at the cost of losing statistical power. Figure 5.6 shows the alterna-

tive boxplots where the data was additionally grouped for genotypes instead of subcompartments. This was done because it is unlikely that the antibody raised against *Zm*FNR2 has an identical affinity for each FNR isoform, so a comparison of total signal density values is less meaningful than a comparison of signal distribution within a genotype. Therefore, a statistical analysis of variance was only performed to compare the distribution within a genotype and not to compare the genotypes to each other. The results for the adjusted calculation of signal densities for each genotype individually are depicted in table 5.4. For each genotype the p-value for the comparison of the signal distribution between individuals is below 0.05, indicating statistical significance apart from *fnr1* mutant plants showing a p-value of 0.07. This is likely due to the high variance of density values for the margin in this genotype.

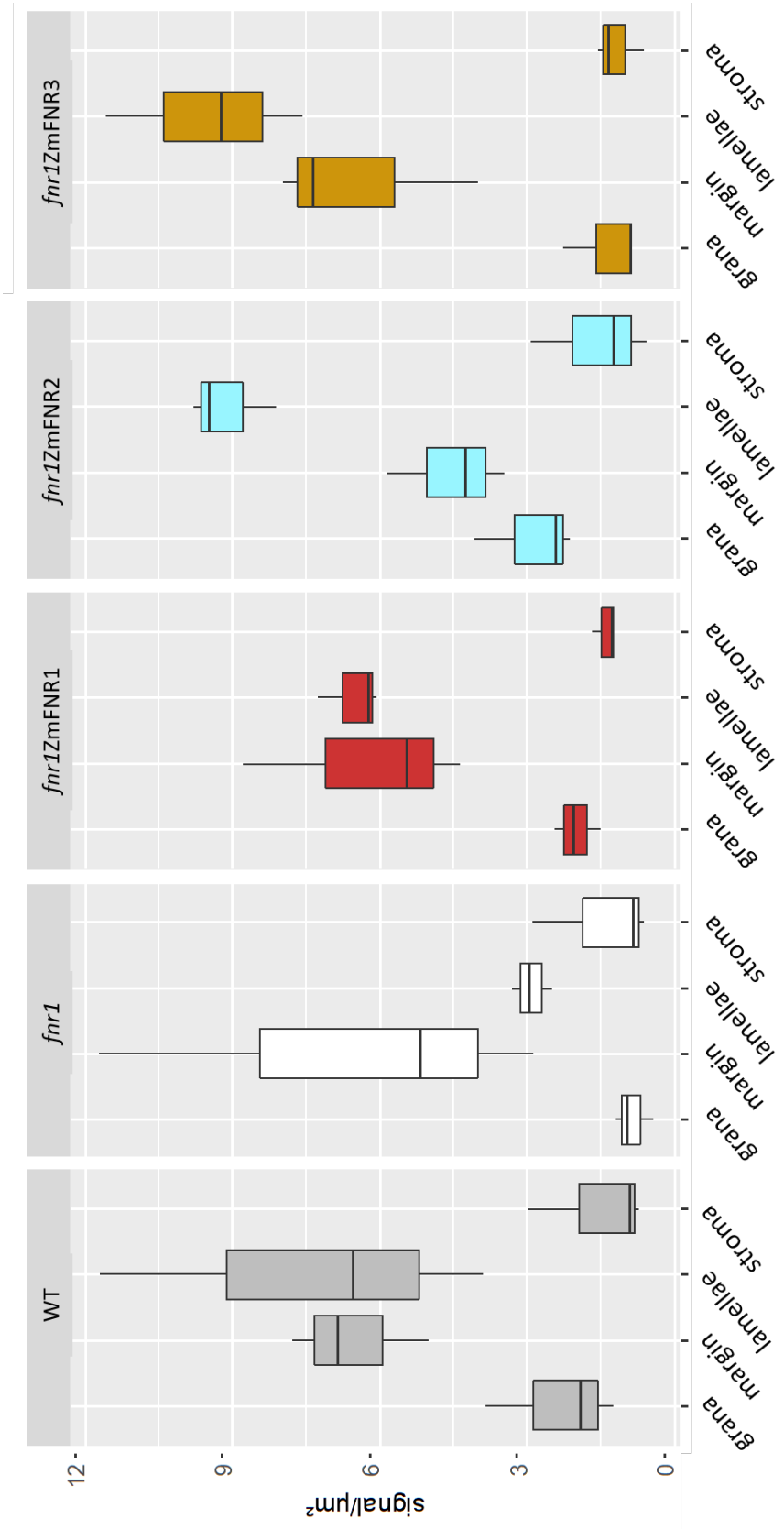

Figure 5.6: **Revised boxplot of IG-labelled FNR signal density in subcompartments of Arabidopsis wild-type, *fnr1* mutants and maize FNR expressor plants.** The same dataset of 5.5 was used but the signal per μm^2 was calculated after adding up the area measurements and signal counts of all micrographs per individual. Statistical analysis is presented in table 5.4.

Table 5.4: **Alternative statistical analysis of signal densities of FNR in sub-compartments (s.comp) of wild-type, *fnr1* mutant and maize FNR expressor plants to compare signal distribution between individuals of the indicated genotypes.** Above: Analysis of variance (ANOVA) was performed on the alternatively calculated signal densities of each individual per genotype. Below: Tukey post hoc test for the combination of lamellae-margin for each genotype individually. A corresponding boxplot on this alternatively processed dataset is presented in figure 5.6.

ANOVA						
	Df	SumSq	MeanSq	F-value	Pr(>F)	
wild-type						
s.comp	3	77.82	25.939	4.903	0.0321	*
Residuals	8	42.33	5.291			
fnr1						
s.comp	3	59.56	19.852	3.449	0.0717	.
Residuals	8	46.04	5.755			
fnr1 ZmFNR1						
s.comp	3	66.02	22.007	14.6	0.00131	**
Residuals	8	12.06	1.507			
fnr1 ZmFNR2						
s.comp	3	97.96	32.65	26.96	0.00016	***
Residuals	8	9.69	1.21			
fnr1 ZmFNR3						
s.comp	3	147.50	49.17	20.67	0.0004	***
Residuals	8	19.03	2.38			

genotype	margin-lamellae	stroma-lamellae	stroma-margin
wild-type	0.970	0.057	0.106
fnr1	0.310	0.874	0.113
fnr1 ZmFNR1	0.986	0.004	0.005
fnr1 ZmFNR2	0.004	0.001	0.045
fnr1 ZmFNR3	0.157	0.001	0.013

The alternative boxplots reveal a clear difference in signal density between the grana/stroma and margin/lamellae regions for all analysed genotypes as in figure 5.5, but this time the ratio of the signal density in the margin and signal density in the lamellae become apparent. In the wild-type, the median signal density for both of

these domains is approximately equal (p=0.97). Upon knock-out of *At*FNR1, the signal from the lamellae decreases drastically compared to the margin level. This suggests that the remaining *At*FNR2 is located mainly at the margins of the thylakoids (and does not become soluble as previously proposed by Lintala et al. [2009]). Because it is reported that there is no FNR-TROL or FNR-Tic62 interaction in this mutant, this implies that there is either an unknown tether for *At*FNR2 present in the thylakoid membrane or that the protein can bind directly to other complexes in the membrane e.g. PSI or Cyt b_6f complex as proposed before (Baniulis et al. [2011] and Zhang et al. [2001], respectively). Presumably, these interactions are disrupted during the sample preparation for electrophoresis, which has lead to the suggestion that all FNR in the mutant is soluble. Analysing the maize FNR expressors, *fnr1*ZmFNR1 plants show a similar pattern to wild-type plants, except with slightly higher labelling density on the lamellae than at the margins, indicating that the expression of *Zm*FNR1 in the *fnr1* mutant background restores the FNR distribution. We are unable to distinguish between the native and the maize isoforms using immunostaining, but because the total lamellae area is significantly smaller than the total margin area it can be assumed, that introduced *Zm*FNR1 is recruited to both membrane domains, otherwise the signal density in the lamellae would be much higher compared to the margin. In contrast, the genotypes *fnr1*ZmFNR2 and *fnr1*ZmFNR3 exhibit a higher FNR signal density in the lamellae than in the margins. However, this effect is only statistically significant in the *fnr1*ZmFNR2 genotype (p=0.004). It indicates that ZmFNR2 is much more strongly recruited to the thylakoid lamellae and that the *At*FNR2 is also more strongly recruited to the lamellae in the presence of *Zm*FNR2. Interestingly, the *fnr1*ZmFNR2 mar-

gin signal density is dramatically lower than in the other genotypes. *fnr1*ZmFNR3 does not show this tendency.

6. Light microscopy

Although electron microscopy delivers high structural detail of the membrane structures and my experiment successfully detected differences in protein distribution with high resolution there are downsides to this method: Although gold-particles are available in different sizes, a statistically convincing co-localization of proteins is problematic (for more information see chapter 1.5). Furthermore, it is impossible to detect signal in a three-dimensional space and - ultimately - in a living sample. We know that FNR tether interactions are highly dynamic and respond to environmental changes (Benz et al. [2009]) and wish to develop methods to observe this. This would provide us with more information on the function of the different FNR-tether complexes and how they would dynamically regulate photosynthetic electron transport. Additionally, it would focus our understanding of FNR distribution from the more broad definition of distribution across membrane compartments discussed before, to a narrower definition of distribution among functional complexes. In this chapter, I describe the development of an immunofluorescence labelling protocol and subsequent laser-scanning microscopy to investigate co-localization of FNR and its tether TROL.

6.1 Laser scanning microscopy

In parallel to the EM approach, I initially explored whether it was possible to see a difference in FNR distribution among the different genotypes by conventional light-microscopy as well. Immunfluorescence labelling approaches are difficult to perform on whole leaves, because the plant cell wall exhibits autofluorescence and also the penetration of the antibody into the cell is impeded. Therefore, chloroplasts were isolated from the plants, fixed and the membranes were permeabilized before immunodecoration with fluorescent probes followed. The same FNR antibody as in the immunogold labelling procedure was used. The autofluorescence of chlorophyll is in the red spectrum of the wavelengths, so the secondary antibodies that were chosen for this experiment were Cy3 (emission in the yellow range) and Alexa488/Cy2 (green) to prevent cross-talk of the signals. The first question to be addressed was whether it is possible at all to distinguish between sub-compartments of the organelle using this technique. Confocal LSM cannot resolve the membrane structure of the thylakoids in the bright field, so it is impossible to distinguish these structures without an appropriate label. Many previous conventional laser microscopy images of chloroplasts have shown an irregular distribution of chlorophyll autofluorescence, suggesting that areas with higher intensities are the appressed regions of the grana stacks and areas with lower intensities either lamellae or stroma (van Spronsen et al. [1989]). Therefore, I hypothesised that the resolution might be high enough to detect differences in sub-compartmental location if the target proteins are clearly separated. To test this hypothesis, wild-type Arabidopsis chloroplasts were isolated from the plant, fixed and immunolabelled with fluorescent probes against PsbA, a subunit

of PSII, and FNR and visualised in a confocal laser-scanning microscope (see figure 6.1). Using Alexa488 conjugated secondary antibody, no unspecific labelling occured when the incubation step with the 1st antibody was omitted (see Appendix, figure 11.1). PsbA as a grana marker was chosen over comparison with chlorophyll autofluorescence, because a single fluorophore is more suitable to produce a clear signal than autofluorescence which has a broad width of wavelengths (García-Plazaola et al. [2015]). As expected, we can observe small insulaes of concentrated PsbA signal in the chloroplasts, corresponding to the grana stacks. FNR also exhibits a similar irregular pattern, but - as becomes apparent in the overlay of PsbA and FNR channel - anti-correlated to PsbA. This means that it is indeed possible to distinguish different sub-compartments of the chloroplasts with this conventional method: PsbA in the grana and FNR in the stroma (as initially proposed) or at the lamellae/margin regions of the thylakoid. However, we now know on the basis of the EM data presented earlier in chapter 5.2, that FNR is unlikely to be soluble in the chloroplast, indicating that the FNR detected in this image is nearly all located at the thylakoid.

Subsequently, the experiment was repeated to compare wild-type with the maize FNR expressor plants in the *fnr*1 background, co-stained with antibodies against FNR and TROL (see figure 6.2). Omitting the incubation step with the 1st antibody resulted in no unspecific labelling when using the Cy2 and Cy3 conjugated secondary antibodies (see Appendix, figure 11.2 and figure 11.3). If via immuno co-staining we are able to detect changes in association between FNR and membrane tethers, a difference is expected between these genotypes, which show variable FNR-tether interactions (chapter 3.1). Interestingly, TROL is mainly distributed in

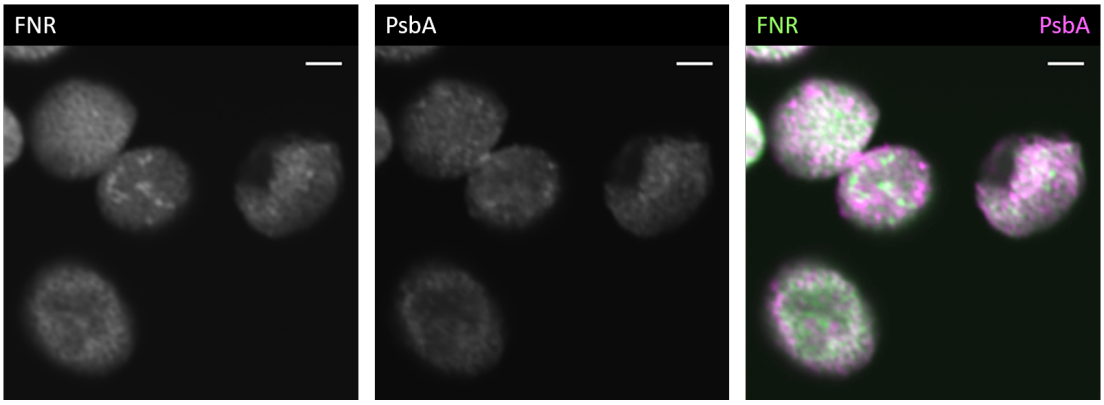

Figure 6.1: **Laser-scanning microscopy image of Arabidopsis wild-type chloroplast immunostained with markers for grana stacks (PsbA) and margin/lamellae (FNR).** Chloroplasts were isolated from *A.thaliana* (wild-type, Columbia ecotype) after 1h dark incubation and cross-linked with 3% formaldehyde. Membranes were permeabilized with 0.1 % TritonX-100 and the sample was immunolabelled for FNR with Cy3 conjugated secondary antibody and PsbA with Alexa488 conjugated secondary antibody. Imaging was performed on a Zeiss LSM 510 META NLO. Scalebar = 1 µm.

the outer areas of the chloroplasts like a corona in all genotypes. FNR in the wild-type plants shows the same irregular distribution as observed in the trial experiment before. The same pattern can be observed in *fnr1*ZmFNR2 and *fnr1*ZmFNR3 plants. However in the *fnr1*ZmFNR1 genotype, FNR is located in the outer areas of the chloroplasts. This is particularly obvious in the overlay images: While FNR is distributed across the whole chloroplasts in all genotypes but *fnr1*ZmFNR1, this genotype shows colocalization of FNR and TROL in the outer areas of the chloroplasts (in white). This is in line with the finding that *Zm*FNR1 predominantly binds to the TROL protein described in chapter 3.1. I therefore designed another experiment to achieve a higher resolution by deconvolution and three dimensional imaging in a light-sheet microscope.

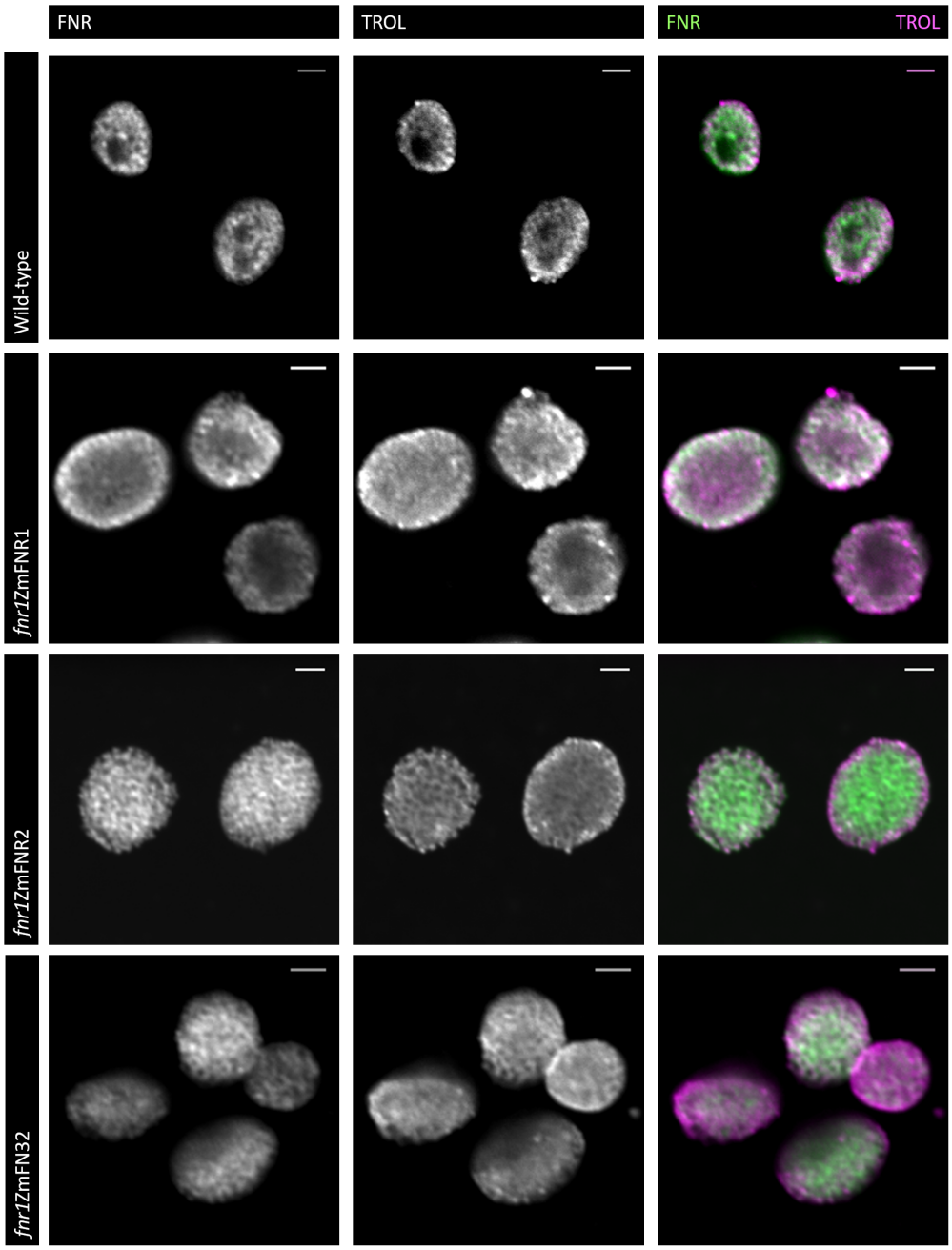

Figure 6.2: **Laser-scanning microscopy image of Arabidopsis wild-type and *fnr1* maize FNR expressor chloroplasts immunostained for FNR and its tether TROL.** Chloroplasts were isolated from maize FNR expressor plants after 1h dark incubation and cross-linked with 3% formaldehyde, permeabilized with 0.1 % TritonX-100 and the sample was immunolabelled for FNR with Cy3 conj. secondary antibody and TROL with Cy2 conj. secondary antibody. Imaging was performed on a Zeiss LSM 510. Scalebar = 1 µm.

6.2 Light sheet microscopy

Antibody-labelling In preparation for further immunofluorescence experiments, I directly labelled highly specific primary antibodies for Cyt *f*, FNR and its tether TROL with Atto dyes of different wavelengths. This serves the double purpose of firstly reducing the washing steps to facilitate an easier sample preparation and secondly reducing the distance from the fluorescent probe to the actual target protein by superseding the secondary antibody. Furthermore, the dye-conjugated antibodies provide a valuable tool for possible future super-resolution imaging approaches, and the dyes were selected accordingly for high quantum yield and high photostability required for these experiments. Both TROL and Cyt *f* (a subunit of the Cytb_6f) were labelled to study co-localization of FNR with its tether proteins. Tic62 was disregarded for this experiment as the available primary antibody is not specific enough (e.g. it also recognizes TROL as described by Benz et al. [2009]). These labelled antisera were purified and consecutively labelled with appropriate Atto dyes tested for optimal concentration to be used in immunolabelling experiments on isolated and fixed chloroplasts (see table 6.1). The antibody recognizing Cyt *f* did not show a satisfactory result, despite increasing the concentration for membrane permeabilization by TritonX-100. This is possibly due to a masking of the Cyt *f* recognition site *in vivo* or an inability of the antibody to penetrate into the thylakoid lumen, so the antibody was not considered for future experiments.

Light-sheet microscopy In collaboration with the Centre of Cellular Nanoanalytics Osnabrück University, fixed chloroplasts of Arabidop-

Table 6.1: **Labelling of antibodies with Atto dye.** Optimised combinations of antibody and Atto dye (ATTO-TEC GmbH) with respective conditions for immunolabelling assays following testing on isolated and fixed wild-type Arabidopsis chloroplasts.

Antibody	Atto dye	Staining conc.	Permeabilization
anti-*Zm*FNR	Atto 488	1 mM	0.1 % TritonX-100
anti-*Zm*TROL	Atto 565	70 mM	0.1 % TritonX-100
anti-Cyt*f*	Atto 565	N/A	0.2 % TritonX-100

sis WT, *fnr1* mutant and maize FNR expressors in the mutant background were recorded as Z-stacks in a lattice light-sheet microscope and images were deconvolved. The microscope is a state of the art live cell imaging platform for multi-color high-speed volumetric imaging using thin light-sheets based on optical lattices, which generate high signal-to-noise ratios (Chen et al. [2014]).

As in other light microscopy experiments we are unable to see the thylakoid membrane structure directly, but in this setup, it is possible to indirectly correlate the autofluorescence to a part of the thylakoid structure, the grana. The selected dyes require excitation by green or yellow wavelengths lasers, which only excite Chl b that associates with PSII in the grana (Blankenship [2014]). Co-localization of chlorophyll and immunolabel would therefore indicate that FNR is associated with the grana or lamellae margins. Because the EM immunogold labelling results indicate that FNR is overwhelmingly bound to the thylakoid, it follows that FNR signals not colocalised with chlorophyll are most likely bound to the stromal lamellae membrane. We therefore measured the co-localization of FNR and TROL, not only in relation to each other, but also to the chlorophyll fluorescence.

Figure 6.3 shows an irregular distribution throughout the chloroplast for both proteins and the chlorophyll autofluorescence (grey in

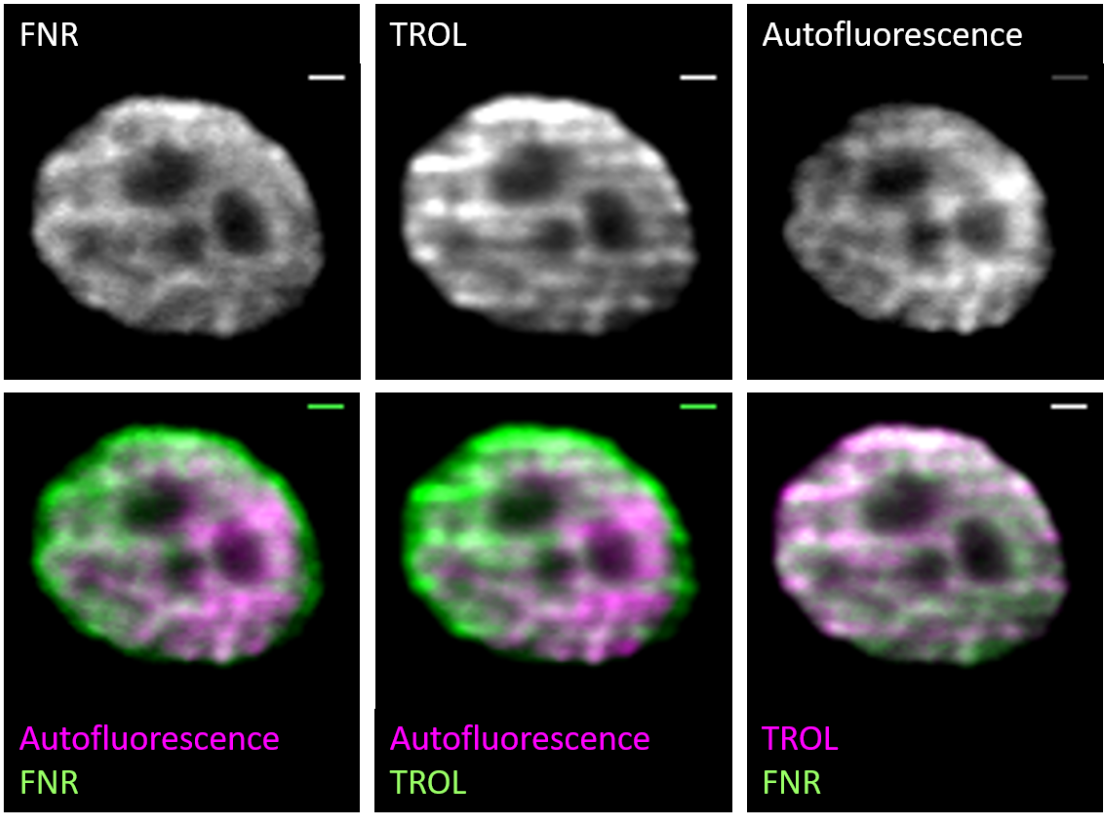

Figure 6.3: **Light-sheet microscopy image of isolated chloroplast from wild-type Arabidopsis immunostained for FNR and its tether TROL.** Chloroplasts were isolated from *A.thaliana* (wild-type, Columbia ecotype) after dark incubation of 1h and cross-linked with 3% formaldehyde. Membranes were permeabilized with 0.1 % TritonX-100 and the sample was immunolabelled for FNR with Atto488 conjugated primary antibody and thylakoid rhodanase-like protein (TROL) with Atto565 conjugated primary antibody. Imaging was performed on a lattice light-sheet microscope, followed by mathematical deconvolution of the image. Scalebar = 1 µm.

upper panels for indicated signal). However, overlaying the channels (presented in the lower panels in pink and green for the indicated combinations) reveals that none of them show a complete co-localization, which would be visible as only white pixels in this colour combination. Rather, a partial co-localization can be observed in each case: Co-localisation is less pronounced for the protein to autofluorescence combinations and more so for FNR and TROL.

Assessing these differences by eye is not accurate and - especially when dealing with Z-stacks - not feasible, so in order to obtain values for co-localisation I analysed the images by calculating the Pearson's Correlation Coefficient (PCC) (Costes et al. [2004]) between two signals using the "Coloc 2" tool in ImageJ and tested whether there are variations between genotypes. The program runs an auto-threshold determination so that reproducibility of the results is not compromised by manual thresholding. In order to exclude as much background as possible, single chloroplasts were defined as region of interest (ROI) to prevent positive skew of the values. However, each Z-stack contains at least 40 single images and chloroplasts also enclose regions devoid of signal (e.g. the stroma or remaining transistory starch) so as a consequence the values might still indicate a higher correlation than it is really the case. This effect applies to all genotypes so a comparison of the values will nonetheless be revelatory.

Only one example of an immunolabelled chloroplast per indicated genotype is depicted in figures 6.4 to 6.7. In total 4 to 8 chloroplasts per genotype with from 40 to 70 images per Z-stack were analysed to calculate the PCC shown in figure 6.8. Presented is a comparison of Pearson's Correlation Coefficient results for different genotypes in all three signal combinations. Values close to zero indicate no spa-

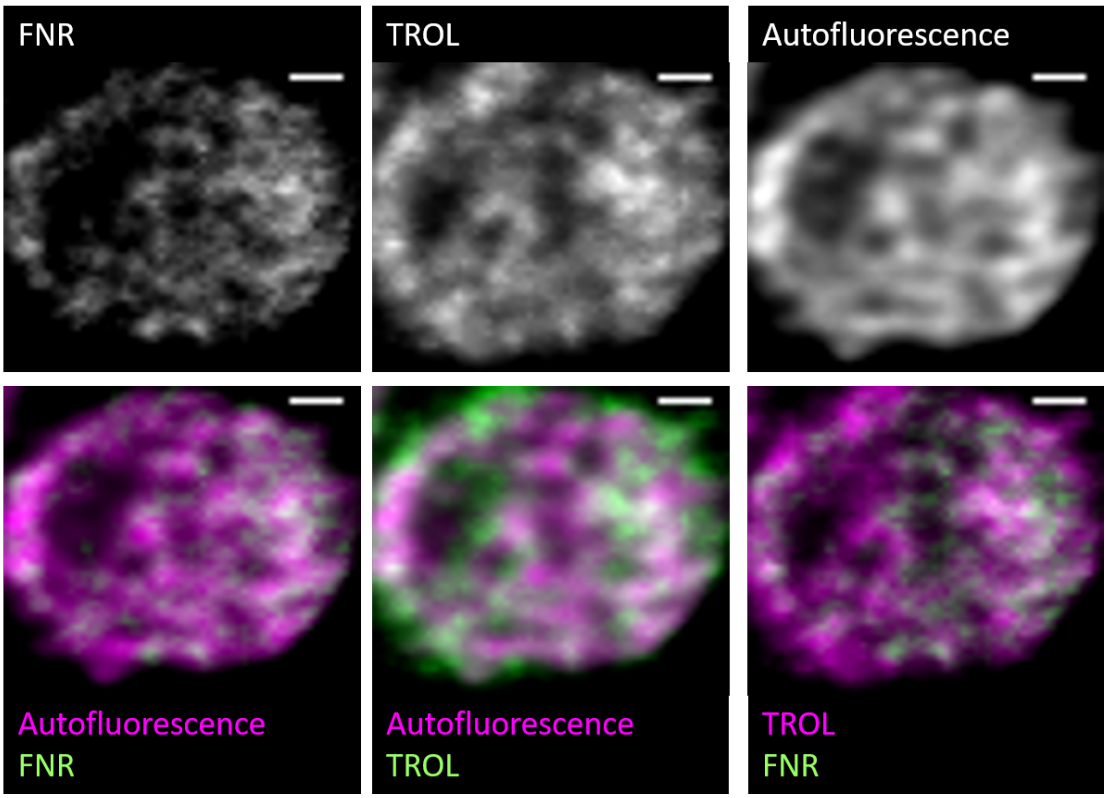

Figure 6.4: **Light-sheet microscopy image of isolated chloroplast from *fnr1* Arabidopsis immunostained for FNR and its tether TROL.** Chloroplasts were isolated from *A.thaliana fnr1* after dark incubation of 1h, and then cross-linked with 3% formaldehyde. Membranes were permeabilized with 0.1 % TritonX-100 and the sample was immunolabelled for FNR with Atto488 conjugated primary antibody and thylakoid rhodanase-like protein (TROL) with Atto565 conjugated primary antibody. Imaging was performed on a lattice light-sheet microscope, followed by mathematical deconvolution of the image. Scalebar = 1 µm.

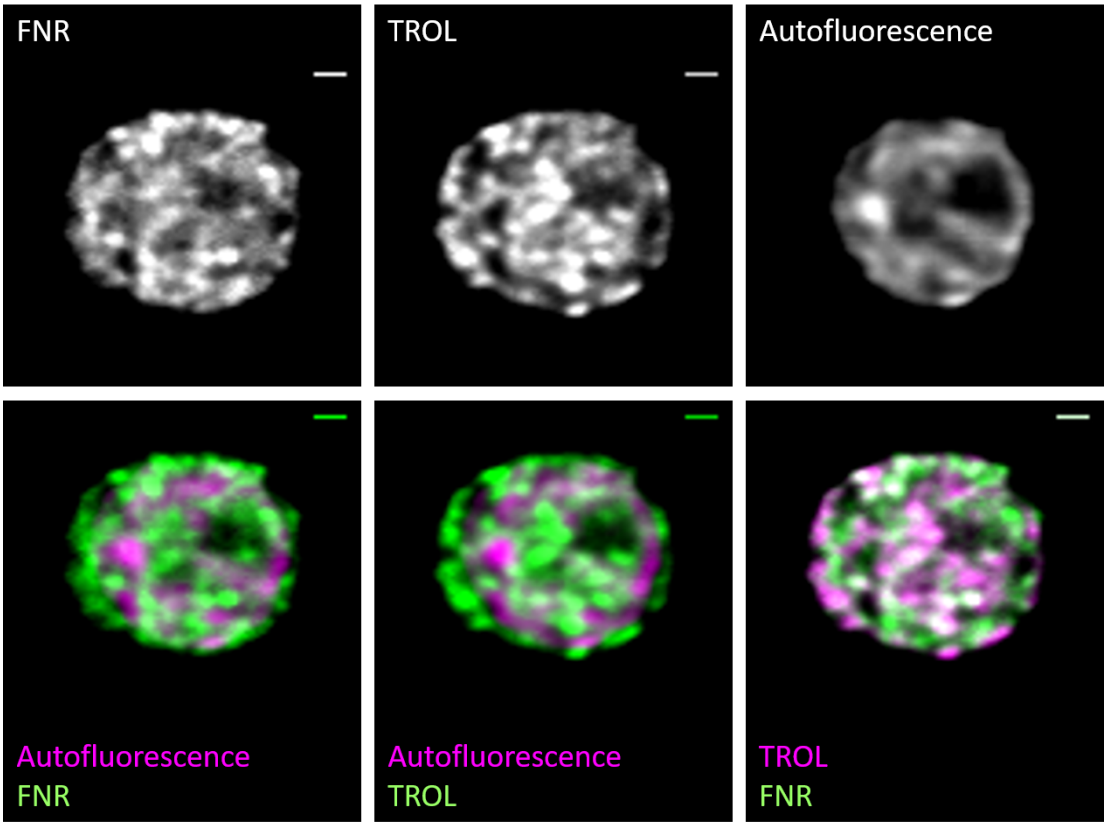

Figure 6.5: **Light-sheet microscopy image of isolated chloroplast from *fnr1* Zm1 Arabidopsis immunostained for FNR and its tether TROL.** Chloroplasts were isolated from *A.thaliana fnr1*Zm1 after dark incubation of 1h, and then cross-linked with 3% formaldehyde. Membranes were permeabilized with 0.1 % TritonX-100 and the sample was immunolabelled for FNR with Atto488 conjugated primary antibody and thylakoid rhodanase-like protein (TROL) with Atto565 conjugated primary antibody. Imaging was performed on a lattice light-sheet microscope, followed by mathematical deconvolution of the image. Scalebar = 1 µm.

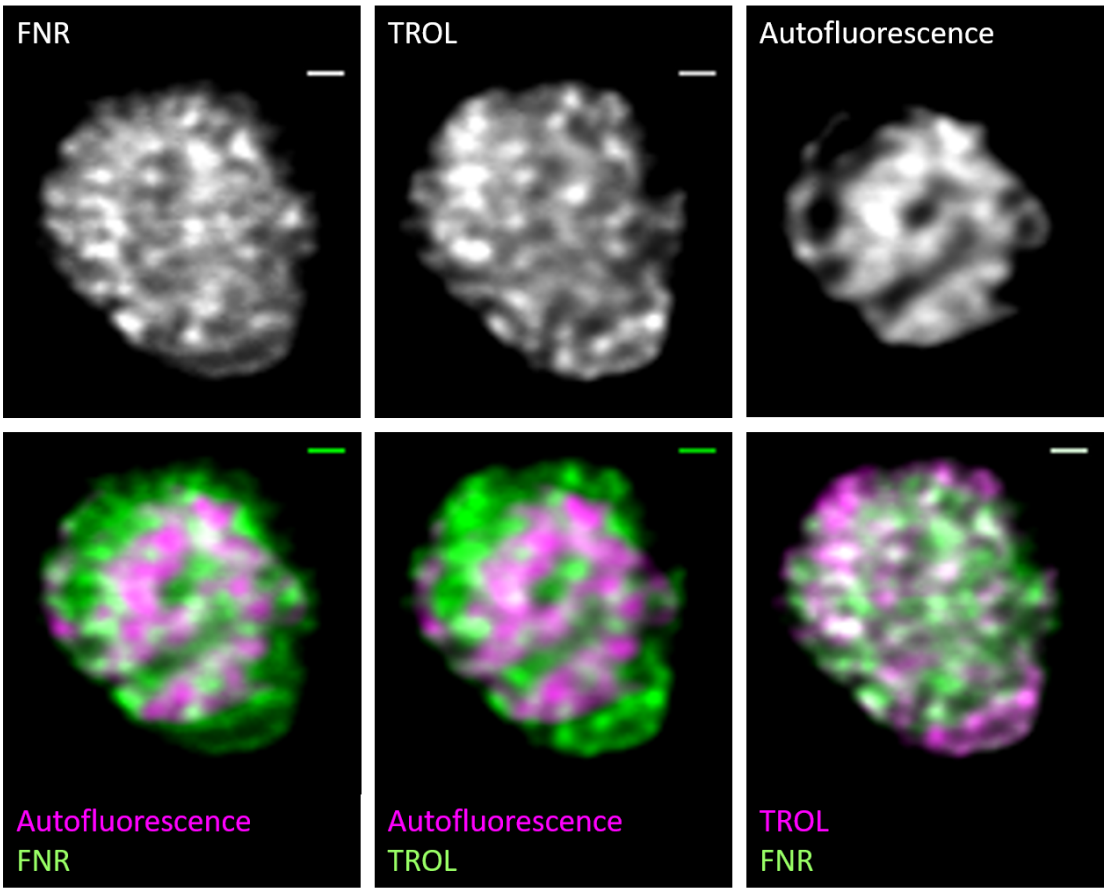

Figure 6.6: **Light-sheet microscopy image of isolated chloroplast from *fnr1* Zm2 Arabidopsis immunostained for FNR and its tether TROL.** Chloroplasts were isolated from *A.thaliana fnr1* Zm2 after dark incubation of 1h, and then cross-linked with 3% formaldehyde. Membranes were permeabilized with 0.1 % TritonX-100 and the sample was immunolabelled for FNR with Atto488 conjugated primary antibody and thylakoid rhodanase-like protein (TROL) with Atto565 conjugated primary antibody. Imaging was performed on a lattice light-sheet microscope, followed by mathematical deconvolution of the image. Scalebar = 1 µm.

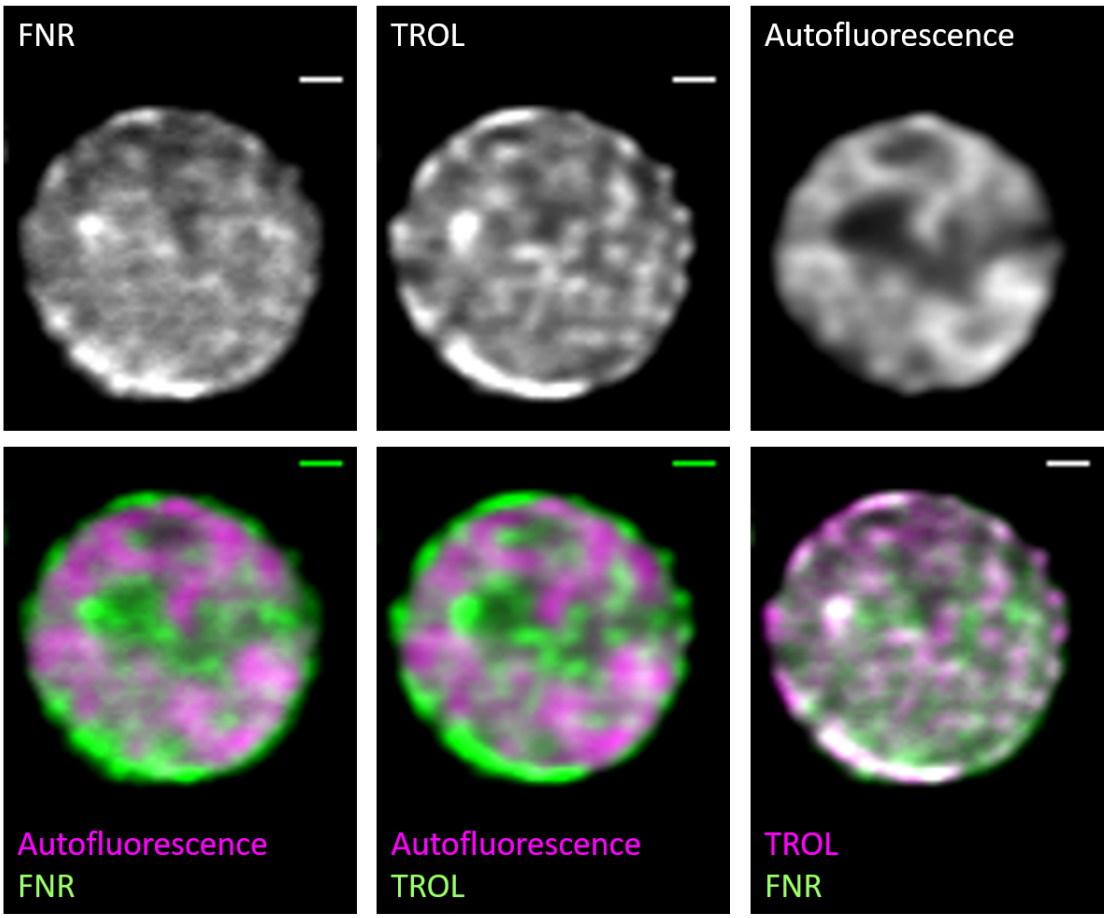

Figure 6.7: **Light-sheet microscopy image of isolated chloroplast from *fnr1* Zm3 Arabidopsis immunostained for FNR and its tether TROL.** Chloroplasts were isolated from *A.thaliana fnr1* Zm3 after dark incubation of 1h, and then cross-linked with 3% formaldehyde. Membranes were permeabilized with 0.1 % TritonX-100 and the sample was immunolabelled for FNR with Atto488 conjugated primary antibody and thylakoid rhodanase-like protein (TROL) with Atto565 conjugated primary antibody. Imaging was performed on a lattice light-sheet microscope, followed by mathematical deconvolution of the image. Scalebar = 1 µm.

tial correlation of the compared fluorophores, whereas a value of 1 indicates a perfect correlation. Despite having a lower total signal due to decreased FNR content, knock-out of Arabidopsis FNR1 does not lead to a proportional re-distribution of the remaining *At*FNR2 away from the PSII regions, as the correlation values between FNR and chlorophyll stay the same. One advantage of the PCC is that it is not sensitive to mean signal intensities, only localisation. This means that even in genotypes with variable FNR (such as the *fnr1* mutant) PCC will accurately detect co-localisation regardless of signal intensity.

The correlation of both FNR and TROL to autofluorescence of chlorophyll goes down upon introduction of any of the three maize FNR, despite their different protein interaction partners. This means that all maize FNR isoforms seem to be recruited into interactions that restrict their localisation to the chlorophyll containing grana margins to some extent. Strikingly, FNR-Chlorophyll correlation is very close to 0, indicating no correlation in the *fnr1*ZmFNR1 genotype, while these chloroplasts simultaneously exhibit slightly enhanced FNR-TROL correlation compared to the other plants. This is in agreement with the observation that *Zm*FNR1 specifically binds to TROL (Twachtmann et al. [2012], see figure 3.3). It also refines the findings of Jurić et al. [2009], who reported localization of TROL to the thylakoids using standard confocal microscopy. The FNR-TROL protein complex might get sequestered away from the margins of the grana stacks and into the lamellae, where there is less autofluorescence. This effect is not pronounced in the *fnr1*ZmFNR2 and *fnr1*ZmFNR3 mutants which show no enhanced FNR-TROL correlation and a lower but still moderate degree of correlation for FNR-Chlorophyll correlation compared to the wild-type. Interest-

ingly, the introduction of any maize FNR isoform leads to a decreased correlation of TROL to Chlorophyll. This suggests that the TROL tether itself is not rigidly allocated to one specific area of the thylakoid membrane, but is able to move between domains. We can only speculate as to why this is the case, but the limited FNR mobility/binding flexibility while retaining protein levels of the native *At*FNR1 might lead to unforeseeable stress response mechanisms e.g. relocation of FNR binding complexes. It is worth mentioning, that the binding of FNR itself does not seem to be required (as *Zm*FNR2 and *Zm*FNR3 do not bind strongly to TROL) for this. Likewise, the decreased FNR-Chlorophyll correlation in *Zm*FNR2 and *Zm*FNR3 suggests that the respective membrane-binding interactions of these isoforms follow the same principle and remove FNR from the margins. This would also explain the unexpectedly high co-localisation of these two FNR isoforms with the tether TROL, even if interaction of these proteins is not detected biochemically (figure 3.3). FNR that is removed from the margin regions of the grana has to be located at the lamellae and the same is true for the TROL protein which could lead to a correlation of the two signals.

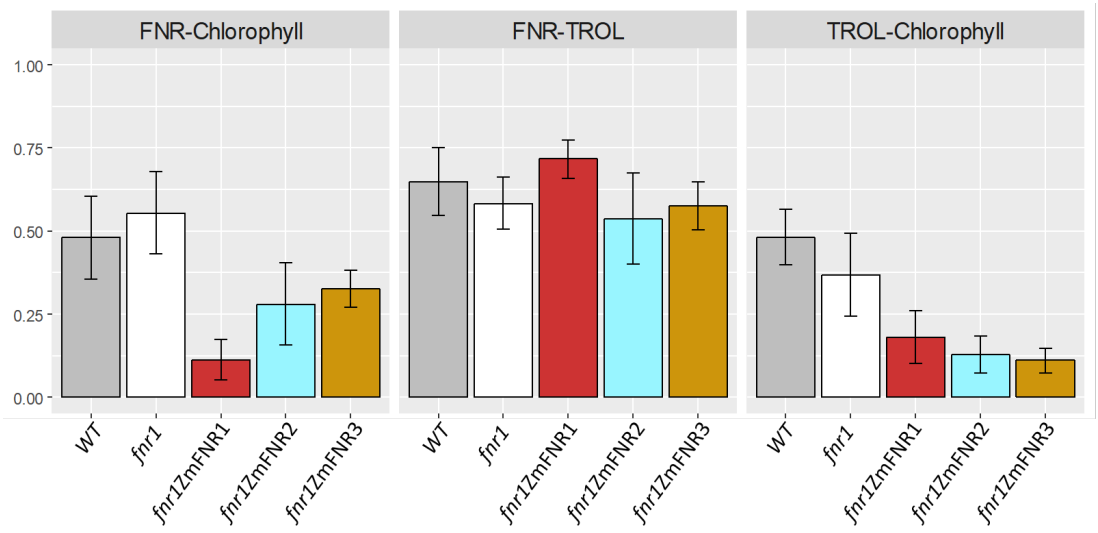

Figure 6.8: **Pearson's Correlation Coefficient calculated for Arabidopsis wild-type, *fnr1* and maize FNR expressor chloroplasts for the indicated fluorophore combinations.**The Coefficient has been calculated for four to eight chloroplasts imaged as 40 to 70 stacks. It describes the covariance between the intensities in two images. A value of +1 = perfect correlation, 0 = no correlation, -1 = perfect anti-correlation. The error bars indicate standard deviation.

7. Loop-tagged FNR as functional tool to investigate dynamic relocalisation

A dynamic relocation of FNR would unquestionally be best observed *in vivo* where immunolabelling approaches in the classic sense are unworkable. Cloning a fluorescent tag onto a terminus of FNR however is not reasonable as the carboxy group of the C-terminal tyrosine is involved in FNR catalytic mechanism (Tejero et al. [2005]), and the N-terminus is critical for membrane recruitment (Twachtmann et al. [2012]) and would also lead to a dysfunctional enzyme. Therefore, I determined to introduce the tag to an internal, preferably protruding loop. GFP with a size of 27 kDa is only slightly smaller than FNR itself and would possibly interfere with the structure of FNR to an extent that might change its capacity to bind the cofactor or two interaction partners if cloned into a loop. Thus, we adapted the immunotagging approach SunTag described by Tanenbaum et al. [2014]. In the planned work scheme Arabidopsis *fnr1* mutant plants will be transformed with GFP-tagged single-chain antibodies (scFv), under control of an inducible oestradiol promoter and with the chloroplast target peptide from FNR. Then, a small

immunotag (GCN4) recognized by the scFv will be inserted in an internal loop of FNR. The GCN4 tag with a size of 19 amino acids is less likely to cause structural perturbations of FNR than a big fluorescent tag. Furthermore, the inducibility of the GFP-scFv expression prevents a build-up of GFP during the maturation of the plant that would cause high nonspecific background-signal.

I identified possible loop structures in FNR by *in silico* analysis of its crystal structure in jmol (see table 7.1). Each described internal loop was tested for its possible involvement in co-factor binding (FAD), interaction partner binding (Fd and NADP(H)) and dimer formation, which is important for membrane recruitment. The remaining loops were checked for conserved sequences via multiple sequence alignment in TEXShade. Conserved loops were excluded because they likely serve an important function in binding or have structural importance. I then scanned for other structural clashes (e.g. proline in the sequence which might be crucial to maintain the tertiary structure). An interference in any of these criteria lead to the exclusion of the loop. Three possible loops were identified via this method and named FNR-LA, FNR-LB and FNR-LC. FNR-LB contravened my criteria, but was recommended upon personal communication with Prof. Toshiharu Hase, Osaka University, suggesting that a mutation in this loop is not likely to inhibit the binding of Fd at this site, despite my analysis.

Table 7.1: **FNR loops identified in the crystal structure using jmol.** The crystal structures are listed in PDBj: FNR-Fd (gaw1), FNR-Tic62 peptide (3mhp). An "X" marks an interference of the indicated loop with the respective criteria. The selected loops are indicated LA, LB and LC and were used for scFv-antigen-tagging.

FNR loop	start AA	end AA	Fd	FAD	NADP(H)	FNR dimer	Tic62	sequence	selected loop
1	Ile 48	Glu 56			x		x		
2	Glu 65	Pro 69				x			
3	Ala 80	Val 92	x	x					
4	Ala 101	Lys 109				x			
5	Asn 122	Glu 126		x					
6	Leu 139	Asp 143						conserved	
7	Met 157	Ala 163							LA
8	Glu 187	Gly 196					x		
9	Pro 205	Thr 206						prolin	
10	Pro 224	Phe 227						conserved	
11	Ser 234	Tyr 246			x				LB
12	Lys 264	Asn 266						conserved	
13	Lys 275	Gly 276			x				
14	Ile 294	Asp 295							LC

```
ZmRFNR2          ..................................................    0
OsRFNR2          ..................................................    0
ZmRFNR1          ..................................................    0
OsRFNR1          ..................................................    0
AtRFNR1          ..................................................    0
AtRFNR2          ..................................................    0
PpFNR2?          ..................................................    0
PpFNR1           ..................................................    0
CrFNR            ..................................................    0
OtFNR            ..................................................    0
PsFNR1           ..................................................    0
PsFNR2?          ..................................................    0
AtLFNR2          ..................................................    0
AtLFNR1          ..................................................    0
OsLFNR2          ..................................................    0
ZmLFNR2          ..................................................    0
ZmLFNR3          ..................................................    0
ZmLFNR1          ..................................................    0
OsLFNR1          ..................................................    0
AFNR             .................................................G    1
SFNR             MYSPGYVATSSRQSDAGNRLFVYEVIGLSQSTMTDGLDYPIRRSG    45
consensus
```

```
ZmRFNR2          ..................................................    0
OsRFNR2          ..................................................    0
ZmRFNR1          ..................................................    0
OsRFNR1          ..................................................    0
AtRFNR1          ..................................................    0
AtRFNR2          ..................................................    0
PpFNR2?          ..................................................    0
PpFNR1           ..................................................    0
CrFNR            ..................................................    0
OtFNR            ..................................................    0
PsFNR1           ..................................................    0
PsFNR2?          ..................................................    0
AtLFNR2          ..................................................    0
AtLFNR1          ..................................................    0
OsLFNR2          ..................................................    0
ZmLFNR2          ..................................................    0
ZmLFNR3          ..................................................    0
ZmLFNR1          ..................................................    0
OsLFNR1          ..................................................    0
AFNR             KIVSIQTVSALQQLNGRTTIATVTDASSEIAKSEGNGKATPVKTD    46
SFNR             STFITVPLKRMNQEMRRITRMGGKIVSIKPLEGDSPLPHTEGIAK    90
consensus
```

```
ZmRFNR2          ..............QASRSKVAVMPVELEKAKEPLLHLYKPKEP     30
OsRFNR2          ..............QASKSKVAVKPLELDNAKEPPLNLYKPKEP     30
ZmRFNR1          ..............QASRSKVSVAPLHLESAKEPPLNTYKPKEP     30
OsRFNR1          ..............QASESKVAVKPLDLESANEPPLNTYKPKEP     30
AtRFNR1          ..............QSSKSKVLVTPLELEDPKETPLNLFRPKEP     30
AtRFNR2          ..............QTSSSKVTVSPIELEDPKDPPLNLYKPKES     30
PpFNR2?          ....................................MHLFKNKEP      9
PpFNR1           .......QRRVFTAALTEQASKVALTADLEGEPEPPMHLFKNKEP     38
CrFNR            ..........KASTAVTTDMSKRTVPTKLEEGEMPLNTYSNKAP     34
OtFNR            .........MSTTADKNIDPNGRAKVPLEMEKMELPLNTYKNKEP     36
PsFNR1           ............QVTTEAPATTKVVKISKKNEEGVVVNKYKPKTP     33
PsFNR2?          ............QVTTEAPATTKVVKISKKNEEGVVVNKYKPKTP     33
AtLFNR2          ..........ITTETDTPTPAKKVEKVSKKNEEGVIVNRYRPKEP     35
AtLFNR1          ..........VTTDTTEAPPVKVVKESKKQEEGIVVNKFKPKNP     34
OsLFNR2          .......STTETTAAPAAEVTTKVEKVSKKQVDGVVTNKYRPKEP     38
ZmLFNR2          ........QVSTTETAEAEPVKKLEKVSKKQEEGLVTNKYKPKEP     37
ZmLFNR3          ............QVSTTETAAAGPAKTSKKQDEGLVTNKYKPKEP     33
ZmLFNR1          ........IRAQASAVEAPATAKAKKESKKQEEGVVTNLYKPKEP     37
OsLFNR1          .........STTDAAAVAAAPAKKEKISKKHDEGVVTNKYRPKEP     36
AFNR             SGAKGFAKPPAEEQLKKKDNKGNTMTQAKAKHADVPVNLYRPNAP     91
SFNR             PSQSEGSGSEAVANPAPESNKTMTTTPKEKKADDIPVNIYRPKTP    135
consensus                                 *    **     * * ******

ZmRFNR2          YTATIVSVERLVGPRAPGETCHVVIDHG.GNVPYWEGQSYGVIPP     74
OsRFNR2          YTATIVSVERLVGPKAPGETCHIVIDHG.GNVPYWEGQSYGVIPP     74
ZmRFNR1          FTATIVSVESLVGPKAPGETCHIVIDHG.GNVPYWEGQSYGVIPP     74
OsRFNR1          YTATIVSVERIVGPKAPGETCHIVIDHG.GNVPYWEGQSYGIIPP     74
AtRFNR1          YTATIVSVERIVGPQAPGETCHIVIDHD.GNVPYWEGQSYGVIPP     74
AtRFNR2          YTAKIVSVERVVGPKAPGETCHIVIDHD.GNLPYWEGQSYGVIPP     74
PpFNR2?          FIGTIKSVERIVGPKAPGETCHIVIDHE.GNVPYWEGQSYGIIPP     53
PpFNR1           FIGTVKSVERIVGPNATGETCHIVIDHG.GQMPYWEGQSYGIIPP     82
CrFNR            FKAKVRSVEKITGPKATGETCHIIIETE.GKIPFWEGQSYGVIPP     78
OtFNR            FVGTIRSVERIVGPNATGETCHIIIEHG.GKMPFWEGQSYGVIPP     80
PsFNR1           YIGRVLLNTKITADDAPGETWHMVFSTE.GELPYREGQSIGVIPT     77
PsFNR2?          YIGRVLLNTKITADDAPGETWHMVFSTE.GELPYREGQSIGVIPT     77
AtLFNR2          YTGKCLLNTKITADDAPGETWHMVFSHQ.GEIPYREGQSVGVIAD     79
AtLFNR1          YTGRCLLNTKITGDDAPGETWHIVFTTE.GEVPYREGQSIGVIPE     78
OsLFNR2          YTGRCLLNTRITGDDAPGETWHMVFSTD.GEIPYREGQSIGVIPD     82
ZmLFNR2          YVGRCLLNTRITGDQAPGETWHMVFSTE.GEVPYREGQSIGVIAD     81
ZmLFNR3          YVGRCLSNTRITGDDAPGETWHMVFSTE.GEIPYREGQSIGIIAD     77
ZmLFNR1          YVGRCLLNTKITGDDAPGETWHMVFSTE.GKIPYREGQSIGVIAD     81
OsLFNR1          YVGKCLLNTKITADDAPGETWHMVFSTE.GEIPYREGQSIGVIAD     80
AFNR             FIGKVISNEPLVKEGGIGIVQHIKFDLTGGNLKYIEGQSIGIIPP    136
SFNR             YIGKVLENYPLVREGAIGTVQHLTFDLSAGDLRYLEGQSIGIIPP    180
consensus        * *  ********* **!***!*****  !  ***!!!!*!*!**
```

```
ZmRFNR2       GENPKKPG..SPNTVRLYSIASTRYGDSFDGKTASLCVRRAVYYD   117
OsRFNR2       GENPKKPG..SPNTVRLYSIASTRYGDSFDGKTASLCVRRAVYYD   117
ZmRFNR1       GENPKKPG..APQNVRLYSIASTRYGDNFDGRTGSLCVRRAVYYD   117
OsRFNR1       GENPKKPG..APHNVRLYSIASTRYGDSFDGRTTSLCVRRAVYYD   117
AtRFNR1       GENPKKPG..APHNVRLYSIASTRYGDSFDGKTASLCVRRAIYYD   117
AtRFNR2       GENPKKPG..APHNVRLYSIASTRYGDFFDGKTASLCVRRAVYYD   117
PpFNR2?       GENPKKPG..QPNSVRLYSIASTRYGDDFDGRTASFCVRRAVYWD    96
PpFNR1        GENPKKPG..QPNTVRLYSIASTRYGDEFDGKTASLCVRRAVYWC   125
CrFNR         GTKINSKGKEVPHGTRLYSIASSRYGDDFDGQTASLCVRRAVYVD   123
OtFNR         GTKVNSKGKEVPHGVRLYSIASSRYGDSYDGLTATLCVRRATYWD   125
PsFNR1        GIDKNG....KPHKLRLYSIASSALGDFGDSKTVSLCVKRLVYTN   118
PsFNR2?       GIDKNG....KPHKLRLYSIASSALGDFGDSKTVSLCVKRLVYTN   118
AtLFNR2       GIDKNG....KPHKVRLYSIASSALGDLGNSETVSLCVKRLVYTN   120
AtLFNR1       GIDKNG....KPHKLRLYSIASSAIGDFGDSKTVSLCVKRLVYTN   119
OsLFNR2       GIDKNG....KPHKLRLYSIASSAIGDFADSKTVSLCVKRLVYTN   123
ZmLFNR2       GEDKNG....KPHKLRLYSIASSALGDFGDSKTVSLCVKRLVYTN   122
ZmLFNR3       GEDKNG....KPHKLRLYSIASSALGDFGDSKTVSLCVKRLVYTN   118
ZmLFNR1       GVDKNG....KPHKVRLYSIASSAIGDFGDSKTVSLCVKRLIYTN   122
OsLFNR1       GVDKNG....KPHKLRLYSIASSALGDFGDSKTVSLCVKRLVYTN   121
AFNR          GVDKNG....KPEKLRLYSIASTRHGDDVDDKTISLCVRQLEYKH   177
SFNR          GEDDKG....KPHKLRLYSIASTRHGDFGDDKTVSLCVRQLEYQN   221
consensus     !***** *  *!***!!!!!!!***!!*****!***!!****!**
```

LA

```
ZmRFNR2       PETGEEDPSKRGVCSNFLCGSKPGDKVQITGPSGKIMLLPEDDPN   162
OsRFNR2       PETGKEDPTKKGICSNFLCDSKPGDKVQITGPSGKIMLLPEDDPN   162
ZmRFNR1       PETGKEDPSKNGVCSNFLCNSKPGDKIQLTGPSGKIMLLPEEDPN   162
OsRFNR1       PETGKEDPSKNGVCSNFLCNSKPGDKVKVTGPSGKIMLLPEEDPN   162
AtRFNR1       PETGKEDPSKAGVCSNFLCNAKPGDKVKITGPSGKVMLLPEDDPK   162
AtRFNR2       PETGKEDPSKNGVCSNFLCDSKPGDKIQITGPSGKVMLLPESDPN   162
PpFNR2?       PETGKEDPAKKGICSNFLCDSKPGDKVQIVGPSGKVLLLPEEDPS   141
PpFNR1        PELQAEDPAKKGICSNFLCDCKPGDKVQITGPSGKVMLLPESDPN   170
CrFNR         PETGKEDPAKKGLCSNFLCDATPGTEISMTGPTGKVLLLPA.DAN   167
OtFNR         PEMNAEDPAKKGICSNFLCDAKPGQEVMMTGPTGQVMLLPK.DPA   169
PsFNR1        .DQGEVV...KGVCSNFLCDLKPGEEVTITGPVGKEMLMPV.DPN   158
PsFNR2?       .DQGEVV...KGVCSNFLCDLKPGEEVTITGPVGKEMLMPV.DPN   158
AtLFNR2       .DQGETV...KGVCSNFLCDLAPGSDVKLTGPVGKEMLMPK.DPN   160
AtLFNR1       .DGGEIV...KGVCSNFLCDLKPGDEAKITGPVGKEMLMPK.DPN   159
OsLFNR2       .DQGEIV...KGVCSNFLCDLKPGSDVKITGPVGKEMLMPK.DPN   163
ZmLFNR2       .DQGEVV...KGVCSNFLCDLKPGAEVKITGPVGKEMLMPK.DPN   162
ZmLFNR3       .DQGEIV...KGVCSNFLCDLKPGADVKITGPVGKEMLMPK.DPN   158
ZmLFNR1       .DAGEIV...KGVCSNFLCDLQPGDNVQITGPVGKEMLMPK.DPN   162
OsLFNR1       .DQGEIV...KGVCSNFLCDLKPGSDVKITGPVGKEMLMPK.DPN   161
AFNR          PESGETV...YGVCSTYLTHIEPGSEVKITGPVGKEMLLPD.DPE   218
SFNR          .EAGETV...QGVCSTYLCNIKEGDDIAITGPVGKEMLLPP.DED   261
consensus     ** ***** **!*!!**!** **!* * **!!*!***!*!  !**
```

LA

```
ZmRFNR2       ATHIMIATGTGVAPYRGYLRRMFMEDV....PTFKFGGLAWLFLG   203
OsRFNR2       ATHIMIATGTGVAPYRGYLRRMFMEDV....PSFKFGGLAWLFLG   203
ZmRFNR1       ATHIMIATGTGVAPFRGYLRRMFMEDV....PNYRFGGLAWLFLG   203
OsRFNR1       ATHIMIATGTGVAPFRGYLRRMFMEDV....PKYRFGGLAWLFLG   203
AtRFNR1       ATHIMIATGTGVAPYRGYLRRMFMENV....PNFKFDGLAWLFLG   203
AtRFNR2       ATHIMIATGTGVAPYRGYLRRMFMENV....PNKTFSGLAWLFLG   203
PpFNR2?       ATHIMVATGTGIAPYRGYLRRMFMEDT.....EFKFNGLAWLFMG   181
PpFNR1        ATHIMVATGTGIAPYRGFLRRMFMEDV....PTFKFGGLAWLFLG   211
CrFNR         APLICVATGTGIAPFRSFWRRCFIENV....PSYKFTGLFWLFMG   208
OtFNR         TPVIMVATGTGIAPMRSYLRRFFLEDI....PSWEFKGLAWLFMG   210
PsFNR1        ATIIMLATGTGIAPFRGYLWKMFFEKH....PDYKFNGLAWLFLG   199
PsFNR2?       ATIIMLATGTGIAPFRGYLWKMFFEKH....PDYKFNGLAWLFLG   199
AtLFNR2       ATVIMLATGTGIAPFRSFLWKMFFEKH....DDYKFNGLAWLFLG   201
AtLFNR1       ATIIMLGTGTGIAPFRSFLWKMFFEEH....EDYKFNGLAWLFLG   200
OsLFNR2       ATIIMLGTGTGIAPFRSFLWKMFFEEH....DDYKFNGLAWLFLG   204
ZmLFNR2       ATIIMLATGTGIAPFRSFLWKMFFEEH....EDYKYTGLAWLFLG   203
ZmLFNR3       ATVIMLATGTGIAPFRSFLWKMFLEEH....EDYKFTGLAWLFLG   199
ZmLFNR1       ATIIMLATGTGIAPFRSFLWKMFFEKH....DDYKFNGLGWLFLG   203
OsLFNR1       ANIIMLATGTGIAPFRSFLWKMFFEKY....DDYKFNGLAWLFLG   202
AFNR          ANVIMLATGTGIAPMRTYLWRMFKDAERAANPEYQFKGFSWLVFG   263
SFNR          ANIVMLATGTGIAPFRAFLWRMFKEQH....EDYKFKGLAWLIFG   302
consensus     ** ****!!!!*!!*!******! *      ***** !**!!**!
```

LB

```
ZmRFNR2       VANSDSLLYDEEFTNYLQQYPDNFRYDKALSREQKNKSGGKMYVQ   248
OsRFNR2       VANTDSLLYDEEFTNYLQQYPDNFRYDKALSREQKNKNGGKMYVQ   248
ZmRFNR1       VANSDSLLYDEEFTSYLKQYPDNFRYDKALSREQKNRSGGKMYVQ   248
OsRFNR1       VANTDSLLYDEEFTSYLKQYPDNFRYDKALSREQKNKNAGKMYVQ   248
AtRFNR1       VANSDSLLYDEEFAGYRKDYPENFRYDKALSREEKNKKGGKMYVQ   248
AtRFNR2       VANTDSLLYDEEFTKYLKDHPDNFRFDKALSREEKNKKGGKMYVQ   248
PpFNR2?       VANTDSLLYHDEFNTYLKEYPDNFRYDIALSREQKNSRGGKLYVQ   226
PpFNR1        VANSDSLLYHDEFTKYKEAFPENFRYDTALSREEKNSKGGKMYVQ   256
CrFNR         VANSDAKLYDEELQAIAKAYPGQFRLDYALSREQNNRKGGKMYIQ   253
OtFNR         VANSDAKLYDDEFQEMVKRFPDQFRIDYALSREDTNKNGGKMYIQ   255
PsFNR1        VPTSSSLIYKEEFEKMKEKSPDKIRVDFAVSREQTNEKGEKMYIQ   244
PsFNR2?       VPTSSSLIYKEEFEKMKEKSPDKIRVDFAVSREQTNE........   236
AtLFNR2       VPTTSSLLYQEEFDKMKAKAPENFRVDYAISREQANDKGEKMYIQ   246
AtLFNR1       VPTSSSLLYKEEFEKMKEKNPDNFRLDFAVSREQTNEKGEKMYIQ   245
OsLFNR2       VPTSSTLLYREEFERMKEIAPERFRLDFAVSREQTNAAGEKMYIQ   249
ZmLFNR2       VPTSDTLLYKEELEKMKEMAPDNFRLDFAVSREQTNAAGEKMYIQ   248
ZmLFNR3       VPTSDSLLYKEELEKMKEMAPDNFRLDFAVSREQTNAAGEKMYIQ   244
ZmLFNR1       VPTSSSLLYKEEFGKMKERAPENFRVDYAVSREQTNAAGERMYIQ   248
OsLFNR1       VPTSSSLLYKEEFDKMKAKAPENFRVDYAVSREQTNAQGEKMYIQ   247
AFNR          VPTTPNILYKEELEEIQQKYPDNFRLTYAISREQKNPQGGRMYIQ   308
SFNR          IPKSENILYKDDLEKMAAEFPDNFRLTYAISREQQNAEGGRMYIQ   347
consensus     ********! *** ***   !***! * !*!!!* !  *******
```

```
ZmRFNR2       DKIEEYSDEIFRLLDGG.AHIYFCGLKGMMPGIQDTLKKVAEQRG    292
OsRFNR2       DKIEEYSDEIFKLLDGG.AHIYFCGLKGMMPGIQDTLKRVAEQRG    292
ZmRFNR1       DKIEEYSDEIFKLLDGG.AHIYFCGLKGMMPGIQDTLKKVAERRG    292
OsRFNR1       DKIEEYSDEIFKLLDGG.AHIYFCGLKGMMPGIQDTLKKVAEQRG    292
AtRFNR1       DKIEEYSDEIFKLLDNG.AHIYFCGLKGMMPGIQDTLKRVAEERG    292
AtRFNR2       DKIEEYSDEIFKLLDNG.AHIYFCGLKGMMPGIQDTLKRVAEERG    292
PpFNR2?       DKMEEYSEELFDKLDKG.AHIYFCGLRGMMPGIQDMLKRVAESRG    270
PpFNR1        DKIEEYSEELFNLLDKG.AHIYFCGLRGMMPGIQDTLKRVAEARG    300
CrFNR         DKVEEYADEIFDLLDNG.AHMYFCGLKGMMPGIQDMLERVAKEKG    297
OtFNR         DKVEEYKDQVFQLLDGG.AHMYFCGLKGMMPGILSMLEGVCKEKG    299
PsFNR1        TRMGEYAKELWGLFKKENTYVYMCGLKGMEKGIDDIITSLAAEEG    289
PsFNR2?       ............................KGIDDIITSLAAEEG    251
AtLFNR2       TRMAQYAAELWELLKKDNTFVYMCGLKGMEKGIDDIMVSLAANDG    291
AtLFNR1       TRMAEYAEELWELLKKDNTFVYMCGLKGMEKGIDDIMVSLAAKDG    290
OsLFNR2       TRMAEYKDELWELLKKDNTYVYMCGLKGMEKGIDDIMIDLAAKDG    294
ZmLFNR2       TRMAEYKEELWELLKKDNTYVYMCGLKGMEKGIDDIMLDLAAKDG    293
ZmLFNR3       TRMADYREELWELLKKDNTYVYMCGLKGMEKGIDDIMLDLAAKDG    289
ZmLFNR1       TRMAEYKEELWELLKKDNTYVYMCGLKGMEKGIDDIMVSLAEKDG    293
OsLFNR1       TRMAEYKEELWELLKKDHTYVYMCGLKGMEKGIDDIMVSLAAKDG    292
AFNR          DRVAEHADELWQLIKNEKTHTYICGLRGMEEGIDAALSAAAAKEG    353
SFNR          HRVAENAEELWNLMQNPKTHTYMCGLKGMEPGIDEAFTALAEQNG    392
consensus     ** *** ***  *****  * ******** *!!** *   **  !
```

LC

```
ZmRFNR2       ESWDQKLSQLKKNKQWHVEVY    313
OsRFNR2       ESWEQKLSQLKKNKQWHVEVY    313
ZmRFNR1       ESWDQKLAQLKKNKQWHVEVY    313
OsRFNR1       ESWEQKLSQLKKNKQWHVEVY    313
AtRFNR1       ESWEQKLTQLRKNKQWHVEVY    313
AtRFNR2       ESWDLKLSQLRKNKQWHVEVY    313
PpFNR2?       ESWETKLAALKKNKQWHVEVY    291
PpFNR1        ENWEEKLAKLKKNKQWHVEVY    321
CrFNR         LNYEEWVEGLKHKNQWHVEVY    318
OtFNR         ISYEEWLEGLKKNGQWHVEVY    320
PsFNR1        IDWNEYKRQMKKSERWNVEVY    310
PsFNR2?       IDWNEYKRQMKKSERWNVEVY    272
AtLFNR2       IDWFDYKKQLKKAEQWNVEVY    312
AtLFNR1       IDWLEYKKQLKRSEQWNVEVY    311
OsLFNR2       IDWLDYKKQLKKSEQWNVEVY    315
ZmLFNR2       INWLDYKKQLKKSEQWNVEVY    314
ZmLFNR3       IDWMQYKKQLKKGEQWNVEVY    310
ZmLFNR1       IDWFDYKKQLKRGDQWNVEVY    314
OsLFNR1       IDWADYKKQLKKGEQWNVEVY    313
AFNR          VTWSDYQKDLKKAGRWHVETY    374
SFNR          KEWTTFQREMKKEHRWHVETY    413
consensus     * *  *  **** *!*!!*!
```

Figure 7.1: **FNR sequence alignment to visualise conserved regions.** Loop A, B and C are marked in red above the top sequence. Very conservative regions indicated by "!", conservative regions indicated by "*". *Zea mays*: *Zm*LFNR1, BAA88236; *Zm*LFNR2, BAA88237; *Zm*LFNR3, ACF85815; *Zm*RFNR1, ACG39703.1; *Zm*RFNR2, ACG35047.1 ; *Oryza sativa* *Os*LFNR2, BAD07827.1; *Os*LFNR1, OS06G0107700; *Os*RFNR1, OS03G0784700; *Os*FNR2, *Os*07g0147900; *Arabidopsis thaliana*: *At*LFNR1, AT5G66190; *At*LFNR2, AT1G20020; *At*RFNR2, AT1G30510; *At*RFNR1, AT4G05390; *Chlamydomonas reinhardtii*: *Cr*FNR, XP001697352.1; *Ostreococcus taurii*: *Ot*FNR, XP003084170.1; *Nostoc* sp. PCC 7120: AFNR, NP488161.1; *Synechocystis* sp. PCC 6803: SFNR, NP441779.1; *Pp*FNR1, XP001774270; *Physcomitrella patens*: *Pp*FNR2, XP001770917; *Pisum sativum*: *Ps*FNR2?, ABK22336; *Ps*FNR1, ABK21671.1

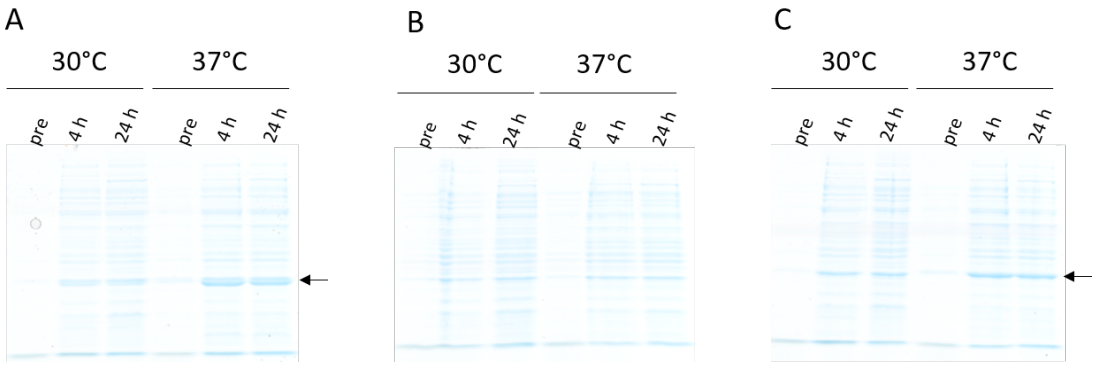

Figure 7.2: **SDS-PAGE of loop-tagged FNR expression optimisation.** The recombinant proteins were expressed in *E.coli* BL21iscr cells at two different temperatures and samples were taken at the indicated time point (pre-induction with IPTG, after 4 hours of induction and after 24 hours of induction) and subjected to SDS-PAGE. **(A)** FNR-LA, **(B)** FNR-LB **(C)** FNR-LC. Black arrows indicate loop-tagged FNR.)

Despite careful selection of loops, it remains crucial to test the tagged version of FNR for its function and capacity to bind to partner proteins *in vivo*. Therefore, the three tagged versions of *Zm*FNR1 were expressed recombinantly and purified. The GCN4 epitope was introduced into the three identified loops of the FNR gene in a pQE-60 expression vector. The expression was performed in *E.coli* BL21Δiscr cells that are mutants in the negative regulator of the FeS cluster assembly machinery (Akhtar and Jones [2008]). It was previously observed that this strain produces large amounts of flavoproteins on heterologous expression (M. Twachtmann, personal communication). Expression of the respective FNR constructs was then tested at two different *E.coli* growth temperatures presented in figure 7.2. FNR-LB did not express in either condition, but FNR-LA and FNR-LC were expressed at 37°C and therefore were chosen for large-scale expression and purification. Although the binding of Fd in the FNR-LB might not be inhibited, it seems like an introduction of amino acids into this loop impairs the stability and therefore the expression of the protein.

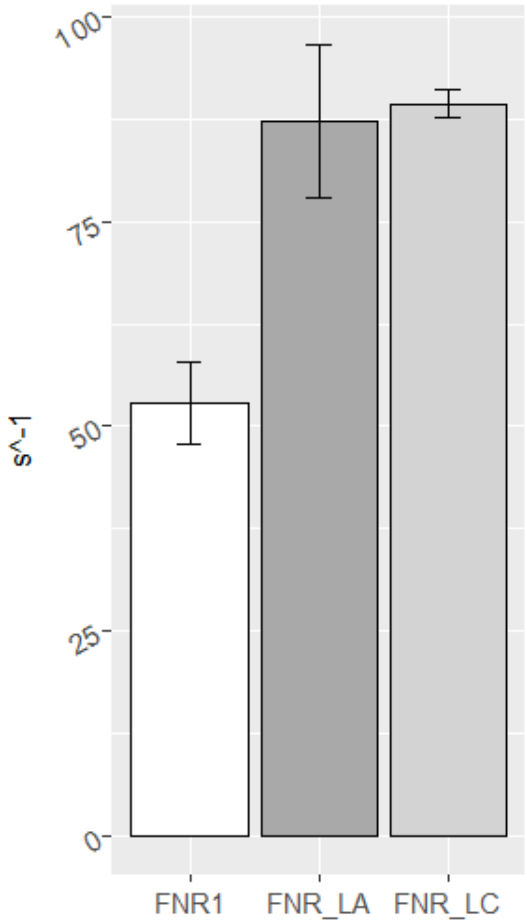

Figure 7.3: **Rate of loop-tagged recombinant FNR enzyme activity.** The rate of enzyme activity of *At*FNR1, FNR-LA and FNR-LC was tested in a cytochrome *c* reduction assay in three experimental replicates. Error bars show the standard error of the rates.

Enzyme activity assay The purified loop-tagged FNR were tested for their enzyme activity rate in an NADP(H) dependent Fd reduction assay, to confirm that interaction with neither partner was disrupted, alongside *Zm*FNR1 for comparison. The calculated rates are shown in the bar chart of figure 7.3. Both loop-tagged enzymes show a similar level of activity (around 90 µM Cyt *C* / µM FNR / s) which even exceeds that of the native FNR (around 50 µM Cyt *C* / µM FNR / s), meaning both loop-tagged enzymes retain their reductase activity *in vitro* and likely cause no structural clashes that hinder Fd or

NADP(H) binding. The ability to oxidise NADP(H) and subsequently reduce Fd even exceeds that of the native protein *Zm*FNR1. This might be for two reasons: the native FNR1 was not purified at the same time as the loop-tagged versions and could have lost part of its activity during storage (despite estimates of concentration being based on the extinction coefficient of the FAD cofactor), or the introduced tag has structurally altered the FNR slightly in favour of accessibility of its active site, and therefore enhances enzyme activity. Okutani et al. [2005] have found a lower overall activity of *Zm*FNR1 compared to *Zm*FNR2 and *Zm*FNR3, so it is possible that a slight structural perturbation enhances the activity of *Zm*FNR1. However, this result is satisfactory in terms of protein functionality and I conclude that these two loop-tagged versions of FNR would not show a drastically different behaviour from the wild-type FNR *in vivo*. On this basis, I propose this system is a valuable tool for future localisation studies of FNR *in vivo*.

Binding assay The capacity of the enzyme to be recruited to the membrane depends on its binding behaviour and partly on its ability to dimerize around homologous peptides of the TROL and Tic62 proteins (Alte et al. [2010]). Therefore, I subjected the purified recombinant FNR enzymes to a size exclusion column each on their own and each in the presence of the TROL peptide that is responsible for FNR dimerisation. The peaks of this size exclusion chromatography are presented in figure 7.4. The monomeric enzyme on its own (red) elutes in a single peak, while the dimer is bigger in size and elutes earlier than the monomer (black). The control in figure 7.4 A shows that *Zm*FNR2 dimerises in the presence of the TROL protein, resulting in two peaks whereas *Zm*FNR3 in figure 7.4 B does

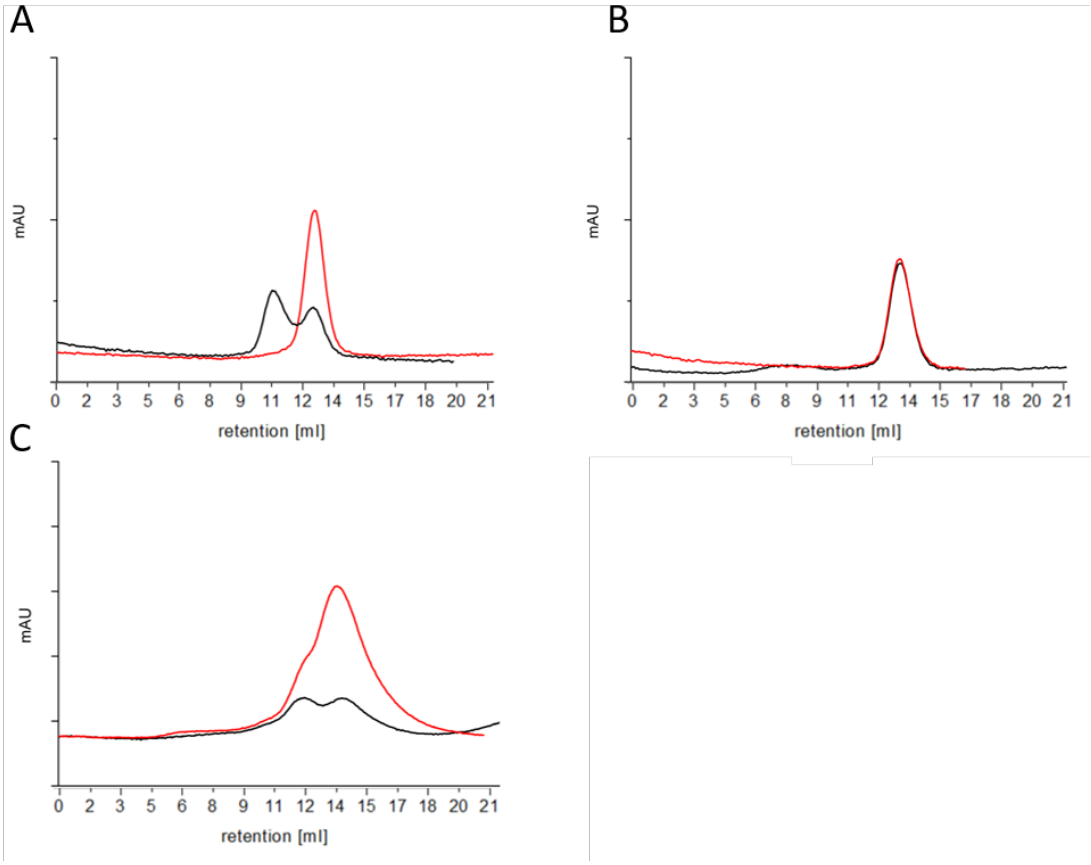

Figure 7.4: **Traces of size exclusion chromatography of the recombinant loop-tagged FNR enzymes to investigate TROL binding.** The recombinant FNR was subjected to size exclusion colum without (red) and with the binding peptide of TROL (black). (**A**) *Zm*FNR2. (**B**) *Zm*FNR3. (**C**) FNR-LA.

not show dimerisation, eluting in a single peak in the presence of TROL. Upon addition of the binding peptide of TROL, FNR-LA elutes in two peaks. This shows that the purified FNR-LA is still able to dimerize upon interaction with TROL peptide. It appears that a portion of FNR-LA remains monomeric, but this could also be a protein contaminant from the purification process. FNR-LC still remains to be tested in regard to its dimerisation capacity.

8. Impact on photosynthesis

In order to investigate the effect of the location of FNR at the thylakoid membrane, and association with its different tethers on its function, I used fluorimetric measurements making use of the inherent light-induced fluorescence of NADP(H), the chlorophyll in PSII and PSI absorption. Hereby, I was also able to investigate the activity of the FNR enzyme itself and the electron transport around the two photosystems, which is presented in the first part of this section. Subsequently, plants adapted to fluctuating light conditions, to simulate stress conditions were also subjected to chlorophyll fluorescence measurements to investigate the impact of location of FNR at the thylakoids on stress response.

8.1 Photosynthetic electron transport

$NADP^+$ reduction The primary function of FNR is the reduction of $NADP^+$, which exhibits no fluorescence to NADP(H) which fluoresces in the blue-green range upon excitation. Although the detection of this change in fluorescence in the cell is complicated by a multitude of factors (e.g. high background, low signal, high chlorophyll fluorescence), it can be exploited for the measurement of $NADP^+$ reduction kinetics in isolated chloroplasts as described by the technical

note from Walz (Walz GmbH [2009]).

We know that in the dark the interaction of FNR with its tethers Tic62 and TROL should be strong due to a low stromal pH (Alte et al. [2010])). Upon illumination, the stromal pH rises and FNR is theoretically released from its tethers. We therefore measured the activity of FNR in the first 40 s of illumination to test whether we can observe a difference in $NADP^+$ reduction depending on the location and interactions of the FNR isoforms. Figure 8.1 shows an average of 9 measurements of $NADP^+$ reduction in wild-type Arabidopsis plants. In the wild type, a fast rise of NADP(H) fluorescence is followed by a slower, curved rise to a steady rise after about 20 s. This suggests that the totality of FNR is not immediately 100% effective and one possible explanation is that this might be because part of the FNR pool is in the lamellae and therefore not immediately in the right location to reduce $NADP^+$. The slow increase in efficiency over the first 20 seconds co-incides with the generation of a pH gradient, consistent with the slow, pH dependent release of FNR from sites on the lamellae and their release to a more efficient active location at the margins.

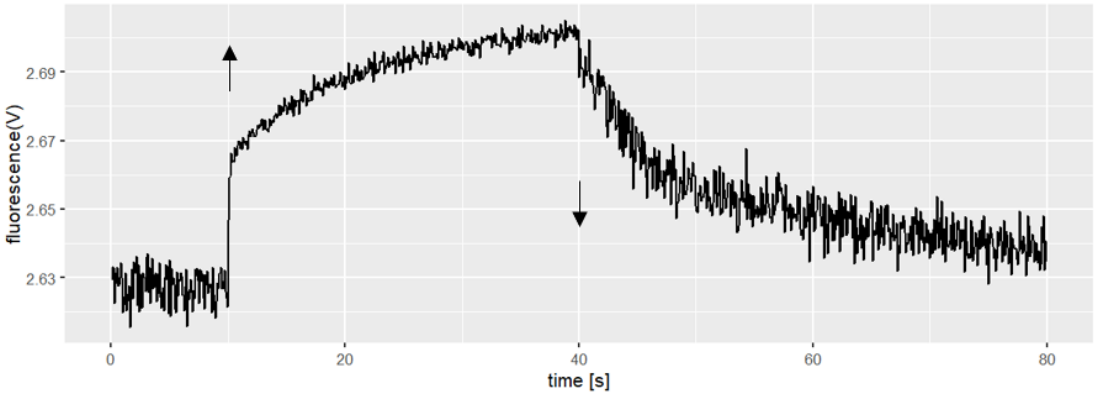

Figure 8.1: **$NADP^+$ reduction kinetics in wild-type Arabidopsis plants.** The trace was averaged out of 9 measurements and normalised for the signal amplitude. Arrows indicate when the light source is switched on and off.

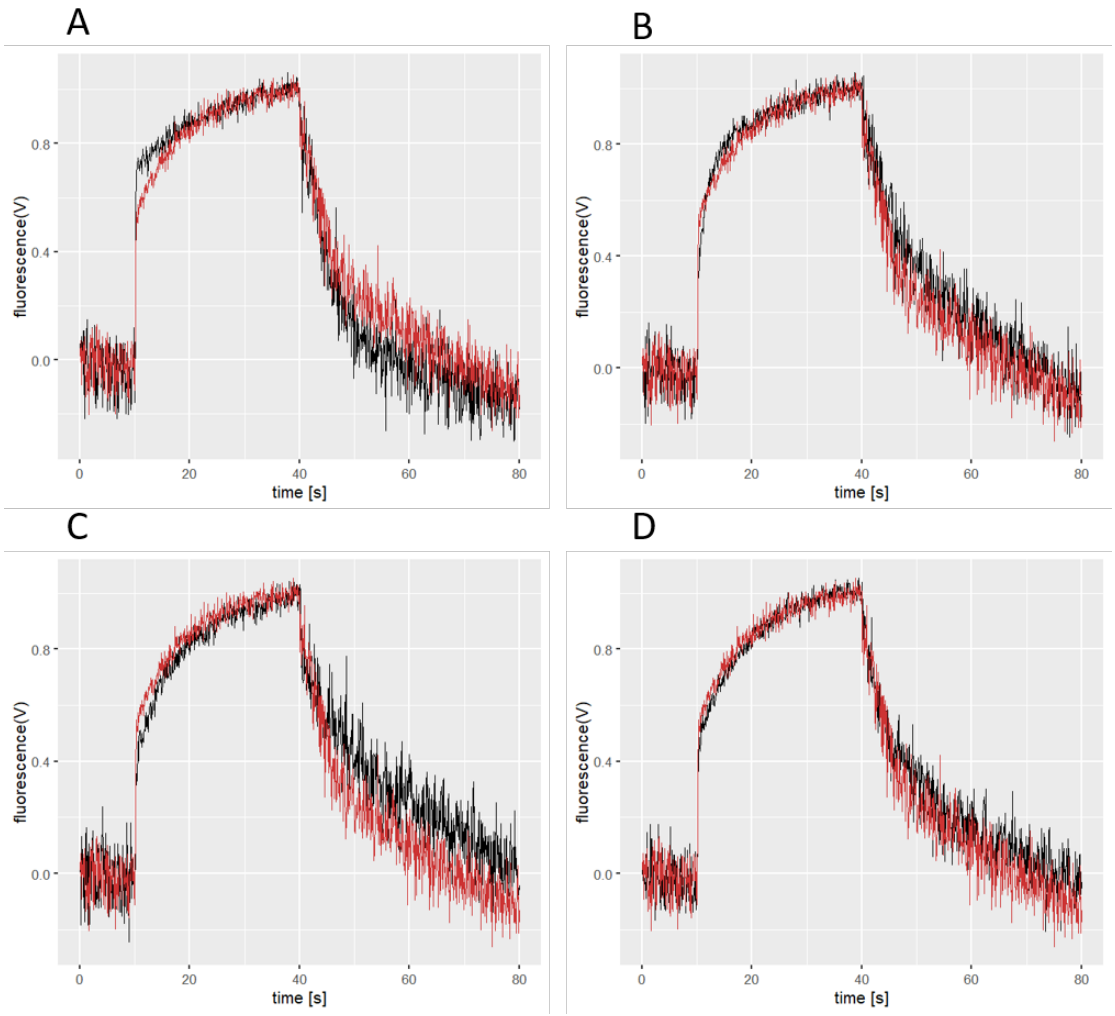

Figure 8.2: **$NADP^+$ reduction kinetics in *fnr1* mutant and maize FNR expressor Arabidopsis plants.** The traces are an average of 9 measurements and were normalised for the signal amplitude and aligned with the wild-type trace in red. **A**: *fnr1*, **B**: *fnr1*ZmFNR1, **C**: *fnr1*ZmFNR2, **D**: *fnr1*ZmFNR3.

If this hypothesis is true, we should see a higher efficiency of FNR when there is a higher FNR density at the margins and also no slow rising phase when there is no FNR binding to either tether. In figure 8.2 the change in NADP(H) signal over the dark to light transition in chloroplasts isolated from *fnr1* mutant (A) and maize FNR expressors (B-D) are presented in comparison to the wild-type (red). In the *fnr1* mutant plants, I previously observed that almost

all of the remaining *At*FNR2 is indeed located at the margin and we know that *At*FNR2 does not interact with either tether in the absence of *At*FNR1. Indeed, we see that the NADP(H) fluorescence trace for these plants (presented in figure 8.2A in black) shows a sharp rise upon illumination and then a less pronounced slow rising phase, which confirms the hypothesis. In contrast, we should see a lower initial efficiency of FNR in genotypes where there is a higher FNR density at the lamellae. As described in chapter 5.2, this is true for *fnr1*ZmFNR2 plants (trace presented in figure 8.2C in black), that show a significantly smaller initial, rapid rising phase in $NADP^+$ reduction, but a longer slow rising phase. This data suggests that the second, slower increase in $NADP^+$ reduction efficiency is likely due to a movement of lamellae tethered FNR to the margins due to weakened tether interactions as a result of the rising stromal pH. *Zm*FNR1 exhibits a very strong binding affinity to the tether TROL (figure 3.3), while the membrane binding behaviour of *Zm*FNR3 is so weak that it cannot be detected by BNP (although some membrane bound *Zm*FNR3 was visible on western blots, see chapter 3.1). The *fnr1*ZmFNR1 and *fnr1*ZmFNR3 plants show a similar distribution of FNR with equal densities at the lamellae and the margins (see chapter 5.2), so any difference we see between them might indicate whether the strength in interaction with a tether or the membrane influences the $NADP^+$ reduction kinetics. *fnr1*ZmFNR3 plants show very similar kinetics to those that can be observed for the wild type (see figure 8.2D). In contrast, *fnr1*ZmFNR1 plants (figure 8.2B) have a shorter fast rising phase than the wild type, followed by a longer slow rising phase that curiously reaches a plateau quicker than the wild type. Therefore, it is likely that the change in activity of FNR is indeed influenced by the binding strength to the tether/membrane.

Electron flow around the photosystems After establishing that FNR location influences the kinetics of $NADP^+$ reduction, I moved on to analyse the impact of this on the electron transport chain. The photosynthetic electron flow around both photosystems was observed by measuring chlorophyll fluorescence and P_{700} reduction state in dual-pulse amplitude modulation experiments upon illumination after dark adaptation. The measured parameters of dark fluorescence yield (F_o), maximal fluorescence yield (F_m) at different time points and - analogous to that - the amount of reduced P_{700} (P_{700}red) and the maximal P_{700} change (P_m) at different time points facilitate the calculation of a range of photosynthetic parameters.

Initially, the effective quantum yields of both PSI (Y(I)) and PSII (Y(II)) of the genotypes were calculated and compared (figure 8.3). Remarkably, in steady-state after a few minutes of illumination, all five genotypes show very little difference in effective quantum yields, regardless of the location of FNR. However, differences can be seen within the first two minutes of illumination, correlating with the time period in which differences in $NADP^+$ kinetics were seen (figure 8.2). Yields are increased in *fnr1*ZmFNR2 and *fnr1*ZmFNR3 genotypes compared to the wild-type and *fnr1* mutant between 0-60 seconds for Y(I), and between 30-120 seconds for Y(II). Such a pattern of initial impact at PSI, followed by an effect on PSII down the line might be expected of changes in FNR, which is functionally associated with PSI. The *fnr1*ZmFNR1 plants show a decrease in Y(I) and Y(II) compared to the wild-type. Again, these differences are pronounced between 0-60 seconds for Y(I), and between 30-120 seconds for Y(II). However, the ratio of Y(I) over Y(II) stays very consistent when the genotypes are compared, apart from the 5 seconds measuring point. The higher this ratio is, the more electrons that do not originate from

PSII are fed into PSI and therefore high values might indicate CET. These differences in photosystem efficiency could reflect different flux through the electron transport chain to NADP(H) via FNR.

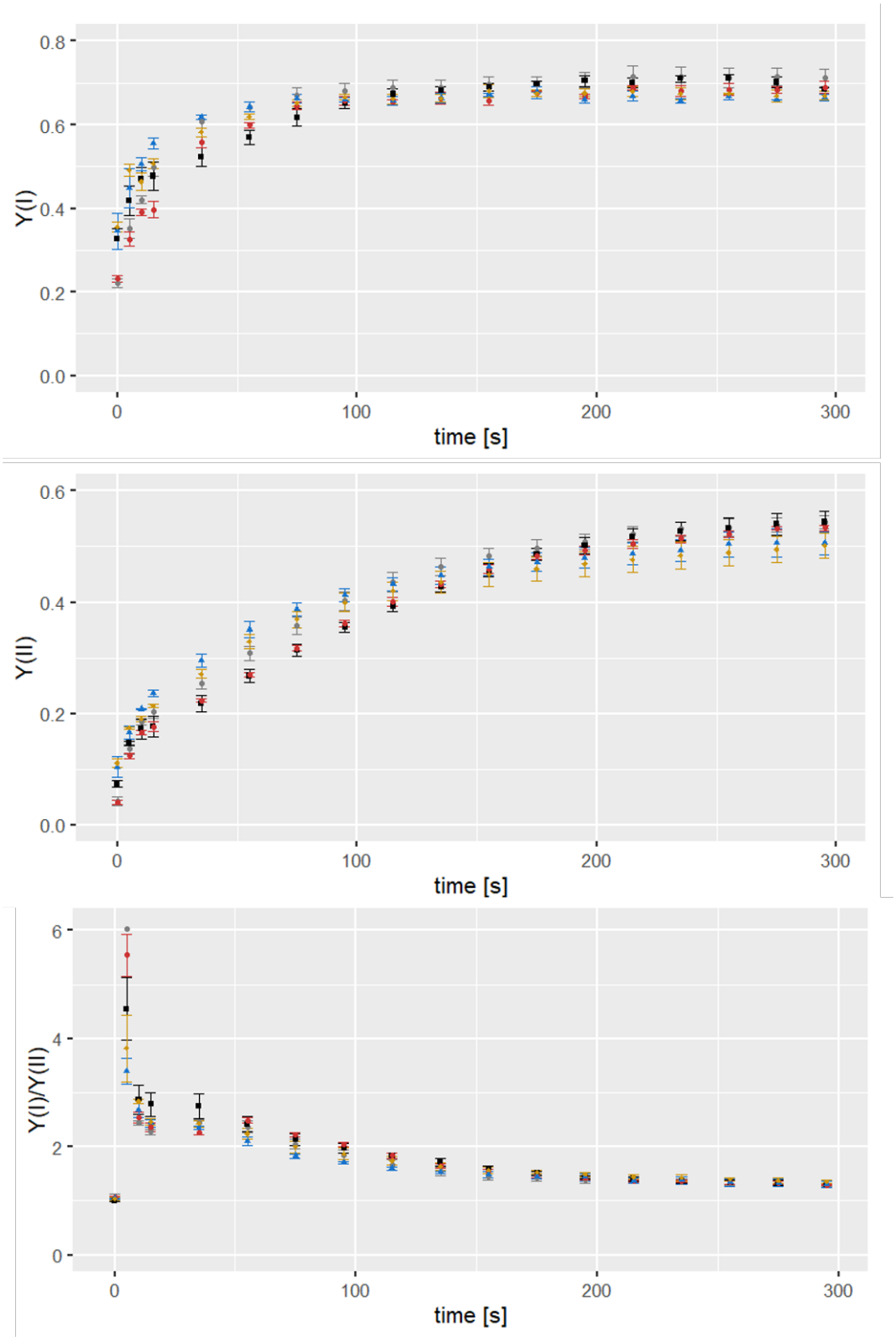

Figure 8.3: **Effective quantum yield of PSI and PSII and ratio of the effective quantum yield of PSI over PSII.** The values were calculated from dual-pulse amplitude modulation measurements. Y(II)=(F_m'-F)/F_m' and Y(I)=1-Y(ND)-Y(NA). WT = grey, *fnr1* = black, *fnr1*ZmFNR1 = red, *fnr1*ZmFNR2 = blue, *fnr1*ZmFNR3 = yellow.

At the same time, the photochemical quenching coefficient (qL) and the non-photochemical quenching (NPQ) were monitored (figure 8.4). The fraction of open reaction centres at PSII is higher in *fnr1*ZmFNR2 and *fnr1*ZmFNR3 in the first two minutes of the measurement, compared to *fnr1* mutants or *fnr1*ZmFNR1 plants, which exhibit similar or slightly lower levels than the wild-type. This suggests that the photochemical efficiency is higher when FNR is bound to Tic62 or bound weakly. It is interesting that *fnr1*ZmFNR2 and *fnr1*ZmFNR3 plants also show higher values in the first 20 seconds of the estimation of the photoprotective mechanism non-photochemical quenching (NPQ), while the *fnr1*ZmFNR1 plants show the same NPQ as the wild-type. After about 40 seconds, the *fnr1* mutant has considerably higher NPQ compared to the other genotypes until the value decreases at about 3 minutes. Also the *fnr1*ZmFNR1 plants show a slightly higher level of NPQ in this time range. Again, the values reach a steady-state after 5 mins with little differences in the genotypes for both qL and NPQ. This data suggests, that FNR location influences the dynamics of electron transport depending on the period of illumination.

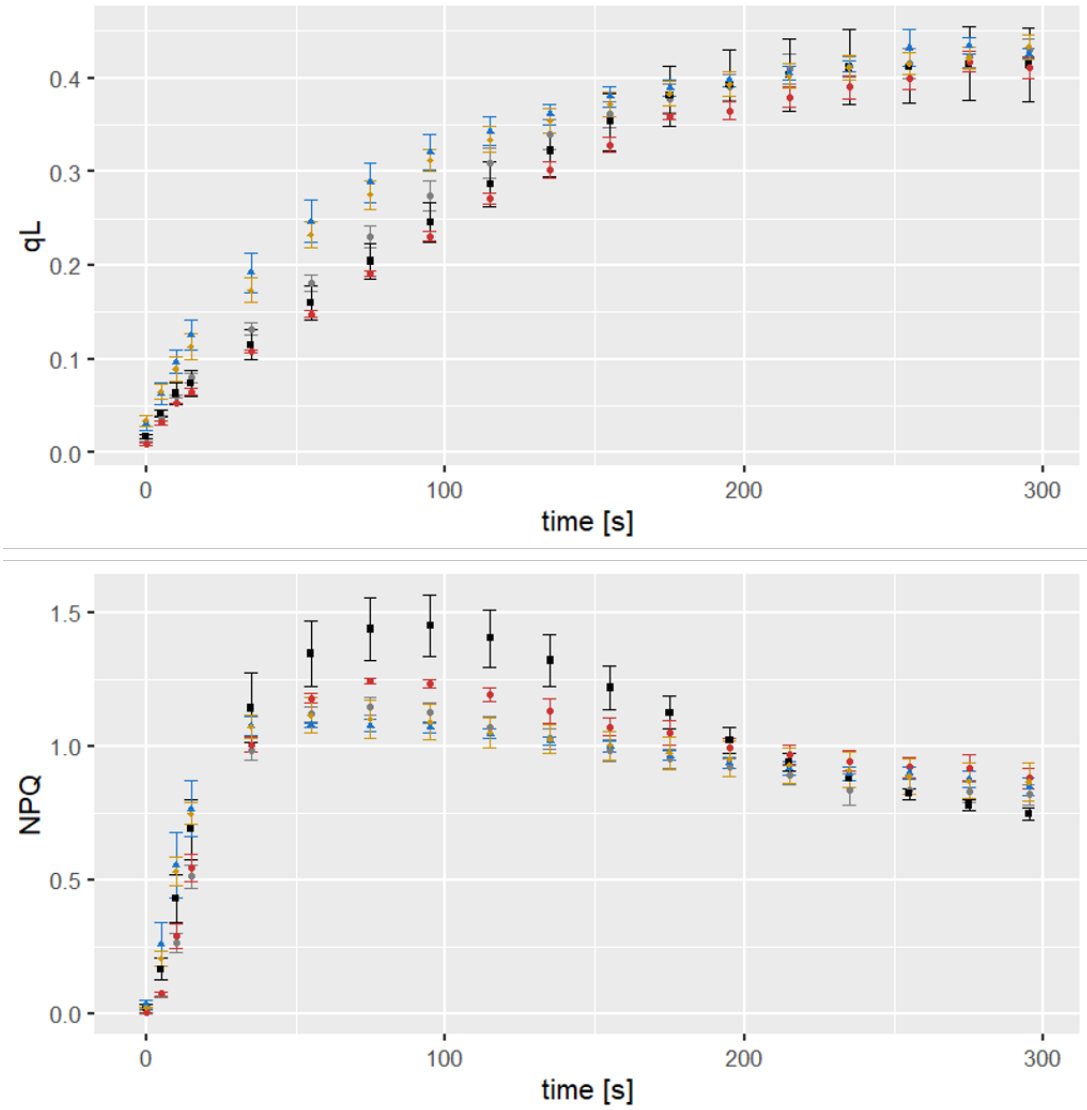

Figure 8.4: **Quantum yield of PSII: qL and NPQ.** Photochemical quenching coefficient qL=(F_m'-F)/(F_m'-Fo')xF_o'/F. Non-photochemical quenching NPQ = (F_m-F_m')/Fm'. WT = grey, *fnr1* = black, *fnr1*ZmFNR1 = red, *fnr1*ZmFNR2 = blue, *fnr1*ZmFNR3 = yellow.

The non-photochemical quantum yield of PSI can be expressed in the two values that are both calculated from P_{700}red: Y(ND) is interpreted as donor side limitation and Y(NA) is a measurement of limitation at the acceptor side (Walz GmbH [2009]). Again, the biggest differences among the genotypes can be observed in the first

40 s upon the onset of light. The *fnr1*ZmFNR1 plants show low donor and high acceptor limitation, a pattern that is opposite to the *fnr1*ZmFNR2 and *fnr1*ZmFNR3 plants, which have low limitation in acceptors and high limitation on the donor side. This might indicate that the electron flow in *fnr1*ZmFNR1 plants is either slowed down due to the acceptor ferredoxin not being re-oxidised fast enough by lower FNR activity, or that electrons are flowing back into the system by CET. At the same time, *fnr1*ZmFNR2 and *fnr1*ZmFNR3 plants are more limited from the donor side although they show a higher photochemical quenching and more quantum yield at PSII (see 8.3). A high acceptor availability would indicate that oxidised Fd is replenished quickly by these isoforms, due to effiecient reduction of $NADP^+$ by FNR .

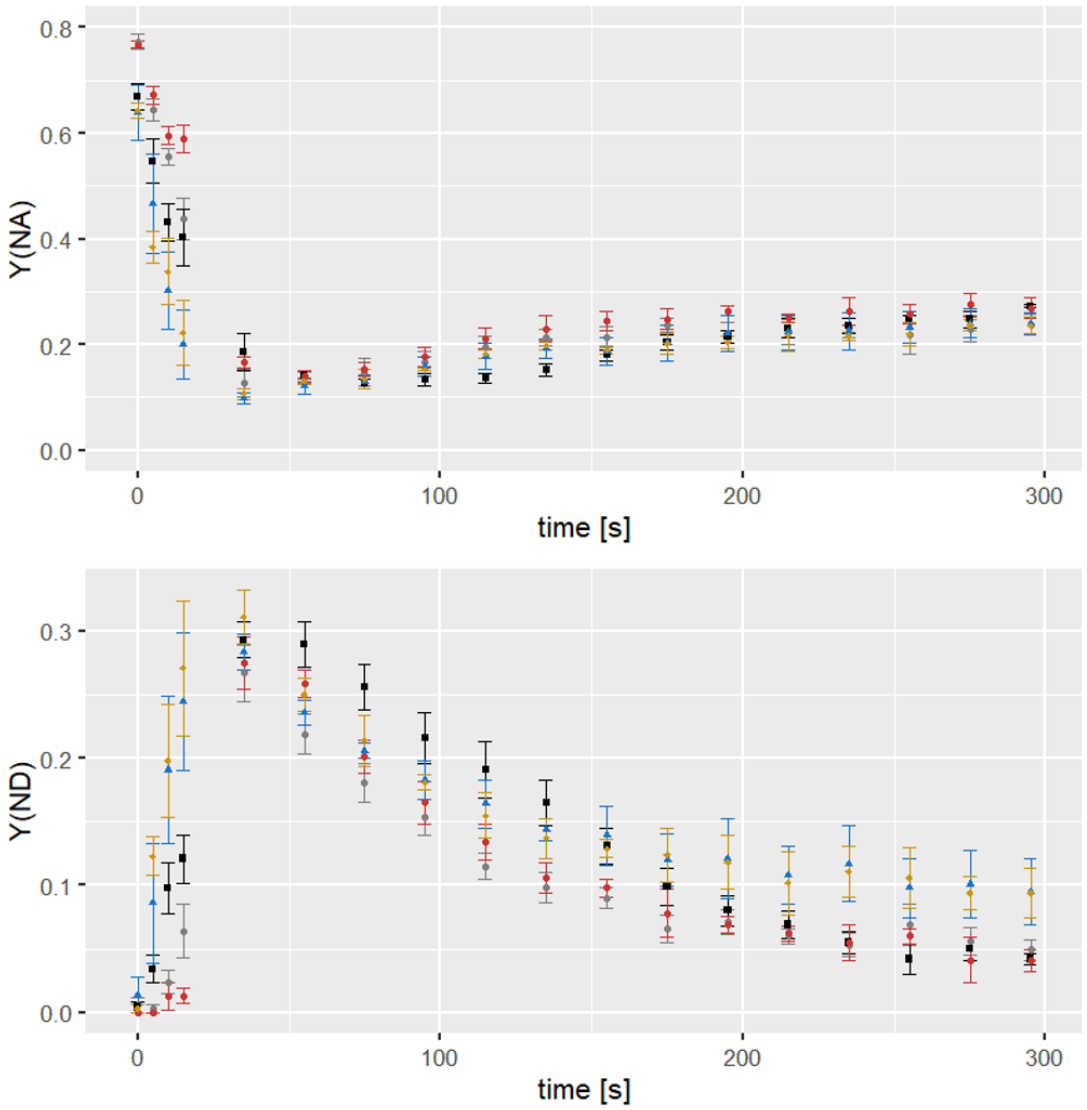

Figure 8.5: **Non-photochemical quantum yield of PSI.** Y(ND)=1-P_{700}red., Y(NA)=(P_m-P_m')/P_m. WT = grey, *fnr1* = black, *fnr1*ZmFNR1 = red, *fnr1*ZmFNR2 = blue, *fnr1*ZmFNR3 = yellow.

Reduction of P_{700} The previous measurements revealed that electron transport around PSI differs between the genotypes in regard to donor and acceptor side limitation. However, we do not know whether this is a consequence of variation in FNR $NADP^+$ reduction activity, electron diversion into CET or upstream regulation at PSII. Therefore, I measured the capacity of these plants to conduct

CET. It has previously been reported that CET is elevated in *fnr1* plants (Hanke et al. [2008]) when P_{700} reduction is more prominent following high light treatment. Lintala et al. [2012] also reported a higher rate of P_{700} re-reduction in *fnr1*x*fnr2* double mutant plants. I measured the reduction state of P_{700} under far-red light. As PSII will not supply electrons under these conditions, a more reduced P_{700} most likely reflects increased return of electrons via cyclic flow. A value of 0 indicates fully oxidised P_{700} and a value of 1 indicates fully reduced P_{700}, which is normally the case in dark state. In the dark, when FNR location is expected to be most varied between genotypes, all genotypes show a P_{700} reduction at the same level (see figure 8.6). However, after 15 min of high-light incubation, P_{700} reduction is increased for all genotypes, indicating that either more electron donors are available, or that electrons are being reintroduced into the electron transport chain by CET. This makes sense in regard to light induction of CET as a stress-response valve for excess light. However, there are differences in the extent of P_{700} reduction: wild-type and *fnr1*ZmFNR1 plants show a similarly small increase, whereas *fnr1*, *fnr1*ZmFNR2 and *fnr1*ZmFNR3 exhibit more reduced P_{700}. The big increase in *fnr1* mutant plants could be explained by the overall lower amount of FNR, possibly leading to a slower reconstitution of oxidised Fd and diversion of these electrons into CET by default. However, the maize FNR expressor plants contain the same amount of total FNR as the WT, so any changes we can observe should be an effect of localisation. Therefore, the increase of active PSI in *fnr1*ZmFNR2 and *fnr1*ZmFNR3 could mean that more electrons are flowing back into the ETC via cyclic flow, either because CET pathways have been upregulated or because more stromal reductant is available for re-introduction into the chain by CET. This

idea is supported by the earlier measurements that these genotypes are not acceptor limited and therefore re-oxidation should not be slowed down on this side (figure 8.5).

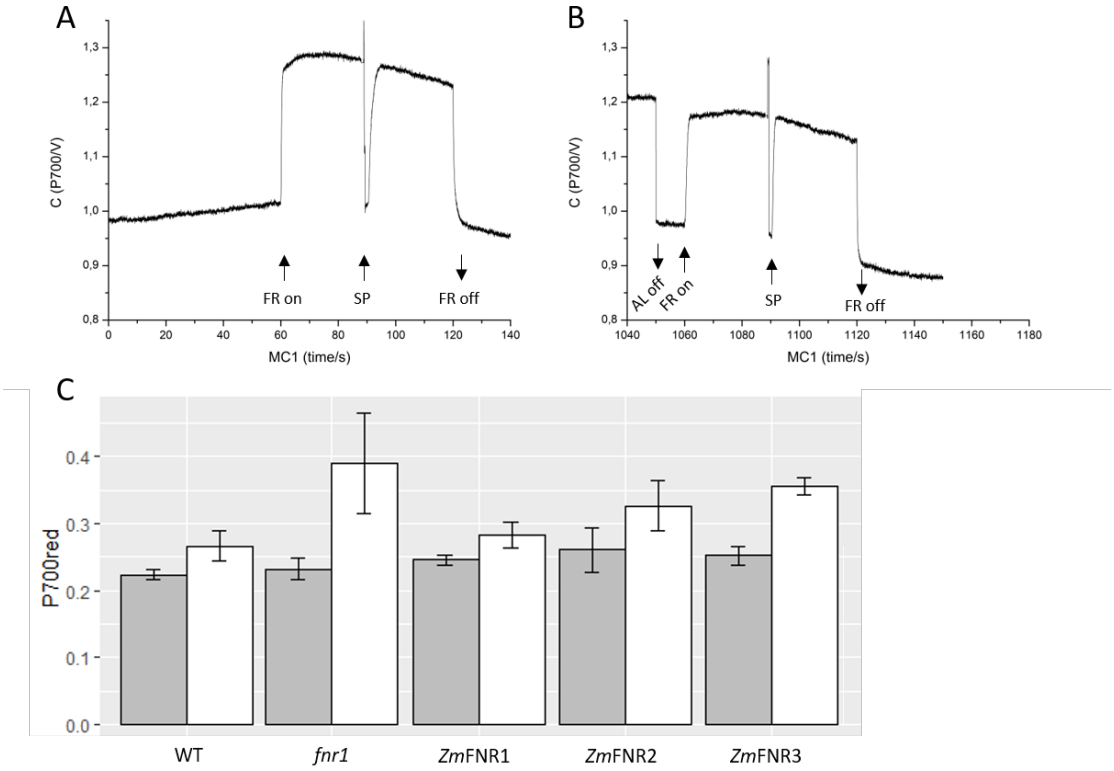

Figure 8.6: **PSI dependent P_{700} re-reduction.** (**A**) Example trace of P_{700} reduction kinetics after dark incubation. (**B**) Example trace of P_{700} reduction kinetics after 15 minutes of high-light treatment. (**C**) The reduction state of P_{700} under far-red light was measured in leaves of four dark incubated plants (grey) and in a leaf of four high-light incubated plants after 15 min (white). Error bars indicate standard error.

8.2 Fluctuating light conditions change electron transport

The photosynthetic measurements suggested that any changes between the different genotypes are most distinct within the first minute of illumination. This raises the idea that FNR location might play a role in a plants adaptation mechanisms to changing light conditions. This is also in line with the proposition that FNR acts in

the distribution of electrons between LET and CET discussed in the introduction chapter 1.2.2 and the results chapter 3.4. In fluctuating light, the plants also show a different fresh weight as discussed before, with *fnr1*ZmFNR1 coping best in these conditions (see figure 3.7).

Therefore, we repeated these photosynthetic measurements on plants grown in fluctuating light conditions. However, to ensure that there is no drastic up- or downregulation in content of the components of the electron transport chain, we analysed representative proteins of different thylakoid complexes via western blots presented in figure 8.7. The blots are comparable to the analysis of the plants grown in constant light conditions (figure 3.4) and no drastic changes in protein content are observable, although PsbA seems to be slightly increased and PsaD seems to be slightly decreased in *fnr1*ZmFNR2 and *fnr1*ZmFNR3 plants. This might indicate that these genotypes respond to fluctuating light conditions by balancing the content of the two photosystems.

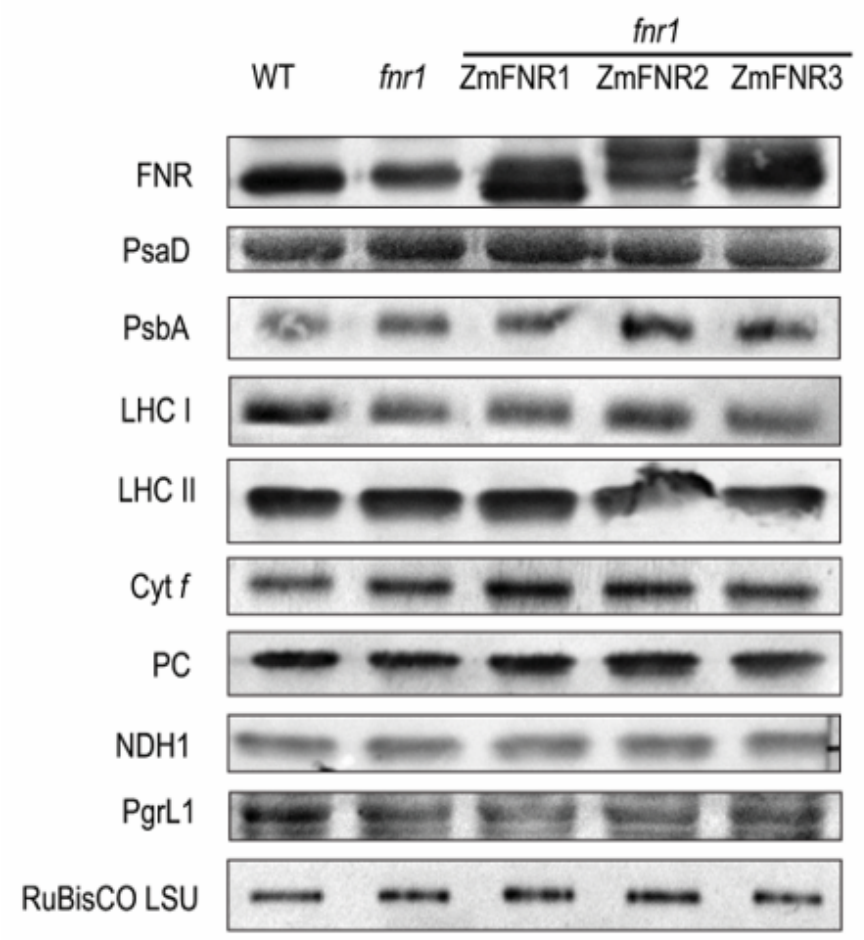

Figure 8.7: **Abundance of photosynthetic components in wild-type and transgenic Arabidopsis grown in fluctuating light.** Leaf extracts or isolated chloroplasts (indicated by cross) were normalised for equal protein content and separated by SDS-PAGE and transferred to a PVDF membrane via western blotting. The membranes were immunodecorated with indicated antisera and the protein was detected via colorimetric changes caused by secondary antibody-conjugated alkaline phosphatase.

I repeated the measurements that are described in section 8.1 on plants grown in fluctuating light conditions, but receiving the same total exposure of photons. I plotted the fluctuating light data onto the previously measured traces in stable light in order to evaluate the change in each parameter for each individual genotype. This could provide information about the response capacity of the plants to fluctuating light: Little or no difference between the conditions

would mean that the capacity to change in response to growth in fluctuating light conditions is either exhausted, or that there is no pressure that requires changes in these parameters, whereas a larger difference between the traces would indicate a greater regulatory response is induced. The most interesting changes can be observed in Y(ND) and Y(NA) (see figure 8.8) and will be discussed in this section, but the full comparison of the datasets for the other parameters can be found in the appendix (see section 11.2).

When comparing the donor limitation of plants grown in the two different light conditions, it becomes evident that there are little changes between growth conditions observable in the wild-type (figure 8.8A), but that *fnr1* mutant plants show a faster induction of Y(ND), dropping to less limitation at the donor site of PSI in fluctuating light (figure 8.8B). These plants might be primed for increased electron cycling as a coping mechanism to the fluctuating light. The maize FNR expressor plants consistently show a decreased donor limitation in steady state conditions (figure 8.8C-E).

Wild-type plants cope with fluctuating light conditions in a way that decreases the acceptor side limitation compared to plants grown in stable light conditions (figure 8.9A), suggesting that the acceptor Fd is re-oxidised quickly by high FNR activity levels or an increase of downstream acceptors. The *fnr1* mutant plants grown in fluctuating light show the same tendency, but fail to keep the acceptor limitation as low as the wild-type after about two minutes of illumination, possibly due to a lower overall FNR content (figure 8.9B). However, it becomes evident that *fnr1*ZmFNR1 are in turn less acceptor limited in fluctuating light compared to the plants grown in stable light (figure 8.9C). This suggests that this genotype is like the wild-type primed to keep up a fast re-oxidation rate of the accep-

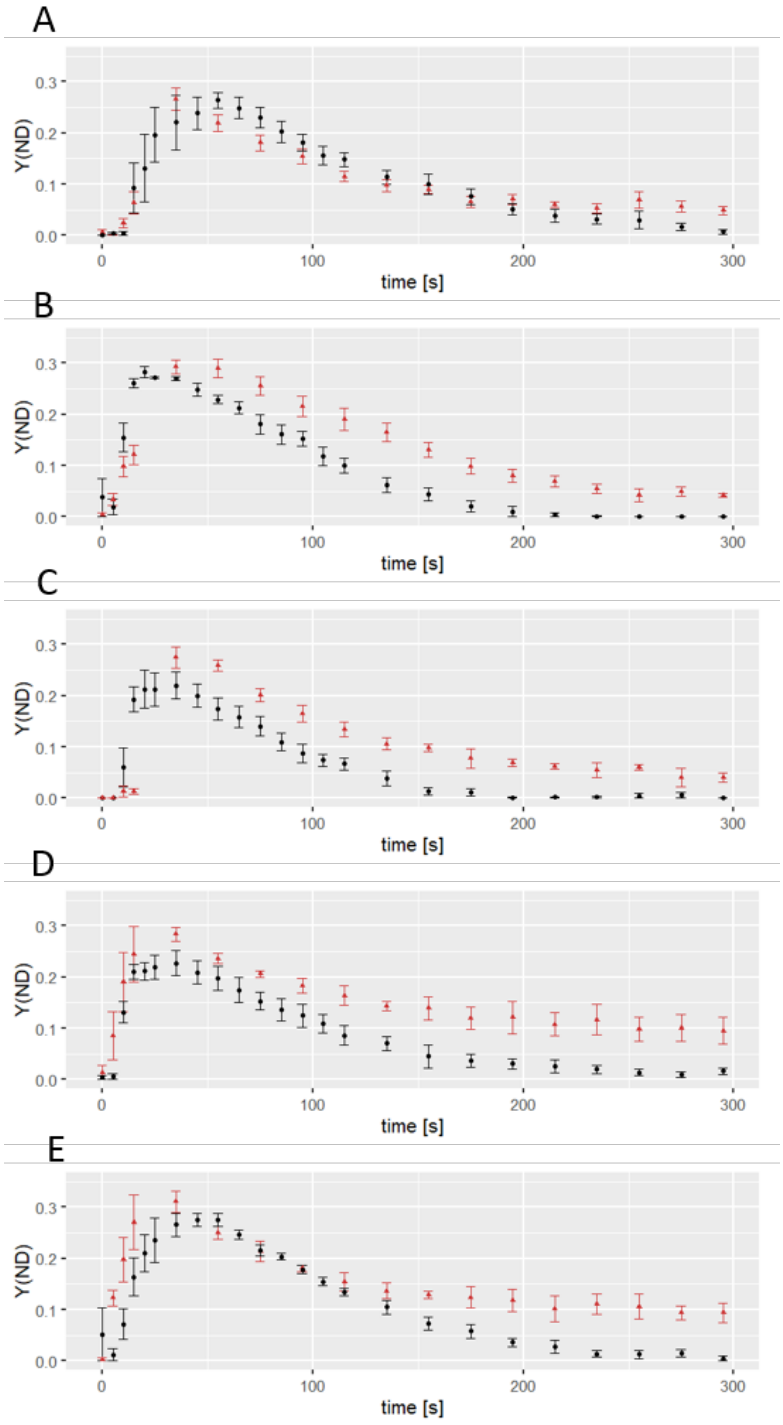

Figure 8.8: **A comparison of donor limitation at PSI in plants grown in stable and fluctuating light conditions.** A comparison of donor limitation at PSI in plants grown in stable (red trace) and fluctuating (black trace) light conditions. Y(ND)=1-P_{700}red. Wild-type (**A**), *fnr1* (**B**), *fnr1* ZmFNR1 (**C**), *fnr1* ZmFNR2 (**D**), *fnr1* ZmFNR3 (**E**).

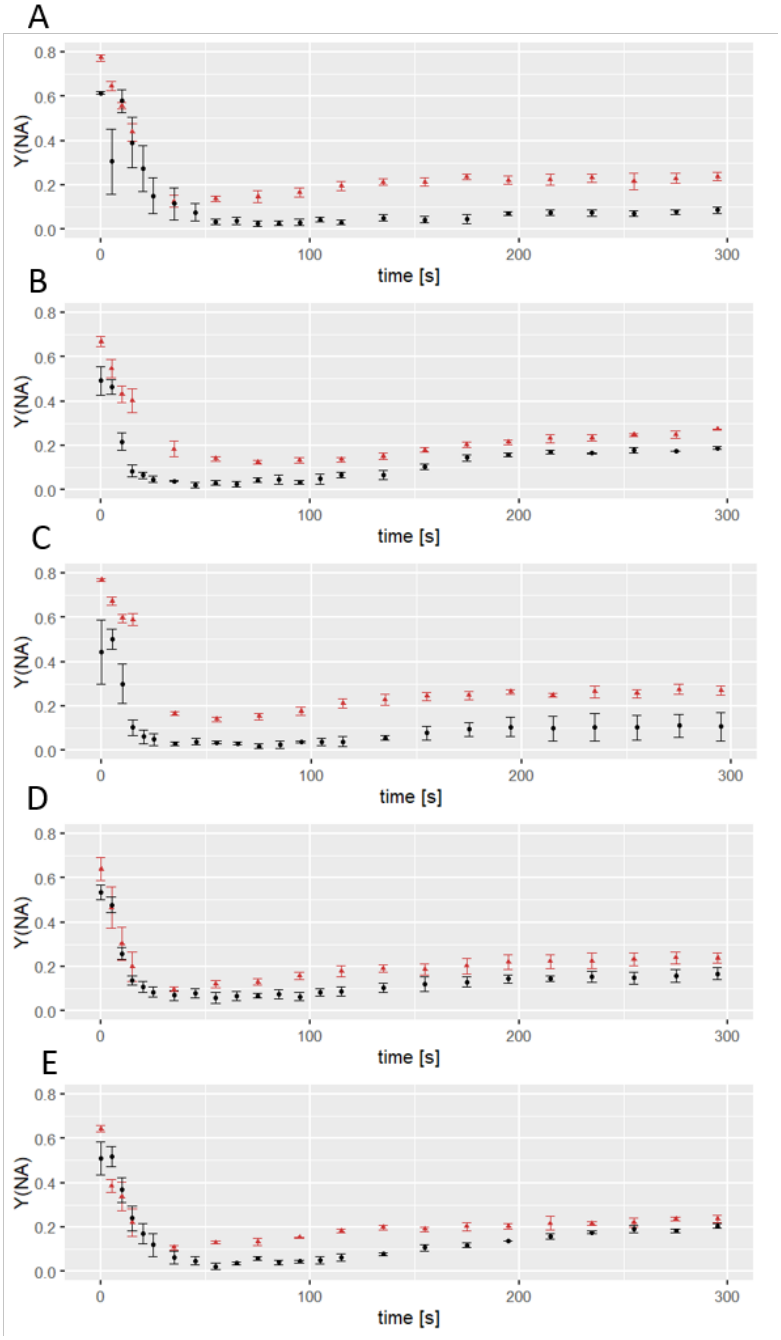

Figure 8.9: **A comparison of acceptor limitation at PSI in plants grown in stable and fluctuating light conditions.** A comparison of acceptor limitation at PSI in plants grown in stable (red trace) and fluctuating (black trace) light conditions. Y(NA)=(P_m-P_m')/P_m. Wild-type (**A**), *fnr1* (**B**), *fnr1*ZmFNR1 (**C**), *fnr1*ZmFNR2 (**D**), *fnr1*ZmFNR3 (**E**).

tor Fd or has more acceptors available in total. The differences of *fnr1*ZmFNR2 and *fnr1*ZmFNR3 between the two light conditions show little response in acceptor limitation (figure 8.9D and E).

The induction of both parameters in fluctuating light differs, with a faster response in *fnr1* plants compared to the wild-type. The same rapidity can be observed for *fnr1*ZmFNR1 plants, but not for *fnr1*ZmFNR2 and *fnr1*ZmFNR3, who show a wild-type like induction speed.

The responses of electron transport around PSI to a regime of fluctuating light therefore primarily seem to lead to decreased acceptor limitation in the wild-type, with no alteration of processes impacting donor limitation. The *fnr1* mutant seems to initiate a greater regulatory response, with faster initial changes in both parameters, followed by a steady state with the opposite trend to the wild-type - no change at the acceptor side but decreased donor limitation. This phenotype could not be completely rescued by introduction of any of the maize FNR proteins, with all showing higher steady state donor limitation. However, expression of *Zm*FNR1 in the *fnr1* background did rescue the lower acceptor limitation seen in the wild-type in steady state. Moreover, the introduction of *Zm*FNR3 to the *fnr1* line results in the only instance where initial increase in donor limitation is actually slower after growth in fluctuating light than in stable light.

9. General discussion

We have established that each maize FNR has unique tether-binding properties and the generated genotypes expressing them in the Arabidopsis *fnr1* genetic background are therefore ideal study objects for my investigation of location and function of FNR at different positions in the chloroplast. I will discuss my findings in the following chapter by examining each genotype individually with regard to FNR location, enzyme kinetics and electron flow. Moreover, I will pay special attention to the proposal that LET is spatially tied to the margin area of the thylakoid and CET happens predominantly at the lamellae, and the suggestion that FNR might act as an enzymatic switch between the two processes by channeling electrons into either pathway (Joliot and Johnson [2011]). I will start my analysis by explaining the biggest side-finding - that FNR is not soluble in the stroma.

9.1 FNR is not soluble

The most profound side-finding of my immunogold localisation studies of FNR is that there is no statistically significant fraction of FNR found in the stroma of any of the five genotypes in the dark (see figure 5.6). This is especially surprising for the *fnr1* mutant and

*fnr1*ZmFNR3 plants, as they show no FNR in the membrane fractions of analysed western blots (see figure 3.1) and therefore were described as having only soluble FNR. However, my finding suggests that the interactions of *At*FNR2 and *Zm*FNR3 with the membranes in these genotypes are possibly very weak and probably broken even by very gentle sample treatment, meaning that these FNR isoforms were misassigned as soluble proteins (e.g. Twachtmann et al. [2012] and Lintala et al. [2009], Lintala et al. [2014]). Even though this suggests that the interactions are very transient and therefore not detectable following mechanical separation of soluble and membrane fractions, the protein is presumably still held in place at the membrane without the need of strong binding to a tethering protein, by interactions that prevent diffusion of FNR into the stroma. The suggested remaining interaction sites for these isoforms of FNR are PSI (Andersen et al. [1992]), Cytb_6f (Zhang et al. [2001])and the thylakoid membrane itself (Grzyb et al. [2008], Grzyb et al. [2018]). The *fnr1* mutant plants only contain *At*FNR2 and do not show severe growth and seed yield limitations, which suggests that this isoform is sufficient to perform the bulk of LET in these plants and I therefore propose that it is likely located at the PSI. Taking into account the mainly margin-location of this isoform on the micrographs, this would support the idea that the margins (by my definition of a functional subcompartment comprising non-appressed membranes adjacent to appressed mebranes) are the thylakoidial domain where LET takes place.

The observation made by Benz et al. [2009] or Palatnik et al. [1997] that the proportions of soluble and membrane bound pools of FNR change in response to redox and pH changes would therefore mean that these changes do not actually have an impact on the

membrane location of FNR but more on the relative strength of the interactions and possibly the binding partners.

My finding contradicts the IG-labelling experiment by Negi et al. [2008], who found that FNR co-localises with GAPDH in the stroma. However, they do not present adequate controls and show no statistical analysis of their data, so this conclusion is questionable. In my own experiment I chose to keep the labelling density very low, because a high antibody concentration resulted in increased background signal. This is another factor that might distort their data. Indeed, van Thor et al. [2000] have performed an indirect IG-labelling of GFP-tagged FNR in *Synechocystis* with a similarly low labelling density and FNR was only found in immediate proximity to the thylakoid membrane. Furthermore, the absence of soluble FNR stands in contrast to Benz et al. [2009] who suggested that FNR-Tic62 can be stroma located as a complex and that this complex is also located at the inner envelope membrane. I did not see any significant amount of FNR in the inner envelope membrane and therefore this compartment was not analysed any further. However, the authors also employed the fractionation of chloroplasts to determine FNR content and distribution, and if transient FNR interactions are easily disrupted, there might be a significant amount of contamination into other fractions. Moreover, the thylakoid network connects to the inner envelope membrane for e.g. lipid synthesis (Wang and Benning [2012]) and there might be some co-isolation of thylakoid fractions with the envelopes.

9.2 The knock-out mutant *fnr1*

This knock-out mutant only contains *At*FNR2, which was previously thought to be soluble, but based on my results is loosely bound to

the thylakoids.

Growth and seed yield The biomass production in stable light conditions (figure 3.5) shows no statistically significant difference to wild-type plants. This also applies to plants grown in fluctuating light (figure 3.7), however the overall biomass production in all plants is roughly 80% lower than in stable light. This is another sign that only *At*FNR2 at the margins is enough to perform sufficient LET. The seed yield is slightly lower in stable light conditions (figure 3.6) when compared to the wild-type, but this difference is not statistically significant. Plants grown in fluctuating light conditions all show yields ranging about 30% of the harvest that stable light grown plants deliver, and there is no difference between the wild-type and the *fnr1* mutant plants (figure 3.8). Palatnik et al. [2003] reported that a downregulation of overall FNR content in tobacco increased susceptibility to oxidative stress. However, the mutants used in this thesis are specifically lacking *At*FNR1. Previous work by Lintala et al. [2007] has revealed that these mutant plants cope with cold-stress conditions and develop a wild-type like phenotype. This suggests that while a non-specific reduction of total FNR is detrimental to the stress response, we do not see the same effect when plants contain wild-type levels of *At*FNR2 and are just deficient in *At*FNR1.

Thylakoid location As described earlier, there is no soluble FNR in the stroma (figure 4.6). Statistically, there is no difference between the labelling densities of the margins and the lamellae, but we see a very high spread in the values of the margin densities, that impacts the p-value and the difference of labelling density between margin and lamellae is higher than that between the stroma or grana and

lamellae (figure 5.6). The remaining *At*FNR2 is mainly located at the grana margins and only very little at the lamellae. I regard this as an indicator that margin-bound *At*FNR2 is sufficient for LET and this explains, why this mutant is able to survive despite the fact that Hajirezaei et al. [2002b] have found a high control coefficient for FNR in tobacco when analysing FNR-antisense plants. More strongly membrane bound FNR in general and lamellae-bound FNR in particular might therefore serve another purpose. It is worth mentioning, that the *fnr1* mutant is the only genotype where a slight shift in total area coverage of different chloroplast regions can be observed, with a higher percentage of stroma and a lower percentage of margin coverage, showing a response on the thylakoid-architectural level (figure 5.4).

$NADP^+$ reduction Previous work in cyanobacteria has revealed that the $NADP^+$ reduction kinetic follows a two-phased rate (Kauny and Sétif [2014]). In the *fnr1* mutant genotype, we only see the rapid reduction phase in $NADP^+$ reduction kinetics with a greatly decreased contribution of the slower second phase (figure 8.2). Based on this, it seems likely that the slow phase corresponds to an increase in catalytically efficient FNR, following its pH dependent release from TROL and Tic62. This means, that in *fnr1* during the first seconds of illumination, the AtFNR2 is instantaneously available for $NADP^+$ reduction and there is little later pH-dependent release. This fits well with the BNP western blots, showing that *At*FNR2 does not bind to any tether (figure 3.3) and the IG-labelling that shows *At*FNR2 location mainly at the margins (figure 5.6). Moreover, this strongly suggests that the remaining *At*FNR2 is located at PSI and therefore in its active location to begin with. This would support the findings

of (Andersen et al. [1992]), who co-purified FNR in a complex with PSI.

Electron transport The deletion of *At*FNR1 has no drastic effects on growth and seed yield in both light conditions tested (figures 3.5, 3.7, 3.6 and 3.8), indicating that it does not put a significant stress on the plants. It has been previously reported by Hanke et al. [2008] that the oxidation state of P_{700} in *fnr1* plants is more reduced following 15 min of high-light (HL) incubation. This was interpreted as a capability of these plants to perform increased CET. I was able to confirm this finding and observed a much more reduced P_{700} than is the case in wild-type plants (figure 8.6). Following HL conditions, P_{700} in wild-type stays oxidised under far-red light, presumably because of the pH-dependent short-term feedback regulation that happens by downregulation of the Cytb_6f at high pH-gradient to prevent damage at PSI (Laisk et al. [2005]) by excess electron pressure. The increased reduction state of P_{700} in *fnr1* plants in HL conditions may therefore represent a regulatory failure to induce photosynthetic control, rather than increased CET.

It has been suggested by Walz GmbH [2009] that measurement of the electron flow around PSI can be used as a way of investigating CET with a low donor limitation and high acceptor limitation indicating increased CET and a high donor limitation and a low acceptor limitation indicating decreased CET. We know from the western blots (figure 3.4), that the amount of known components of the two different CET pathways (PGRL1 and NDH-SU) do not change in abundance between the genotypes, so this will not contribute to any observed changes, but changes would rather be due to FNR location/binding or regulation of these pathways. If a knock-

out of *fnr1* would have an effect on CET, this should be reflected in the Y(ND) and Y(NA) values of these plants compared to the wild-type. Immediately after dark, we can observe higher Y(ND) and lower Y(NA) values in the *fnr1* mutant plants compared to wild-type plants (figure 8.5). This means that less electrons are arriving at the donor side of PSI and they are less limited at the acceptor side than in the wild-type plants. In steady state conditions after 5 min of low actinic light, the difference between *fnr1* mutant and wild-type plants disappears. This indicates, that plants lacking *At*FNR1 do not perform more CET, indeed less electrons are arriving from PC directly after the onset of illumination when wild-type plants induce CET (Joliot and Joliot [2008 Jul-Aug]). This further endorses the idea that the high P_{700} re-reduction observed under HL conditions in this genotype might rather be due to an impaired Cytb_6f downregulation than increased CET. Munekage et al. [2002] and Joliot and Joliot [2002] have also found P_{700} in pgr5 and pgrl1 mutants to be constantly reduced in HL conditions. This might be an indication that *At*FNR1 is involved in the same mechanism.

9.3 The TROL-bound *fnr1* ZmFNR1

The TROL-bound *Zm*FNR1 does not recruit the remaining *At*FNR2 back into a strong dimer-tether interaction (figure 3.1). Almost all of the FNR visible on the BNP is located at TROL (figure 3.3) and just very small amounts can be detected in some of the high-molecular weight complexes which are suggested to contain Tic62 (Benz et al. [2009]). In the wild-type, there is much less FNR found at the tether TROL, which suggests that the *Zm*FNR1 binds stronger to TROL than the Arabidopsis isoforms.

Growth and seed yield In stable light conditions, all maize FNR expressor plants perform better than the wild-type and *fnr1* mutants in terms of biomass production (figure 3.5). As *At*FNR2 seems to be sufficient to provide LET, any additional FNR might enhance growth and the lost flexibility in binding behaviour might actually be beneficial in stable light conditions. In fluctuating light, this genotype is the only one who can retain this improved growth compared to the wild-type and *fnr1* mutant (figure 3.7). TROL-bound FNR seems to therefore have a positive effect in plants grown in fluctuating light. However, this increased biomass does not translate into increased seed in fluctuating light (figure 3.8) and the seed yield even suffers in *fnr1* ZmFNR1 plants in stable light conditions compared to the wild-type (figure 3.6). This suggests that any beneficial effect mainly acts during the vegetative state of the plants with no knock-on effect during reproduction and that this genotype has a poor resource allocation under stable light, inefficiently channelling its photosynthetic power into growth processes.

Thylakoid location In the *fnr1*ZmFNR1 genotype, we can observe an evenly distributed signal density of FNR between the margin and lamellae, which resembles that of the wild-type plants (figure 5.6). However, although FNR is seemingly distributed as in wild-types, the binding behaviour of the two FNR isoforms differs. *Zm*FNR1 is strongly bound to the tether TROL, while *At*FNR2 is not recruited back into a strong binding FNR-dimer (figure 3.1) to form a complex with the TROL tether. I therefore propose, that *At*FNR2 remains mainly in the margins as in the *fnr1* background genotype, while the additional TROL-bound *Zm*FNR1 binds to the tether in the lamellae and also the margin regions. This means that the lamellae-bound FNR is likely in a complex with TROL. In the LSFM immunofluorescence experiment, we also see the strongest TROL-FNR correlation in this genotype (figure 6.8), which confirms this finding. The co-localisation experiment deserves some additional thoughts here. A lower co-localisation of TROL and chlorophyll in the maize FNR expressor plants would indicate that TROL moves into the lamellae in certain circumstances, because the chlorophyll that is in the lamellae is not detected in this experimental setup. This is detected in all maize FNR expressor plants, which suggests that the direct interaction of FNR with the TROL protein is not the trigger for this movement, and the reasons for this remain unclear.

$NADP^+$ reduction In *fnr1*ZmFNR1 plants, we see a shorter fast reduction phase and a longer second, slow reduction phase than in the wild-type plants (figure 8.2). Furthermore, the plateau is reached more quickly. This is the only genotype that does not fit a two-component model well (C. Duffy, personal communication). The location and binding behaviour of *At*FNR2 should not have changed

in this genotype and I therefore suggest that the fast rising time in the $NADP^+$ reduction can be assigned to the activity of this isoform. We know from Alte et al. [2010], that the release of FNR from the tethers happens in a pH-dependent manner and that binding between FNR and TROL is stronger than between FNR and Tic62. Therefore faster release of FNR would contribute to the increased activity of the slow reduction phase. The pH-dependent release of two, potentially independent FNR tether interactions (strong *Zm*FNR1-TROL and weak putative *At*FNR2 interactions) may be the cause of these complex kinetics. Although the kinetics differ between wild-type and *fnr1*ZmFNR1, the signal densities of FNR in the margin and lamellae are the same, therefore it is more likely that the binding strength to the tether and pH-dependent release of FNR rather than the absolute location cause the difference in kinetics.

Electron transport The introduction of *Zm*FNR1 into the *fnr1* genetic background rescues the phenotype of far-red induced P_{700} reduction kinetics (figure 8.6). Even in HL, P_{700} is re-reduced only to a small extent, just as is the case in wild-type plants. This raises the idea that TROL-bound FNR might be required to keep this PSI protective mechanism functional. Photosynthetic control is dependent on the generation of a high pH gradient (Joliot and Johnson [2011], Tikhonov [2015]). These plants show a slightly higher NPQ induction than the wild-type when grown in stable light conditions, proving that they are capable of building up a higher pH gradient in these conditions in principle (figure 8.4). This is in line with the observation that donor limitation is lower in these plants at the onset of illumination compared to wild-type plants (figure 8.5), indicating a comparatively higher electron influx which might be caused by

CET. In steady-state conditions however,they show no difference to the wild-type. These findings combined indicate that *fnr1*ZmFNR1 plants are able to divert electrons into CET on the onset of illumination while simultaneously maintaining the ability to downregulate the Cytb_6f to protect PSI from overreduction and possible damage or ROS formation at hight light intensities.

TROL-bound FNR might be situated at Cytb_6f for its function in CET induction and PSI photoprotection. Furthermore, Jurić et al. [2009] suggested that the rhodanese-like domain of TROL might be able to interact with PQ and stated that a lack of TROL leads to increased reduction of the PET chain at high light intensities, which would match the hypothesis that TROL-bound FNR might play a role in photosynthetic control, possibly in combination with PGR5 and PGRL1 (see section 9.2). This could either be caused by the inability to build up a sufficient pH gradient in the absence of TROL in the first place or a secondary, unknown mechanism. When grown in fluctuating light, the plants in contrast become donor limited more quickly compared to grown in stable light conditions, but they also relax more quickly (figure 8.8). This might indicate that *fnr1*ZmFNR1 plants are able to react faster because there is more FNR in a complex with TROL. This would explain, why the *fnr1*ZmFNR1 plants outperform the other maize FNR expressor plants in fluctuating light in terms of biomass production.

9.4 The Tic62-bound *fnr1* ZmFNR2

This genotype has no or barely detectable levels of TROL-bound FNR. All the tightly bound FNR is located at Tic62 complexes, but to a lesser extent than is the case in wild-type plants (figure 3.3). This is the only genotype that is able to recruit the remaining *At*FNR2 back into a tightly bound tether interaction as a heterodimer (figure 3.1). There is a possibility, that ZmFNR2 can form a homodimer, as it crystallizes as a dimer (Twachtmann et al. [2012]), but there is no direct evidence of this *in vivo*.

Growth and seed yield These plants are unremarkable in terms of biomass production and show similar levels of seed yield to wild-type and the *fnr1* genetic background in both growth conditions (figures 3.5, 3.7, 3.6 and 3.8).

Thylakoid location *fnr1* ZmFNR2 is the only genotype where there is a statistically significant difference between the margin and lamellae signal density, showing a higher density of FNR at the lamellae than at the margins (figure 5.6). This suggests that the introduced *Zm*FNR2 binds to Tic62 situated at the lamellae and recruits some of the remaining *At*FNR2 into a heterodimeric complex at Tic62. The immunofluorescence experiment does not deliver much more information, because there was no suitable antibody for Tic62 at hand, but FNR in *fnr1* ZmFNR2 mutant plants correlates with TROL to a lesser extent than the FNR in *fnr1* ZmFNR1 genotype (figure 6.8), which is consistent with the BNP.

$NADP^+$ reduction The *fnr1* ZmFNR2 plants show a lower initial efficiency of FNR with a much smaller initial rapid reduction phase

compared to the wild-type (figure 8.2). This could be because the *At*FNR2 recruited to Tic62 is not immediately available for $NADP^+$ reduction. In turn, a greater relative slow reduction phase is observable, which might correspond to a slow, pH-dependent release of FNR from the tether Tic62, as proposed by Alte et al. [2010].

Electron transport The far-red P_{700} reduction in HL is ambiguous in *fnr1*ZmFNR2 plants (figure 8.6). They show a tendency to be more reduced after HL treatment, but the standard error is quite high so more repetitions are necessary to evaluate whether the difference between dark and HL is bigger than in the wild-type. These plants show a lower NPQ than the wild type (8.4), suggesting that less CET is happening to build up a pH gradient and the electrons are rather channelled into LET. This is interesting, because $NADP^+$ reduction kinetics indicate that they initially have less free *At*FNR2 available to perform LET (figure 8.2). However, this could mean that in the dark, *At*FNR2 and *Zm*FNR2 are recruited by Tic62 and are rapidly released upon illumination to be available for $NADP^+$ reduction in LET. The *fnr1*ZmFNR2 has an overall higher donor limitation (figure 8.5), which reinforces the hypothesis that electrons are more favourably diverted into LET rather than CET.

9.5 The loosely bound *fnr1* ZmFNR3

*Zm*FNR3 is not visible on BNP, indicating that it does not bind strongly enough to a tether to withstand the detergent treatment necessary for BNP (figure 3.3). It is therefore also incapable of recruiting *At*FNR2 into such a complex.

Growth and seed yield In terms of biomass, these plants grow as well as the genotypes in stable light conditions and there is no statistically significant difference to the wild-type in fluctuating light conditions either (figures 3.5 and 3.7). However, the seed yield in these plants is significantly worse compared to the wild-type in stable light conditions (figure 3.6) and almost comes to a total breakdown in seed production in fluctuating light conditions (figure 3.8). This indicates that these plants are not disadvantaged in the vegetative state but are severely challenged during reproduction and the inability to recruit wild-type equivalent levels of FNR into stable complexes with TROL or Tic62 results in poor resource allocation or stress.

Thylakoid location Again, this is a genotype where, based on western blots, I did not expect FNR to be located at the thylakoid membranes, but just like for *At*FNR2 in the *fnr1* genotype background it can be observed that *Zm*FNR3 is strongly associated to the margins and lamellae (figure 5.6). Originally, it was postulated that these two isoforms cannot dimerise, because strong membrane binding is not restored, but there is a possibility that these two isoforms can still form a heterodimer that is very loosely attached to the membrane. As in the case of the *fnr1* mutant plants, the question arises as to how the two isoforms bind to the membrane. I stated before that for the *At*FNR2, PSI is a likely binding partner because the mutant

plants retain their ability to perform LET and this would also be the case for any *Zm*FNR3 that might be involved in LET. Although we see a slightly higher density of FNR signal in the lamellae, this effect is not statistically significant and it therefore resembles wild-type distributions. This indicates that a big part of the *Zm*FNR3 will be located at the lamellae, but a smaller pool of margin-bound *Zm*FNR3 is also conceivable in case this isoform is taking part in LET.

NADP$^+$ reduction Very surprisingly, the NADP$^+$ reduction kinetics in this genotype looks closest to the wild-type of all other genotypes (figure 8.2). If the initial fast reduction phase is assigned to *At*FNR2 activity again, then the second slow rising phase would show a slow induction of *Zm*FNR3 activity. This is interesting because the original proposition was that this reflects the mechanism of pH-dependent release from a tether. There are two possible interpretations of this: either there might be a pH-dependent effect on the loosely bound *Zm*FNR3 at the thylakoid, meaning that location, rather than binding partner is the principle cause of the slow component of NADP$^+$ reduction, or the slow rising phase in NADP$^+$ reduction is not due to pH-dependent release of FNR but of some other effect. It is possible that *Zm*FNR3 binds to Tic62 or TROL very transiently and that this effect is also pH-dependent.

Electron transport The high far-red P_{700} reduction after HL treatment that we can observe in the *fnr1* plants is not resolved in this genotype (figure 8.6). These plants also show a higher re-reduction in far-red, indicating that the mechanism that keeps P_{700} oxidised in the wild-type requires a strongly tether-bound (presumably TROL-

bound) FNR. It has been reported by Colombo et al. [2016] that Arabidopsis mutants lacking short-term regulatory processes like NPQ, state transitions or photosynthetic control are severely impaired in seed production in fluctuating light conditions and it is therefore possible that an the poor seed yield of these plants is a reflection of an impaired photosynthetic control mechanism. The electron transport in stable light conditions looks similar to that of the *fnr1*ZmFNR2 plants. In fluctuating light, the donor limitation of these plants is induced a bit later. This is contrary to what happens in *fnr1* and *fnr1*ZmFNR1 plants, so there might be another level of regulation involved.

9.6 Wild-type

With the newly gained knowledge that FNR is not truly soluble in the stroma, previous work that has divided the isoforms into soluble and membrane bound based on gel electrophoresis (Matthijs et al. [1986], Shin et al. [1985], Benz et al. [2009], Palatnik et al. [1997], Hanke et al. [2005], Okutani et al. [2005], Lintala et al. [2007]) should be revised. It is probably more accurate to divide into loose and strong membrane binding. Hereby, strong membrane binding is the association to the tethers Tic62 and TROL. Weak membrane binding is not so easily defined, but they might be transient interactions with PSI, Cyt b_6f or weak interactions with the tethers are also conceivable. Wild-type Arabidopsis chloroplasts contain two isoforms of FNR, with *At*FNR1 showing a stronger binding affinity to membrane tethers and *At*FNR2 more loosely bound, which is predominantly to the margin regions of the thylakoids when *At*FNR1 is absent as we now know. *At*FNR2 can be pulled back into a heterodimeric interaction with *At*FNR1 at the tethers. Both knock-out plants are viable (Lintala et al. [2009]), so both FNR isoforms can fulfill their function in LET. On the BNP, we can see that membrane-bound FNR is overwhelmingly located at Tic62 and only a small proportion at the TROL protein. It has been proposed before, that Tic62 binding is a way to store the inactivate FNR in the dark, possibly to prevent it from degradation (Benz et al. [2009]), and my findings support this idea, because we see a slow reduction of $NADP^+$ in *fnr1*ZmFNR2 expressing plants. I hypothesise that the FNR-TROL interaction might play an important role in the protection of PSI at high light intensities, because we can see this effect especially pronounced in *fnr1*ZmFNR1 plants. This would also explain, why we

only see very little TROL-bound FNR on the BNP in plants harvested in the dark. Furthermore, TROL-bound FNR might play a role in CET at the onset of light. My findings align with the hypothesis of Joliot and Johnson [2011] that FNR plays a crucial role in channelling electrons into CET or LET and plays a role in the photosynthesis control mechanism.

10. Conclusion and outlook

My work shows that FNR is solely located at the thylakoid membrane and its function is influenced by its binding partner, the binding strength and the sub-thylakoidial location. I performed the localisation studies on plants adapted in the dark, just like the biochemical preparations, so this data only shows the location of FNR when it is inactive. It would however be very interesting to repeat this in light adapted plants to further test the hypothesis that the sub-thylakoidial location is a factor in determining FNR function. For example, if the pH-dependent release of FNR from its tether Tic62 in the light would lead to more FNR available for LET, we would expect to see a decrease in lamellae-bound FNR and an increase in margin-located FNR in *Zm*FNR2 plants. We do not know, whether the FNR isoforms (*Zm*FNR3, *At*FNR2) that were previously regarded as unable to bind to a tether can in fact bind very transiently and therefore, it cannot be excluded, that loose tether binding is still a requirement for FNR to be located at the thylakoid membranes, especially the lamellae. Therefore, this experiment could be performed on *tictrol* double mutants where tether binding of FNR is completely eliminated. Additionally, I have to remark that the difference in signal density between lamellae and grana in *fnr1* is not statistically significant, presumably due to the overall very low la-

belling density of FNR in this genotype. Although the tendency is quite clear, it would need further repetition to be sure that there is more FNR at the margins than in the lamellae in this genotype. Moreover, I have only analysed one biological replicate for the Cyt *f* IG-labelling in wild-type plants and although it reproduced results that were published previously, the labelling density with this antibody is very low and further replicates would therefore be advisable to provide more statistical power. It might be interesting to also monitor the Cyt *f* distribution in *fnr1* plants, just in case a putative binding of FNR binding to the Cyt b_6f impacts its distribution in the thylakoid membranes. My method of combining semi-automatic area recognition and IG-labelling has proven to be sensitive to subtle changes in signal distribution and this experimental design could be extended to other experimental designs to further investigate the lateral heterogeneity of the thylakoids with regard to other components that are not detectable on freeze-fracture cryo-EM, for example the distribution of PC in various conditions. My hypothesis that TROL-bound FNR plays a role in the photoprotection of PSI in HL could be tested by subjecting isolated wild-type chloroplasts to HL prior to a BNP. If a dynamic re-location of FNR into TROL complexes is involved in a mechanism of photoprotection, we should be able to see more TROL-bound FNR in HL treated plants compared to low light or dark conditions. Apart from this, the biomass and seed yield of plants grown in HL conditions could provide further information. If TROL-bound FNR serves in a protection mechanism, we might observe an increased performance in *Zm*FNR1 plants compared to the other genotypes, as these plants have an increased amount of TROL-FNR.

10. Bibliography

M. Kalim Akhtar and Patrik R. Jones. Deletion of iscR stimulates recombinant clostridial Fe-Fe hydrogenase activity and H2-accumulation in Escherichia coli BL21(DE3). *Applied Microbiology and Biotechnology*, 78(5):853–862, April 2008. ISSN 0175-7598. doi: 10.1007/s00253-008-1377-6.

Per-Åke Albertsson. Interaction between the lumenal sides of the thylakoid membrane. *FEBS Letters*, 149(2):186–190, 1982. ISSN 1873-3468. doi: 10.1016/0014-5793(82)81098-3.

John F. Allen. Botany. State transitions–a question of balance. *Science (New York, N.Y.)*, 299(5612):1530–1532, March 2003. ISSN 1095-9203. doi: 10.1126/science.1082833.

David R. Allred and L. Andrew Staehelin. Spatial organization of the cytochrome b6-f complex within chloroplast thylakoid membranes. *Biochimica Et Biophysica Acta*, 849(1):94–103, April 1986. ISSN 0006-3002.

Ferdinand Alte, Anna Stengel, J. Philipp Benz, Eike Petersen, Jürgen Soll, Michael Groll, and Bettina Bölter. Ferredoxin:NADPH oxidoreductase is recruited to thylakoids by binding to a polyproline type II helix in a pH-dependent manner. *Proceedings of the National Academy of Sciences of the United States of America*, 107(45):19260–19265, November 2010. ISSN 1091-6490. doi: 10.1073/pnas.1009124107.

Birgitte Andersen, Henrik V. Scheller, and Birger L. Møller. The PSI-E subunit of photosystem I binds ferredoxin:NADP+ oxidore-

ductase. *FEBS letters*, 311(2):169–173, October 1992. ISSN 0014-5793.

Jan M. Anderson. Photoregulation of the Composition, Function, and Structure of Thylakoid Membranes. *Annual Review of Plant Physiology*, 37(1):93–136, 1986. doi: 10.1146/annurev.pp.37.060186.000521.

Jan M. Anderson, Peter Horton, Eun-Ha Kim, and Wah Soon Chow. Towards elucidation of dynamic structural changes of plant thylakoid architecture. *Philosophical Transactions of the Royal Society B: Biological Sciences*, 367(1608):3515–3524, December 2012. ISSN 0962-8436. doi: 10.1098/rstb.2012.0373.

Bertil Andersson and Jan M. Anderson. Lateral heterogeneity in the distribution of chlorophyll-protein complexes of the thylakoid membranes of spinach chloroplasts. *Biochimica Et Biophysica Acta*, 593(2):427–440, December 1980. ISSN 0006-3002.

Adrián K. Arakaki, Eduardo A. Ceccarelli, and Néstor Carrillo. Plant-type ferredoxin-NADP+ reductases: A basal structural framework and a multiplicity of functions. *FASEB journal: official publication of the Federation of American Societies for Experimental Biology*, 11(2):133–140, February 1997. ISSN 0892-6638.

Daniel I. Arnon, M. B. Allen, and F. R. Whatley. Photosynthesis by isolated chloroplasts. *Nature*, 174(4426):394–396, August 1954. ISSN 0028-0836.

Kozi Asada. The water-water cycle in chloroplasts: Scavenging of Active Oxygens and Dissipation of Excess Photons. *Annual Review of Plant Physiology and Plant Molecular Biology*, 50:601–639, June 1999. ISSN 1040-2519. doi: 10.1146/annurev.arplant.50.1.601.

Kozi Asada, Kuniaki Kiso, and Kyoko Yoshikawa. Univalent reduction of molecular oxygen by spinach chloroplasts on illumination. *The Journal of Biological Chemistry*, 249(7):2175–2181, April 1974. ISSN 0021-9258.

Jotham R. Austin and L. Andrew Staehelin. Three-Dimensional Architecture of Grana and Stroma Thylakoids of Higher Plants as Determined by Electron Tomography. *Plant Physiology*, 155(4):1601–1611, April 2011. ISSN , 1532-2548. doi: 10.1104/pp.110.170647.

Mordhay Avron and Andre T. Jagendorf. A TPNH Diaphorase from chloroplasts. *Archives of Biochemistry and Biophysics*, 65 (2):475–490, December 1956. ISSN 0003-9861. doi: 10.1016/0003-9861(56)90207-7.

Mordhay Avron and Andre T. Jagendorf. Some further investigations on chloroplast TPNH diaphorase. *Archives of Biochemistry and Biophysics*, 72(1):17–24, November 1957. ISSN 0003-9861. doi: 10.1016/0003-9861(57)90169-8.

Danas Baniulis, Huamin Zhang, Taisiya Zakharova, S. Saif Hasan, and William A. Cramer. Purification and crystallization of the cyanobacterial cytochrome b6f complex. *Methods in Molecular Biology (Clifton, N.J.)*, 684:65–77, 2011. ISSN 1940-6029. doi: 10.1007/978-1-60761-925-37.

Peter Bankhead, Maurice B. Loughrey, José A. Fernández, Yvonne Dombrowski, Darragh G. McArt, Philip D. Dunne, Stephen McQuaid, Ronan T. Gray, Liam J. Murray, Helen G. Coleman, Jacqueline A. James, Manuel Salto-Tellez, and Peter W. Hamilton. QuPath: Open source software for digital pathology image analysis. *Scientific Reports*, 7(1):16878, December 2017. ISSN 2045-2322. doi: 10.1038/s41598-017-17204-5.

Christopher J. Batie and Henry Kamin. Electron transfer by ferredoxin:NADP+ reductase. Rapid-reaction evidence for participation of a ternary complex. *The Journal of Biological Chemistry*, 259(19):11976–11985, October 1984. ISSN 0021-9258.

Stéphane Bellafiore, Frédy Barneche, Gilles Peltier, and Jean-David Rochaix. State transitions and light adaptation require chloroplast thylakoid protein kinase STN7. *Nature*, 433(7028):892–895, February 2005. ISSN 1476-4687. doi: 10.1038/nature03286.

Derek S. Bendall and Robert S. Manasse. Cyclic photophosphorylation and electron transport. *Biochimica et Biophysica Acta (BBA) - Bioenergetics*, 1229(1):23–38, April 1995. ISSN 0005-2728. doi: 10.1016/0005-2728(94)00195-B.

Philipp Benz, Anna Stengel, Minna Lintala, Youn.-H. Lee, Arnim Weber, Katrin Philippar, Irene L. Gügel, Shuji Kaieda, Takahisha Ikegami, Paula Mulo, J'urgen Soll, and Bettina Bölter. Arabidopsis Tic62 and ferredoxin-NADP(H) oxidoreductase form light-regulated complexes that are integrated into the chloroplast redox poise. *The Plant Cell*, 21(12):3965–3983, December 2009. ISSN 1532-298X. doi: 10.1105/tpc.109.069815.

Robert E. Blankenship. *Molecular Mechanisms of Photosynthesis*. John Wiley & Sons, May 2014. ISBN 978-1-4051-8976-7.

Egbert J. Boekema, Jan F. van Breemen, Henny van Roon, and Jan P. Dekker. Arrangement of photosystem II supercomplexes in crystalline macrodomains within the thylakoid membrane of green plant chloroplasts. *Journal of Molecular Biology*, 301(5):1123–1133, September 2000. ISSN 0022-2836. doi: 10.1006/jmbi.2000.4037.

Monika Bojko, Jerzy Kruk, and Stanislaw Wieckowski. Plastoquinones are effectively reduced by ferredoxin:NADP+ oxidoreductase in the presence of sodium cholate micelles Significance for cyclic electron transport and chlororespiration. *Phytochemistry*, 64(6):1055–1060, November 2003. ISSN 0031-9422. doi: 10.1016/S0031-9422(03)00506-5.

M. Calvin. The path of carbon in photosynthesis. *Science (New York, N.Y.)*, 135(3507):879–889, March 1962. ISSN 0036-8075.

Bi-Chang Chen, Wesley R. Legant, Kai Wang, Lin Shao, Daniel E. Milkie, Michael W. Davidson, Chris Janetopoulos, Xufeng S. Wu, John A. Hammer, Zhe Liu, Brian P. English, Yuko Mimori-Kiyosue, Daniel P. Romero, Alex T. Ritter, Jennifer Lippincott-Schwartz, Lillian Fritz-Laylin, R. Dyche Mullins, Diana M.

Mitchell, Joshua N. Bembenek, Anne-Cecile Reymann, Ralph Böhme, Stephan W. Grill, Jennifer T. Wang, Geraldine Seydoux, U. Serdar Tulu, Daniel P. Kiehart, and Eric Betzig. Lattice light-sheet microscopy: Imaging molecules to embryos at high spatiotemporal resolution. *Science (New York, N.Y.)*, 346 (6208):1257998, October 2014. ISSN 1095-9203. doi: 10.1126/science.1257998.

Orinda Chew, James Whelan, and A. Harvey Millar. Molecular definition of the ascorbate-glutathione cycle in Arabidopsis mitochondria reveals dual targeting of antioxidant defenses in plants. *The Journal of Biological Chemistry*, 278(47):46869–46877, November 2003. ISSN 0021-9258. doi: 10.1074/jbc.M307525200.

Monica Colombo, Marjaana Suorsa, Fabio Rossi, Roberto Ferrari, Luca Tadini, Roberto Barbato, and Paolo Pesaresi. Photosynthesis Control: An underrated short-term regulatory mechanism essential for plant viability. *Plant Signaling & Behavior*, 11(4):e1165382, 2016. ISSN 1559-2324. doi: 10.1080/15592324.2016.1165382.

Sylvain V. Costes, Dirk Daelemans, Edward H. Cho, Zachary Dobbin, George Pavlakis, and Stephen Lockett. Automatic and quantitative measurement of protein-protein colocalization in live cells. *Biophysical Journal*, 86(6):3993–4003, June 2004. ISSN 0006-3495. doi: 10.1529/biophysj.103.038422.

Giovanni DalCorso, Paolo Pesaresi, Simona Masiero, Elena Aseeva, Danja Schünemann, Giovanni Finazzi, Pierre Joliot, Roberto Barbato, and Dario Leister. A complex containing PGRL1 and PGR5 is involved in the switch between linear and cyclic electron flow in Arabidopsis. *Cell*, 132(2):273–285, January 2008. ISSN 1097-4172. doi: 10.1016/j.cell.2007.12.028.

Bertram Daum and Werner Kühlbrandt. Electron tomography of plant thylakoid membranes. *Journal of Experimental Botany*, 62 (7):2393–2402, January 2011. ISSN 0022-0957, 1460-2431. doi: 10.1093/jxb/err034.

Bertram Daum, Daniela Nicastro, Jotham Austin, J. Richard McIntosh, and Werner Kühlbrandt. Arrangement of Photosystem II and ATP Synthase in Chloroplast Membranes of Spinach and Pea. *The Plant Cell*, 22(4):1299–1312, April 2010. ISSN 1040-4651, 1532-298X. doi: 10.1105/tpc.109.071431.

Jan P. Dekker and Egbert J. Boekema. Supramolecular organization of thylakoid membrane proteins in green plants. *Biochimica et Biophysica Acta (BBA) - Bioenergetics*, 1706(1):12–39, January 2005. ISSN 0005-2728. doi: 10.1016/j.bbabio.2004.09.009.

Sávio Pinho dos Reis, Aline Medeiros Lima, and Cláudia Regina Batista de Souza. Recent Molecular Advances on Downstream Plant Responses to Abiotic Stress. *International Journal of Molecular Sciences*, 13(7):8628–8647, June 2012. ISSN 1422-0067. doi: 10.3390/ijms13078628.

Kenneth H. Dudley, Anders Ehrenberg, Peter Hemmerich, and Franz Müller. Spektren und Strukturen der am Flavin-Redoxsystem beteiligten Partikeln. Studien in der Flavinreihe IX [1]. *Helvetica Chimica Acta*, 47(5):1354–1383, 1964. ISSN 1522-2675. doi: 10.1002/hlca.19640470531.

Henry J. H. Fenton. LXXIII.—Oxidation of tartaric acid in presence of iron. *Journal of the Chemical Society, Transactions*, 65(0):899–910, January 1894. ISSN 0368-1645. doi: 10.1039/CT8946500899.

Miki Fujita, Yasunari Fujita, Yoshiteru Noutoshi, Fuminori Takahashi, Yoshihiro Narusaka, Kazuko Yamaguchi-Shinozaki, and Kazuo Shinozaki. Crosstalk between abiotic and biotic stress responses: A current view from the points of convergence in the stress signaling networks. *Current Opinion in Plant Biology*, 9(4):436–442, August 2006. ISSN 1369-5266. doi: 10.1016/j.pbi.2006.05.014.

José Ignacio García-Plazaola, Beatriz Fernández-Marín, Stephen O. Duke, Antonio Hernández, Fernando López-Arbeloa, and José María Becerril. Autofluorescence: Biological functions and

technical applications. *Plant Science*, 236:136–145, July 2015. ISSN 0168-9452. doi: 10.1016/j.plantsci.2015.03.010.

Sebastian Gnan, Tom Marsh, and Paula X. Kover. Inflorescence photosynthetic contribution to fitness releases Arabidopsis thaliana plants from trade-off constraints on early flowering. *PloS One*, 12(10):e0185835, 2017. ISSN 1932-6203. doi: 10.1371/journal.pone.0185835.

Joanna Grzyb, Mariusz Gagoś, Wiesław I. Gruszecki, Monika Bojko, and Kazimierz Strzałka. Interaction of ferredoxin:NADP+ oxidoreductase with model membranes. *Biochimica et Biophysica Acta (BBA) - Biomembranes*, 1778(1):133–142, January 2008. ISSN 0005-2736. doi: 10.1016/j.bbamem.2007.09.028.

Joanna Grzyb, Katarzyna Gieczewska, Justyna Łabuz, and Olga Sztatelman. Detailed characterization of Synechocystis PCC 6803 ferredoxin:NADP+ oxidoreductase interaction with model membranes. *Biochimica et Biophysica Acta (BBA) - Biomembranes*, 1860(2):281–291, February 2018. ISSN 0005-2736. doi: 10.1016/j.bbamem.2017.10.012.

Mohammad-Reza Hajirezaei, Martin Peisker, Henning Tschiersch, Javier F. Palatnik, Estela M. Valle, Néstor Carrillo, and Uwe Sonnewald. Small changes in the activity of chloroplastic NADP(+)-dependent ferredoxin oxidoreductase lead to impaired plant growth and restrict photosynthetic activity of transgenic tobacco plants. *The Plant Journal: For Cell and Molecular Biology*, 29(3):281–293, February 2002a. ISSN 0960-7412.

Mohammad-Reza Hajirezaei, Martin Peisker, Henning Tschiersch, Javier F. Palatnik, Estela M. Valle, Néstor Carrillo, and Uwe Sonnewald. Small changes in the activity of chloroplastic NADP(+)-dependent ferredoxin oxidoreductase lead to impaired plant growth and restrict photosynthetic activity of transgenic tobacco plants. *The Plant Journal: For Cell and Molecular Biology*, 29(3):281–293, February 2002b. ISSN 0960-7412.

Guy Thomas Hanke, Satoshi Okutani, Yoshinori Satomi, Toshifumi Takao, Akira Suzuki, and Toshiharu Hase. Multiple iso-proteins of FNR in Arabidopsis: Evidence for different contributions to chloroplast function and nitrogen assimilation. *Plant, Cell & Environment*, 28(9):1146–1157, September 2005. ISSN 1365-3040. doi: 10.1111/j.1365-3040.2005.01352.x.

Guy Thomas Hanke, Tsuyoshi Endo, Fumihiko Satoh, and Toshiharu Hase. Altered photosynthetic electron channelling into cyclic electron flow and nitrite assimilation in a mutant of ferredoxin:NADP(H) reductase. *Plant, Cell & Environment*, 31(7): 1017–1028, July 2008. ISSN 1365-3040. doi: 10.1111/j.1365-3040.2008.01814.x.

Miroslava Herbstová, Stefanie Tietz, Christopher Kinzel, Maria V. Turkina, and Helmut Kirchhoff. Architectural switch in plant photosynthetic membranes induced by light stress. *Proceedings of the National Academy of Sciences of the United States of America*, 109(49):20130–20135, December 2012. ISSN 0027-8424. doi: 10.1073/pnas.1214265109.

Rene Hermann, Paul Walther, and Martin Müller. Immunogold labeling in scanning electron microscopy. *Histochemistry and Cell Biology*, 106(1):31–39, July 1996. ISSN 1432-119X. doi: 10.1007/BF02473200.

Alexander P. Hertle, Thomas Blunder, Tobias Wunder, Paolo Pesaresi, Mathias Pribil, Ute Armbruster, and Dario Leister. PGRL1 is the elusive ferredoxin-plastoquinone reductase in photosynthetic cyclic electron flow. *Molecular Cell*, 49(3):511–523, February 2013. ISSN 1097-4164. doi: 10.1016/j.molcel.2012.11.030.

Noriko Ishikawa, Atsushi Takabayashi, Fumihiko Sato, and Tsuyoshi Endo. Accumulation of the components of cyclic electron flow around photosystem I in C4 plants, with respect to the requirements for ATP. *Photosynthesis Research*, 129(3):261–277, September 2016. ISSN 1573-5079. doi: 10.1007/s11120-016-0251-0.

Masakazu Iwai, Kenji Takizawa, Ryutaro Tokutsu, Akira Okamuro, Yuichiro Takahashi, and Jun Minagawa. Isolation of the elusive supercomplex that drives cyclic electron flow in photosynthesis. *Nature*, 464(7292):1210–1213, April 2010. ISSN 1476-4687. doi: 10.1038/nature08885.

Masakazu Iwai, Makio Yokono, Kazuo Kurokawa, Akira Ichihara, and Akihiko Nakano. Live-cell visualization of excitation energy dynamics in chloroplast thylakoid structures. *Scientific Reports*, 6: 29940, July 2016. ISSN 2045-2322. doi: 10.1038/srep29940.

Masakazu Iwai, Melissa S. Roth, and Krishna K. Niyogi. Subdiffraction-resolution live-cell imaging for visualizing thylakoid membranes. *The Plant Journal*, 96(1):233–243, October 2018. ISSN 1365-313X. doi: 10.1111/tpj.14021.

Matthew P. Johnson, Tomasz K. Goral, Christopher D. P. Duffy, Anthony P. R. Brain, Conrad W. Mullineaux, and Alexander V. Ruban. Photoprotective Energy Dissipation Involves the Reorganization of Photosystem II Light-Harvesting Complexes in the Grana Membranes of Spinach Chloroplasts. *The Plant Cell*, 23 (4):1468–1479, April 2011. ISSN 1040-4651, 1532-298X. doi: 10.1105/tpc.110.081646.

Matthew P. Johnson, Cvetelin Vasilev, John D. Olsen, and C. Neil Hunter. Nanodomains of Cytochrome b6f and Photosystem II Complexes in Spinach Grana Thylakoid Membranes[W][OPEN]. *The Plant Cell*, 26(7):3051–3061, July 2014. ISSN 1040-4651. doi: 10.1105/tpc.114.127233.

Pierre Joliot and Giles N. Johnson. Regulation of Cyclic and Linear Electron Flow in Higher Plants. *Proceedings of the National Academy of Sciences of the United States of America*, 108(32):13317–13322, August 2011. ISSN 1091-6490. doi: 10.1073/pnas.1110189108.

Pierre Joliot and Anne Joliot. Cyclic electron transfer in plant leaf. *Proceedings of the National Academy of Sciences*, 99(15):

10209–10214, July 2002. ISSN 0027-8424, 1091-6490. doi: 10.1073/pnas.102306999.

Pierre Joliot and Anne Joliot. Quantification of the electrochemical proton gradient and activation of ATP synthase in leaves. *Biochimica Et Biophysica Acta*, 1777(7-8):676–683, 2008 Jul-Aug. ISSN 0006-3002. doi: 10.1016/j.bbabio.2008.04.010.

Pierre Joliot, Jérôme Lavergne, and Daniel Béal. Plastoquinone compartmentation in chloroplasts. I. Evidence for domains with different rates of photo-reduction. *Biochimica et Biophysica Acta (BBA) - Bioenergetics*, 1101(1):1–12, July 1992. ISSN 0005-2728. doi: 10.1016/0167-4838(92)90460-U.

Pierre Joliot, Daniel Béal, and Anne Joliot. Cyclic electron flow under saturating excitation of dark-adapted Arabidopsis leaves. *Biochimica Et Biophysica Acta*, 1656(2-3):166–176, June 2004. ISSN 0006-3002. doi: 10.1016/j.bbabio.2004.03.010.

null Jose Quiles M and null Cuello. Association of ferredoxin-NADP oxidoreductase with the chloroplastic pyridine nucleotide dehydrogenase complex in barley leaves. *Plant Physiology*, 117(1):235–244, May 1998. ISSN 1532-2548.

Snjezana Jurić, Kroata Hazler-Pilepić, Ana Tomasić, Hrvoje Lepedus, Branka Jelicić, Sujith Puthiyaveetil, Tihana Bionda, Lea Vojta, John F. Allen, Enrico Schleiff, and Hrvoje Fulgosi. Tethering of ferredoxin:NADP+ oxidoreductase to thylakoid membranes is mediated by novel chloroplast protein TROL. *The Plant Journal: For Cell and Molecular Biology*, 60(5):783–794, December 2009. ISSN 1365-313X. doi: 10.1111/j.1365-313X.2009.03999.x.

Jocelyn Kauny and Pierre Sétif. NADPH fluorescence in the cyanobacterium Synechocystis sp. PCC 6803: A versatile probe for in vivo measurements of rates, yields and pools. *Biochimica Et Biophysica Acta*, 1837(6):792–801, June 2014. ISSN 0006-3002. doi: 10.1016/j.bbabio.2014.01.009.

Mahbuba Khatoon, Kayo Inagawa, Pavel Pospísil, Amu Yamashita, Miho Yoshioka, Björn Lundin, Junko Horie, Noriko Morita, Anjana Jajoo, Yoko Yamamoto, and Yasusi Yamamoto. Quality control of photosystem II: Thylakoid unstacking is necessary to avoid further damage to the D1 protein and to facilitate D1 degradation under light stress in spinach thylakoids. *The Journal of Biological Chemistry*, 284(37):25343–25352, September 2009. ISSN 1083-351X. doi: 10.1074/jbc.M109.007740.

Helmut Kirchhoff. Architectural switches in plant thylakoid membranes. *Photosynthesis Research*, 116(2):481–487, October 2013. ISSN 1573-5079. doi: 10.1007/s11120-013-9843-0.

Helmut Kirchhoff, Winfried Haase, Sandra Wegner, Ravi Danielsson, Ralf Ackermann, and Per-Ake Albertsson. Low-light-induced formation of semicrystalline photosystem II arrays in higher plant chloroplasts. *Biochemistry*, 46(39):11169–11176, October 2007. ISSN 0006-2960. doi: 10.1021/bi700748y.

Helmut Kirchhoff, Chris Hall, Magnus Wood, Miroslava Herbstová, Onie Tsabari, Reinat Nevo, Dana Charuvi, Eyal Shimoni, and Ziv Reich. Dynamic control of protein diffusion within the granal thylakoid lumen. *Proceedings of the National Academy of Sciences of the United States of America*, 108(50):20248–20253, December 2011. ISSN 1091-6490. doi: 10.1073/pnas.1104141109.

Haniyeh Koochak, Sujith Puthiyaveetil, Daniel L. Mullendore, Meng Li, and Helmut Kirchhoff. The structural and functional domains of plant thylakoid membranes. *The Plant Journal*, 97(3):412–429, February 2019. ISSN 0960-7412. doi: 10.1111/tpj.14127.

Marina Kozuleva, Tatjana Goss, Manuel Twachtmann, Katherina Rudi, Jennifer Trapka, Jennifer Selinski, Boris Ivanov, Prashanth Garapati, Heinz-Juergen Steinhoff, Toshiharu Hase, Renate Scheibe, Johann P. Klare, and Guy T. Hanke. Ferredoxin:NADP(H) Oxidoreductase Abundance and Location Influences Redox Poise and Stress Tolerance. *Plant Physiol-*

ogy, 172(3):1480–1493, November 2016. ISSN 1532-2548. doi: 10.1104/pp.16.01084.

David M. Kramer and John R. Evans. The importance of energy balance in improving photosynthetic productivity. *Plant Physiology*, 155(1):70–78, January 2011. ISSN 1532-2548. doi: 10.1104/pp.110.166652.

Ulrich K. Laemmli. Cleavage of structural proteins during the assembly of the head of bacteriophage T4. *Nature*, 227(5259):680–685, August 1970. ISSN 0028-0836.

Agu Laisk, Hillar Eichelmann, Vello Oja, and Richard B. Peterson. Control of cytochrome b6f at low and high light intensity and cyclic electron transport in leaves. *Biochimica Et Biophysica Acta*, 1708(1):79–90, June 2005. ISSN 0006-3002. doi: 10.1016/j.bbabio.2005.01.007.

Adrian M. Lennon, Peerada Prommeenate, and Peter J. Nixon. Location, expression and orientation of the putative chlororespiratory enzymes, Ndh and IMMUTANS, in higher-plant plastids. *Planta*, 218(2):254–260, December 2003. ISSN 0032-0935. doi: 10.1007/s00425-003-1111-7.

Minna Lintala, Yagut Allahverdiyeva, Heidi Kidron, Mirva Piippo, Natalia Battchikova, Marjaana Suorsa, Eevi Rintamäki, Tiina A. Salminen, Eva-Mari Aro, and Paula Mulo. Structural and functional characterization of ferredoxin-NADP+-oxidoreductase using knock-out mutants of Arabidopsis. *The Plant Journal: For Cell and Molecular Biology*, 49(6):1041–1052, March 2007. ISSN 0960-7412. doi: 10.1111/j.1365-313X.2006.03014.x.

Minna Lintala, Yagut Allahverdiyeva, Saijaliisa Kangasjärvi, Nina Lehtimäki, Mika Keränen, Eevi Rintamäki, Eva-Mari Aro, and Paula Mulo. Comparative analysis of leaf-type ferredoxin-NADP oxidoreductase isoforms in Arabidopsis thaliana. *The Plant Journal: For Cell and Molecular Biology*, 57(6):1103–1115, March 2009. ISSN 1365-313X. doi: 10.1111/j.1365-313X.2008.03753.x.

Minna Lintala, Nina Lehtimäki, J. Philipp Benz, Andreas Jungfer, Jürgen Soll, Eva-Mari Aro, Bettina Bölter, and Paula Mulo. Depletion of leaf-type ferredoxin-NADP(+) oxidoreductase results in the permanent induction of photoprotective mechanisms in Arabidopsis chloroplasts. *The Plant Journal: For Cell and Molecular Biology*, 70(5):809–817, June 2012. ISSN 1365-313X. doi: 10.1111/j.1365-313X.2012.04930.x.

Minna Lintala, Natalie Schuck, Ina Thormählen, Andreas Jungfer, Katrin L. Weber, Andreas P. M. Weber, Peter Geigenberger, Jürgen Soll, Bettina Bölter, and Paula Mulo. Arabidopsis tic62 trol mutant lacking thylakoid-bound ferredoxin-NADP+ oxidoreductase shows distinct metabolic phenotype. *Molecular Plant*, 7(1): 45–57, January 2014. ISSN 1752-9867. doi: 10.1093/mp/sst129.

Shilpi Mahajan and Narendra Tuteja. Cold, salinity and drought stresses: An overview. *Archives of Biochemistry and Biophysics*, 444(2):139–158, December 2005. ISSN 0003-9861. doi: 10.1016/j.abb.2005.10.018.

Hans C. P. Matthijs, Sean J. Coughlan, and Geoffrey Hind. Removal of ferredoxin:NADP+ oxidoreductase from thylakoid membranes, rebinding to depleted membranes, and identification of the binding site. *Journal of Biological Chemistry*, 261(26):12154–12158, September 1986. ISSN 0021-9258, 1083-351X.

Terry M. Mayhew. Mapping the distributions and quantifying the labelling intensities of cell compartments by immunoelectron microscopy: Progress towards a coherent set of methods. *Journal of Anatomy*, 219(6):647–660, December 2011. ISSN 1469-7580. doi: 10.1111/j.1469-7580.2011.01438.x.

Alan H. Mehler. Studies on reactions of illuminated chloroplasts. I. Mechanism of the reduction of oxygen and other Hill reagents. *Archives of Biochemistry and Biophysics*, 33(1):65–77, August 1951. ISSN 1096-0384.

Wilhelm Menke. Structure and Chemistry of Plastids. *Annual Re-*

view of Plant Physiology, 13(1):27–44, June 1962. ISSN 0066-4294. doi: 10.1146/annurev.pp.13.060162.000331.

Hara P. Misra and Irvin Fridovich. The generation of superoixide radical during the autoxidation of ferredoxins. *The Journal of Biological Chemistry*, 246(22):6886–6890, November 1971. ISSN 0021-9258.

Peter Mitchell. Coupling of phosphorylation to electron and hydrogen transfer by a chemi-osmotic type of mechanism. *Nature*, 191: 144–148, July 1961. ISSN 0028-0836.

Laura Mosebach, Claudia Heilmann, Risa Mutoh, Philipp Gäbelein, Janina Steinbeck, Thomas Happe, Takahisa Ikegami, Guy Hanke, Genji Kurisu, and Michael Hippler. Association of Ferredoxin:NADP+ oxidoreductase with the photosynthetic apparatus modulates electron transfer in Chlamydomonas reinhardtii. *Photosynthesis Research*, 134(3):291–306, December 2017. ISSN 1573-5079. doi: 10.1007/s11120-017-0408-5.

Conrad W. Mullineaux. Function and evolution of grana. *Trends in Plant Science*, 10(11):521–525, November 2005. ISSN 1360-1385. doi: 10.1016/j.tplants.2005.09.001.

Paula Mulo. Chloroplast-targeted ferredoxin-NADP+ oxidoreductase (FNR): Structure, function and location. *Biochimica et Biophysica Acta (BBA) - Bioenergetics*, 1807(8):927–934, August 2011. ISSN 0005-2728. doi: 10.1016/j.bbabio.2010.10.001.

Paula Mulo, Sari Sirpiö, Marjaana Suorsa, and Eva-Mari Aro. Auxiliary proteins involved in the assembly and sustenance of photosystem II. *Photosynthesis Research*, 98(1):489–501, October 2008. ISSN 1573-5079. doi: 10.1007/s11120-008-9320-3.

Yuri Munekage, Masaya Hojo, Jörg Meurer, Tsuyoshi Endo, Masao Tasaka, and Toshiharu Shikanai. PGR5 is involved in cyclic electron flow around photosystem I and is essential for photoprotection in Arabidopsis. *Cell*, 110(3):361–371, August 2002. ISSN 0092-8674.

Yuri Munekage, Mihoko Hashimoto, Chikahiro Miyake, Ken-ichi Tomizawa, Tsuyoshi Endo, Masao Tasaka, and Toshiharu Shikanai. Cyclic electron flow around photosystem I is essential for photosynthesis. *Nature*, 429(6991):579–582, June 2004. ISSN 1476-4687. doi: 10.1038/nature02598.

Yuri Nakajima Munekage, Françoise Eymery, Dominique Rumeau, Stephan Cuiné, Masateru Oguri, Naoya Nakamura, Akiho Yokota, Bernard Genty, and Gilles Peltier. Elevated expression of PGR5 and NDH-H in bundle sheath chloroplasts in C4 flaveria species. *Plant & Cell Physiology*, 51(4):664–668, April 2010. ISSN 1471-9053. doi: 10.1093/pcp/pcq030.

László Mustárdy, Karolyn Buttle, Gábor Steinbach, and Gyozo Garab. The three-dimensional network of the thylakoid membranes in plants: Quasihelical model of the granum-stroma assembly. *The Plant Cell*, 20(10):2552–2557, October 2008. ISSN 1040-4651. doi: 10.1105/tpc.108.059147.

Naoya Nakamura, Megumi Iwano, Michel Havaux, Akiho Yokota, and Yuri Nakajima Munekage. Promotion of cyclic electron transport around photosystem I during the evolution of NADP-malic enzyme-type C4 photosynthesis in the genus Flaveria. *The New Phytologist*, 199(3):832–842, August 2013. ISSN 1469-8137. doi: 10.1111/nph.12296.

Surendra S. Negi, Andrew A. Carol, Shivangi Pandya, Werner Braun, and Louise E. Anderson. Co-localization of glyceraldehyde-3-phosphate dehydrogenase with ferredoxin-NADP reductase in pea leaf chloroplasts. *Journal of structural biology*, 161(1):18–30, January 2008. ISSN 1047-8477. doi: 10.1016/j.jsb.2007.08.016.

Lukáš Nosek, Dmitry Semchonok, Egbert J. Boekema, Petr Ilík, and Roman Kouřil. Structural variability of plant photosystem II megacomplexes in thylakoid membranes. *The Plant Journal*, 89 (1):104–111, 2017. ISSN 1365-313X. doi: 10.1111/tpj.13325.

Satoshi Okutani, Guy T. Hanke, Yoshinori Satomi, Toshifumi Takao,

Genji Kurisu, Akira Suzuki, and Toshiharu Hase. Three maize leaf ferredoxin:NADPH oxidoreductases vary in subchloroplast location, expression, and interaction with ferredoxin. *Plant Physiology*, 139(3):1451–1459, November 2005. ISSN 0032-0889. doi: 10.1104/pp.105.070813.

Junko Ooyabu, Masako Ohtsuka, Yasuhiro Kashino, Hiroyuki Koike, and Kazuhiko Satoh. The expression pattern of NAD(P)H oxidases and the cyclic electron transport pathway around photosystem I of Synechocystis sp. PCC6803 depend on growth conditions. *Bioscience, Biotechnology, and Biochemistry*, 72(12):3180–3188, December 2008. ISSN 1347-6947. doi: 10.1271/bbb.80370.

Javier F. Palatnik, Estela M. Valle, and Néstor Carrillo. Oxidative stress causes ferredoxin-NADP+ reductase solubilization from the thylakoid membranes in methyl viologen-treated plants. *Plant Physiology*, 115(4):1721–1727, December 1997. ISSN 0032-0889.

Javier F. Palatnik, Vanesa B. Tognetti, Hugo O. Poli, Ramiro E. Rodríguez, Nicolás Blanco, Martha Gattuso, Mohammad-Reza Hajirezaei, Uwe Sonnewald, Estela M. Valle, and Néstor Carrillo. Transgenic tobacco plants expressing antisense ferredoxin-NADP(H) reductase transcripts display increased susceptibility to photo-oxidative damage. *The Plant Journal: For Cell and Molecular Biology*, 35(3):332–341, August 2003. ISSN 0960-7412.

Dominick J. Paolillo. The three-dimensional arrangement of intergranal lamellae in chloroplasts. *Journal of Cell Science*, 6(1):243–255, January 1970. ISSN 0021-9533.

Guenter A. Peschek and Uwe B. Sleytr. Thylakoid morphology of the cyanobacteria Anabaena variabilis and Nostoc MAC grown under light and dark conditions. *Journal of Ultrastructure Research*, 82 (2):233–239, February 1983. ISSN 0022-5320. doi: 10.1016/S0022-5320(83)90056-4.

Mathias Pribil, Mathias Labs, and Dario Leister. Structure and dynamics of thylakoids in land plants. *Journal of Experimen-*

tal Botany, 65(8):1955–1972, May 2014. ISSN 1460-2431. doi: 10.1093/jxb/eru090.

Core Team R. R: A Language and Environment for Statistical Computing. R Foundation for Statistical Computing, 2013.

Ramiro E. Rodriguez, Anabella Lodeyro, Hugo O. Poli, Matias Zurbriggen, Martin Peisker, Javier F. Palatnik, Vanesa B. Tognetti, Henning Tschiersch, Mohammad-Reza Hajirezaei, Estela M. Valle, and Néstor Carrillo. Transgenic tobacco plants overexpressing chloroplastic ferredoxin-NADP(H) reductase display normal rates of photosynthesis and increased tolerance to oxidative stress. *Plant Physiology*, 143(2):639–649, February 2007. ISSN 0032-0889. doi: 10.1104/pp.106.090449.

Joanna Sacharz, Vasco Giovagnetti, Petra Ungerer, Giulia Mastroianni, and Alexander V. Ruban. The xanthophyll cycle affects reversible interactions between PsbS and light-harvesting complex II to control non-photochemical quenching. *Nature Plants*, 3(2):16225, February 2017. ISSN 2055-0278. doi: 10.1038/nplants.2016.225.

Ulrich Schreiber and Christof Klughammer. New NADPH / 9-AA module for the DUAL-PAM-100: Description, operation and examples of application, 2009.

Veit Schubert. Super-resolution Microscopy – Applications in Plant Cell Research. *Frontiers in Plant Science*, 8, April 2017. ISSN 1664-462X. doi: 10.3389/fpls.2017.00531.

Jan M. Schuller, James A. Birrell, Hideaki Tanaka, Tsuyoshi Konuma, Hannes Wulfhorst, Nicholas Cox, Sandra K. Schuller, Jacqueline Thiemann, Wolfgang Lubitz, Pierre Sétif, Takahisa Ikegami, Benjamin D. Engel, Genji Kurisu, and Marc M. Nowaczyk. Structural adaptations of photosynthetic complex I enable ferredoxin-dependent electron transfer. *Science (New York, N.Y.)*, 363 (6424):257–260, January 2019. ISSN 1095-9203. doi: 10.1126/science.aau3613.

Yosepha Shahak, David Crowther, and Geoffrey Hind. The involvement of ferredoxin-NADP+ reductase in cyclic electron transport in chloroplasts. *Biochimica et Biophysica Acta (BBA) - Bioenergetics*, 636(2):234–243, July 1981. ISSN 0005-2728. doi: 10.1016/0005-2728(81)90097-9.

Toshiharu Shikanai. Central role of cyclic electron transport around photosystem I in the regulation of photosynthesis. *Current Opinion in Biotechnology*, 26:25–30, April 2014. ISSN 1879-0429. doi: 10.1016/j.copbio.2013.08.012.

Eyal Shimoni, Ophir Rav-Hon, Itzhak Ohad, Vlad Brumfeld, and Ziv Reich. Three-dimensional organization of higher-plant chloroplast thylakoid membranes revealed by electron tomography. *The Plant Cell*, 17(9):2580–2586, September 2005. ISSN 1040-4651. doi: 10.1105/tpc.105.035030.

Masateru Shin. [40] Ferredoxin-NADP reductase from spinach. In *Methods in Enzymology*, volume 23 of *Photosynthesis and Nitrogen Part A*, pages 440–447. Academic Press, January 1971. doi: 10.1016/S0076-6879(71)23116-5.

Masateru Shin and Daniel I. Arnon. Enzymic mechanisms of pyridine nucleotide reduction in chloroplasts. *The Journal of Biological Chemistry*, 240:1405–1411, March 1965. ISSN 0021-9258.

Masateru Shin, Hiroshi Ishida, and Yukinori Nozaki. A New Protein Factor, Connectein, as a Constituent of the Large Form of Ferredoxin-NADP Reductase. *Plant and Cell Physiology*, 26(3): 559–563, April 1985. ISSN 0032-0781. doi: 10.1093/oxfordjournals.pcp.a076940.

Anna Stengel, Philipp Benz, Mónica Balsera, Jürgen Soll, and Bettina Bölter. TIC62 redox-regulated translocon composition and dynamics. *The Journal of Biological Chemistry*, 283(11):6656–6667, March 2008. ISSN 0021-9258. doi: 10.1074/jbc.M706719200.

Marjaana Suorsa, Sari Järvi, Michele Grieco, Markus Nurmi, Malgorzata Pietrzykowska, Marjaana Rantala, Saijaliisa Kangasjärvi,

Virpi Paakkarinen, Mikko Tikkanen, Stefan Jansson, and Eva-Mari Aro. Proton Gradient Regulation5 Is Essential for Proper Acclimation of Arabidopsis Photosystem I to Naturally and Artificially Fluctuating Light Conditions. *The Plant Cell*, 24(7):2934–2948, July 2012. ISSN , 1532-298X. doi: 10.1105/tpc.112.097162.

Renata Szymańska, Jolanta Dłużewska, Ireneusz Slesak, and Jerzy Kruk. Ferredoxin:NADP+ oxidoreductase bound to cytochrome b_6f complex is active in plastoquinone reduction: Implications for cyclic electron transport. *Physiologia Plantarum*, 141(3): 289–298, March 2011. ISSN 1399-3054. doi: 10.1111/j.1399-3054.2010.01434.x.

Atsushi Takabayashi, Masahiro Kishine, Kozi Asada, Tsuyoshi Endo, and Fumihiko Sato. Differential use of two cyclic electron flows around photosystem I for driving CO2-concentration mechanism in C4 photosynthesis. *Proceedings of the National Academy of Sciences of the United States of America*, 102(46):16898–16903, November 2005. ISSN 0027-8424. doi: 10.1073/pnas.0507095102.

Daisuke Takagi, Shigeo Takumi, Masaki Hashiguchi, Takehiro Sejima, and Chikahiro Miyake. Superoxide and Singlet Oxygen Produced within the Thylakoid Membranes Both Cause Photosystem I Photoinhibition. *Plant Physiology*, 171(3):1626–1634, July 2016. ISSN 1532-2548. doi: 10.1104/pp.16.00246.

Marvin E. Tanenbaum, Luke A. Gilbert, Lei S. Qi, Jonathan S. Weissman, and Ronald D. Vale. A Protein-Tagging System for Signal Amplification in Gene Expression and Fluorescence Imaging. *Cell*, 159(3):635–646, October 2014. ISSN 0092-8674. doi: 10.1016/j.cell.2014.09.039.

Bernhard Teicher H and Vibe Scheller. The NAD(P)H dehydrogenase in barley thylakoids is photoactivatable and uses NADPH as well as NADH. *Plant Physiology*, 117(2):525–532, June 1998. ISSN 1532-2548.

Jesús Tejero, Inmaculada Pérez-Dorado, Celia Maya, Marta

Martínez-Júlvez, Julia Sanz-Aparicio, Carlos Gómez-Moreno, Juan A. Hermoso, and Milagros Medina. C-terminal tyrosine of ferredoxin-NADP+ reductase in hydride transfer processes with NAD(P)+/H. *Biochemistry*, 44(41):13477–13490, October 2005. ISSN 0006-2960. doi: 10.1021/bi051278c.

Jean-Claude Thomas, Bettina Ughy, Bernard Lagoutte, and Ghada Ajlani. A second isoform of the ferredoxin:NADP oxidoreductase generated by an in-frame initiation of translation. *Proceedings of the National Academy of Sciences of the United States of America*, 103(48):18368–18373, November 2006. ISSN 0027-8424. doi: 10.1073/pnas.0607718103.

Alexander N. Tikhonov. Induction events and short-term regulation of electron transport in chloroplasts: An overview. *Photosynthesis Research*, 125(1-2):65–94, August 2015. ISSN 1573-5079. doi: 10.1007/s11120-015-0094-0.

Hans-Wilhelm Trissl and Christian Wilhelm. Why do thylakoid membranes from higher plants form grana stacks? *Trends in Biochemical Sciences*, 18(11):415–419, November 1993. ISSN 0968-0004.

Manuel Twachtmann, Bianca Altmann, Norifumi Muraki, Ingo Voss, Satoshi Okutani, Genji Kurisu, Toshiharu Hase, and Guy T. Hanke. N-terminal structure of maize ferredoxin:NADP+ reductase determines recruitment into different thylakoid membrane complexes. *The Plant Cell*, 24(7):2979–2991, July 2012. ISSN 1532-298X. doi: 10.1105/tpc.111.094532.

Olivier Vallon, Laurence Bulte, Paola Dainese, Jaqueline Olive, Roberto Bassi, and Francis-Andre Wollman. Lateral redistribution of cytochrome b6/f complexes along thylakoid membranes upon state transitions. *Proceedings of the National Academy of Sciences of the United States of America*, 88(18):8262–8266, September 1991. ISSN 0027-8424.

Allison M.L. van de Meene, Martin F. Hohmann-Marriott, Wim F.J.

Vermaas, and Robert W. Roberson. The three-dimensional structure of the cyanobacterium Synechocystis sp. PCC 6803. *Archives of Microbiology*, 184(5):259–270, January 2006. ISSN 1432-072X. doi: 10.1007/s00203-005-0027-y.

Cornelius B. van Niel. On the morphology and physiology of the purple and green sulphur bacteria. *Archiv für Mikrobiologie*, 3(1): 1–112, January 1932. ISSN 1432-072X. doi: 10.1007/BF00454965.

Edwin van Spronsen, V Sarafis, G.J. Brakenhoff, Hans van der Voort, and N Nanninga. Three-dimensional structure of living chloroplasts as visualized by confocal scanning laser microscopy. *Protoplasma*, 148:8–14, February 1989. doi: 10.1007/BF01403986.

Jasper J. van Thor, Robert Jeanjean, Michel Havaux, Klaas A. Sjollema, Francoise Joset, Klaas J. Hellingwerf, and Hans C. P. Matthijs. Salt shock-inducible Photosystem I cyclic electron transfer in Synechocystis PCC6803 relies on binding of ferredoxin:NADP+ reductase to the thylakoid membranes via its CpcD phycobilisome-linker homologous N-terminal domain. *Biochimica et Biophysica Acta (BBA) - Bioenergetics*, 1457(3):129–144, April 2000. ISSN 0005-2728. doi: 10.1016/S0005-2728(00)00072-4.

Alexander V. Vener, Paul J. M. van Kan, Peter R. Rich, Itzhak Ohad, and Bertil Andersson. Plastoquinol at the quinol oxidation site of reduced cytochrome bf mediates signal transduction between light and protein phosphorylation: Thylakoid protein kinase deactivation by a single-turnover flash. *Proceedings of the National Academy of Sciences*, 94(4):1585–1590, February 1997. ISSN 0027-8424, 1091-6490. doi: 10.1073/pnas.94.4.1585.

Berkley J. Walker, Deserah D. Strand, David M. Kramer, and Asaph B. Cousins. The response of cyclic electron flow around photosystem I to changes in photorespiration and nitrate assimilation. *Plant Physiology*, 165(1):453–462, May 2014. ISSN 1532-2548. doi: 10.1104/pp.114.238238.

Heinz Walz GmbH. Dual-PAM-100 Measuring System for Simulta-

neous Assessment of P700 and Chlorophyll Fluorescence, February 2009. 2. Edition.

Zhen Wang and Christoph Benning. Chloroplast lipid synthesis and lipid trafficking through ER-plastid membrane contact sites. *Biochemical Society Transactions*, 40(2):457–463, April 2012. ISSN 1470-8752. doi: 10.1042/BST20110752.

Jean M. Whatley. The Endosymbiotic Origin of Chloroplasts. In Kwang W. Jeon and Jonathan Jarvik, editors, *International Review of Cytology*, volume 144, pages 259–299. Academic Press, January 1993. doi: 10.1016/S0074-7696(08)61517-X.

Hiroshi Yamamoto and Toshiharu Shikanai. In planta mutagenesis of Src homology 3 domain-like fold of NdhS, a ferredoxin-binding subunit of the chloroplast NADH dehydrogenase-like complex in Arabidopsis: A conserved Arg-193 plays a critical role in ferredoxin binding. *The Journal of Biological Chemistry*, 288(51):36328–36337, December 2013. ISSN 1083-351X. doi: 10.1074/jbc.M113.511584.

Chao Yang, Hongtao Hu, Hongyan Ren, Yuzhu Kong, Hongwei Lin, Jiangfan Guo, Lingling Wang, Yi He, Xiaomeng Ding, Magda Grabsztunowicz, Paula Mulo, Tao Chen, Yu Liu, Zhongchang Wu, Yunrong Wu, Chuanzao Mao, Ping Wu, and Xiaorong Mo. Light-induced rice1 regulates light dependent attachment of leaf-type ferredoxin-nadp+ oxidoreductase to the thylakoid membrane in rice and arabidopsis. *The Plant Cell*, 28(3):712–728, March 2016. ISSN 1532-298X. doi: 10.1105/tpc.15.01027.

Giuliana Zanetti and Giorgio Forti. Studies on the triphosphopyridine nucleotide-cytochrome f reductase of chloroplasts. *The Journal of Biological Chemistry*, 241(2):279–285, January 1966. ISSN 0021-9258.

Huamin Zhang, Julian P. Whitelegge, and William A. Cramer. Ferredoxin:NADP+ oxidoreductase is a subunit of the chloroplast cytochrome b6f complex. *The Journal of Biological Chem-*

istry, 276(41):38159–38165, October 2001. ISSN 0021-9258. doi: 10.1074/jbc.M105454200.

Vadim Zinchuk, Olga Zinchuk, and Teruhiko Okada. Quantitative Colocalization Analysis of Multicolor Confocal Immunofluorescence Microscopy Images: Pushing Pixels to Explore Biological Phenomena. *Acta Histochemica et Cytochemica*, 40(4):101–111, August 2007. ISSN 0044-5991. doi: 10.1267/ahc.07002.

Francesca Zito, Giovanni Finazzi, Rrené Delosme, Wolfgang Nitschke, Daniel Picot, and Francis-Andre Wollman. The Qo site of cytochrome b6f complexes controls the activation of the LHCII kinase. *The EMBO Journal*, 18(11):2961–2969, June 1999. ISSN 0261-4189, 1460-2075. doi: 10.1093/emboj/18.11.2961.

11. Appendix

11.1 Immunfluorescence control experiments

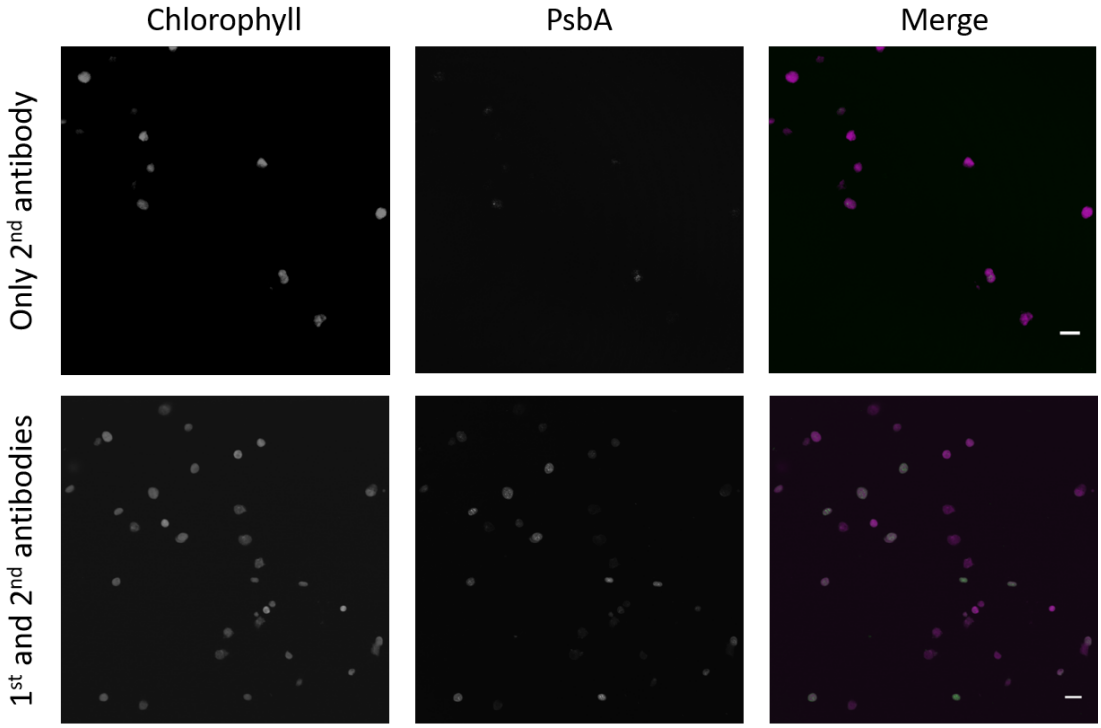

Figure 11.1: **Laser-scanning microscopy image of Arabidopsis wild-type chloroplast immunostained for PsbA.** Chloroplasts were isolated from *A.thaliana* (wild-type, Columbia ecotype) after 1h dark incubation and cross-linked with 3% formaldehyde. Membranes were permeabilized with 0.1 % TritonX-100 and the sample was immunolabelled for PsbA with Alexa488 conjugated secondary antibody. For the labelling control (upper panels) the incubation step with the 1st antibody was omitted. Imaging was performed on a Zeiss LSM 510 META NLO. Scalebar = 20 µm.

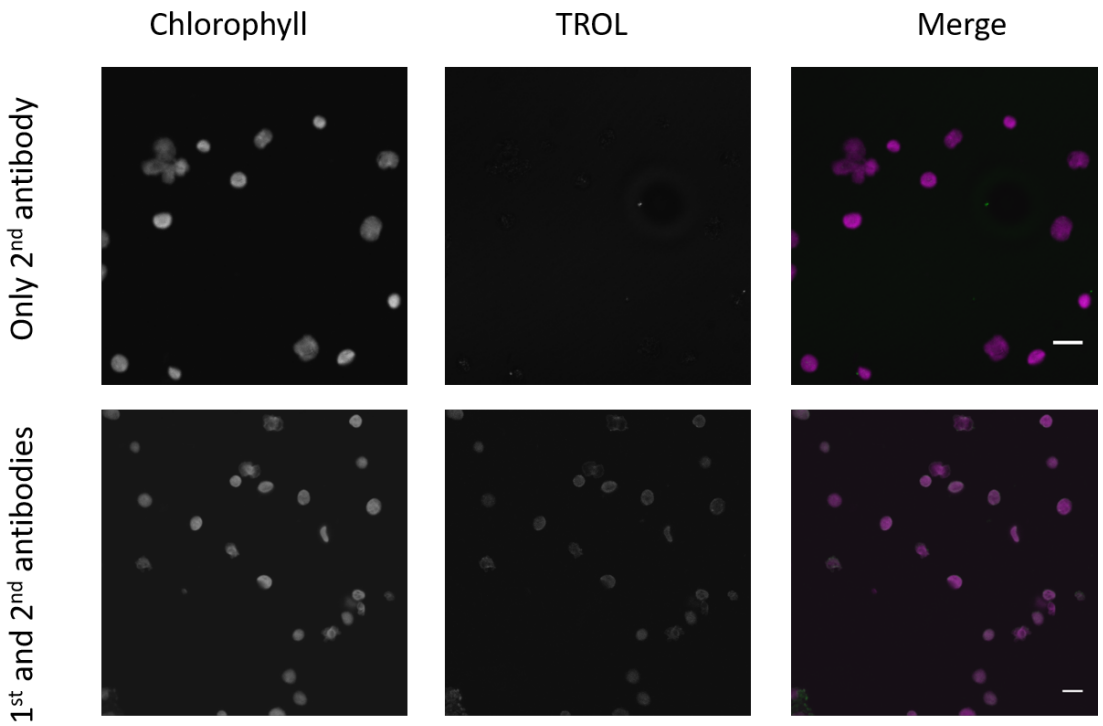

Figure 11.2: **Laser-scanning microscopy image of Arabidopsis wild-type chloroplast immunostained for TROL.** Chloroplasts were isolated from *A.thaliana* (wild-type, Columbia ecotype) after 1h dark incubation and cross-linked with 3% formaldehyde. Membranes were permeabilized with 0.1 % TritonX-100 and the sample was immunolabelled for TROL with Cy2 conjugated secondary antibody. For the labelling control (upper panels) the incubation step with the 1st antibody was omitted. Imaging was performed on a Zeiss LSM 510 META NLO. Scalebar = 20 µm.

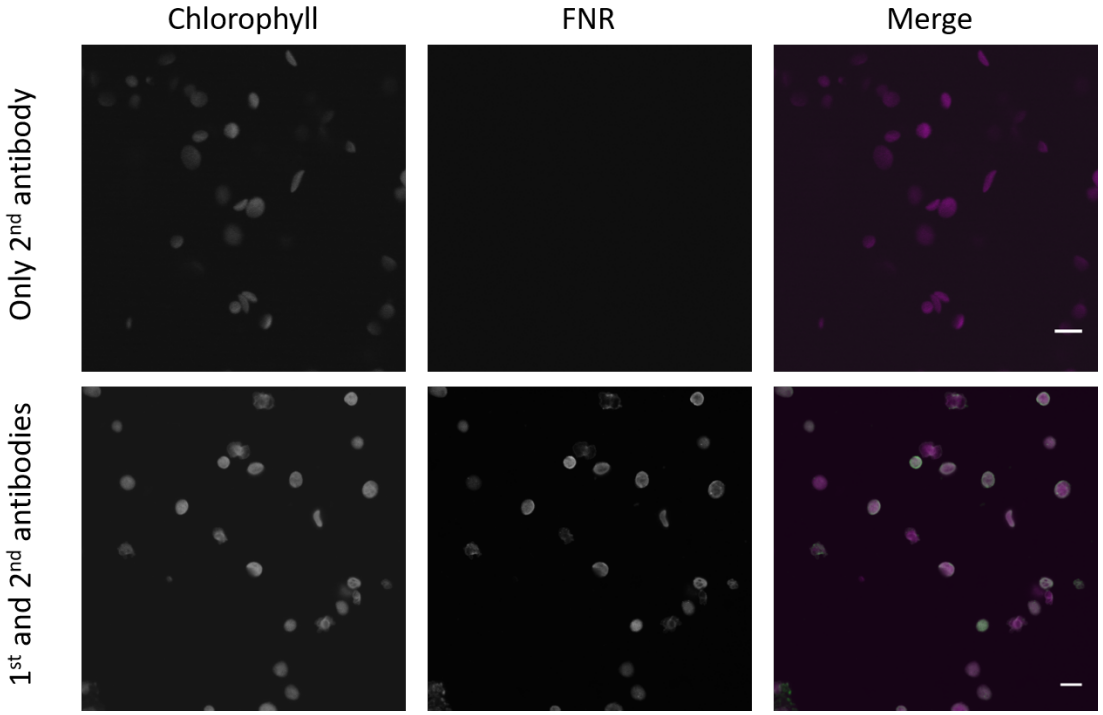

Figure 11.3: **Laser-scanning microscopy image of Arabidopsis wild-type chloroplast immunostained for FNR.** Chloroplasts were isolated from *A.thaliana* (wild-type, Columbia ecotype) after 1h dark incubation and cross-linked with 3% formaldehyde. Membranes were permeabilized with 0.1 % TritonX-100 and the sample was immunolabelled for FNR with Cy3 conjugated secondary antibody. For the labelling control (upper panels) the incubation step with the 1st antibody was omitted. Imaging was performed on a Zeiss LSM 510 META NLO. Scalebar = 20 µm.

11.2 Electron flow around the photosystems in plants grown in fluctuating light

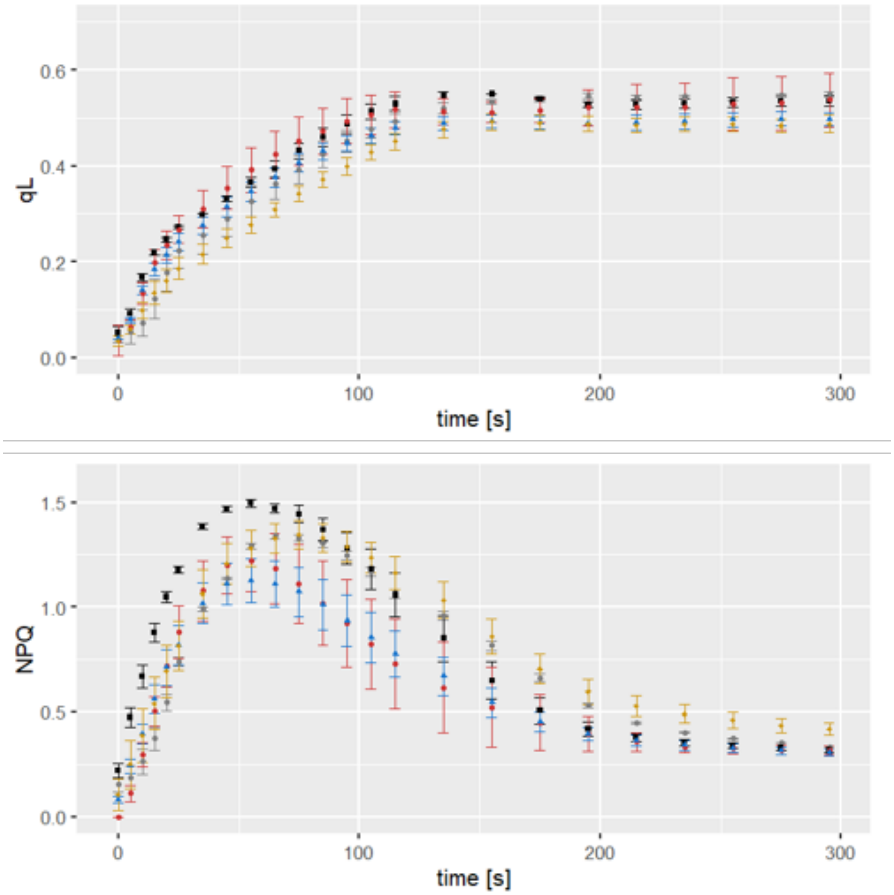

Figure 11.4: **Quantum yield of PSII: qL and NPQ of plants grown in fluctuating light.** Photochemical quenching coefficient qL=(Fm'-F)/(Fm'-Fo')xFo'/F. Non-photochemical quenching NPQ = (Fm-Fm')/Fm'. WT = grey, *fnr1* = black, *fnr1*ZmFNR1 = red, *fnr1*ZmFNR2 = blue, *fnr1*ZmFNR3 = yellow.

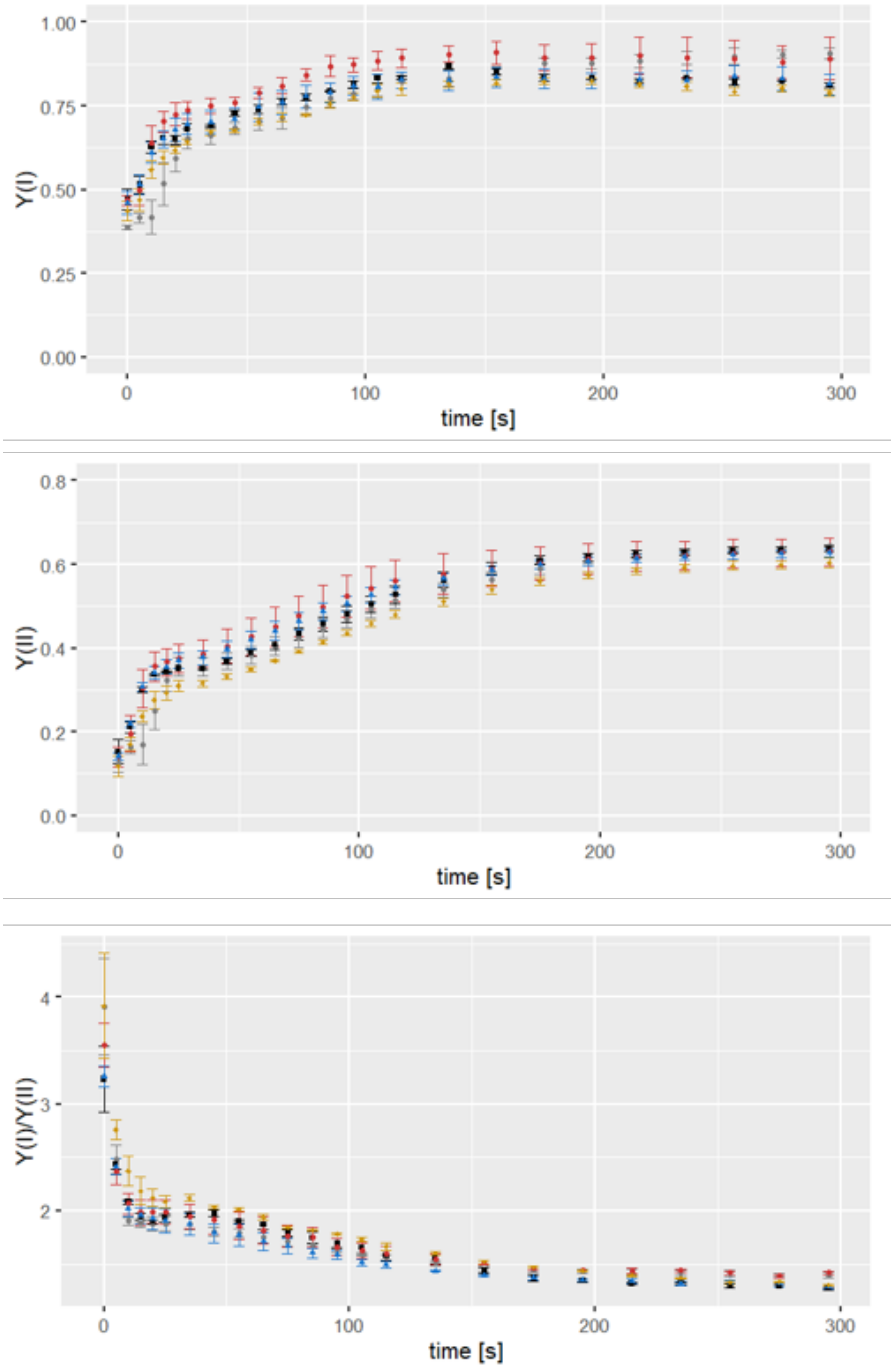

Figure 11.5: **Effective quantum yield of PSI and PSII and ratio of the effective quantum yield of PSI over PSII of plants grown in fluctuating light.** The values were calculated from dual-pulse amplitude modulation measurements. Y(II)=(Fm'-F)/Fm' and Y(I)=1-Y(ND)-Y(NA). WT = grey, *fnr1* = black, *fnr1*ZmFNR1 = red, *fnr1*ZmFNR2 = blue, *fnr1*ZmFNR3 = yellow.

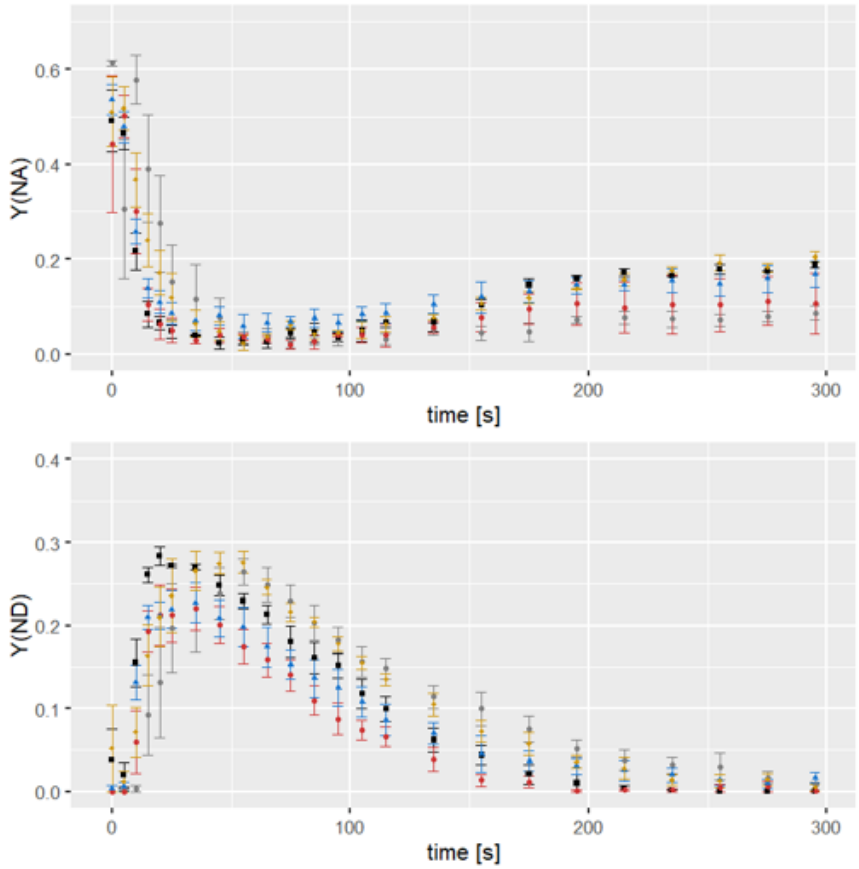

Figure 11.6: **Non-photochemical quantum yield of PSI of plants grown in fluctuating light.** Y(ND)=1-P_{700}red., Y(NA)=(Pm-Pm')/Pm. WT = grey, *fnr1* = black, *fnr1*ZmFNR1 = red, *fnr1*ZmFNR2 = blue, *fnr1*ZmFNR3 = yellow.

11.3 Sequences and vector maps

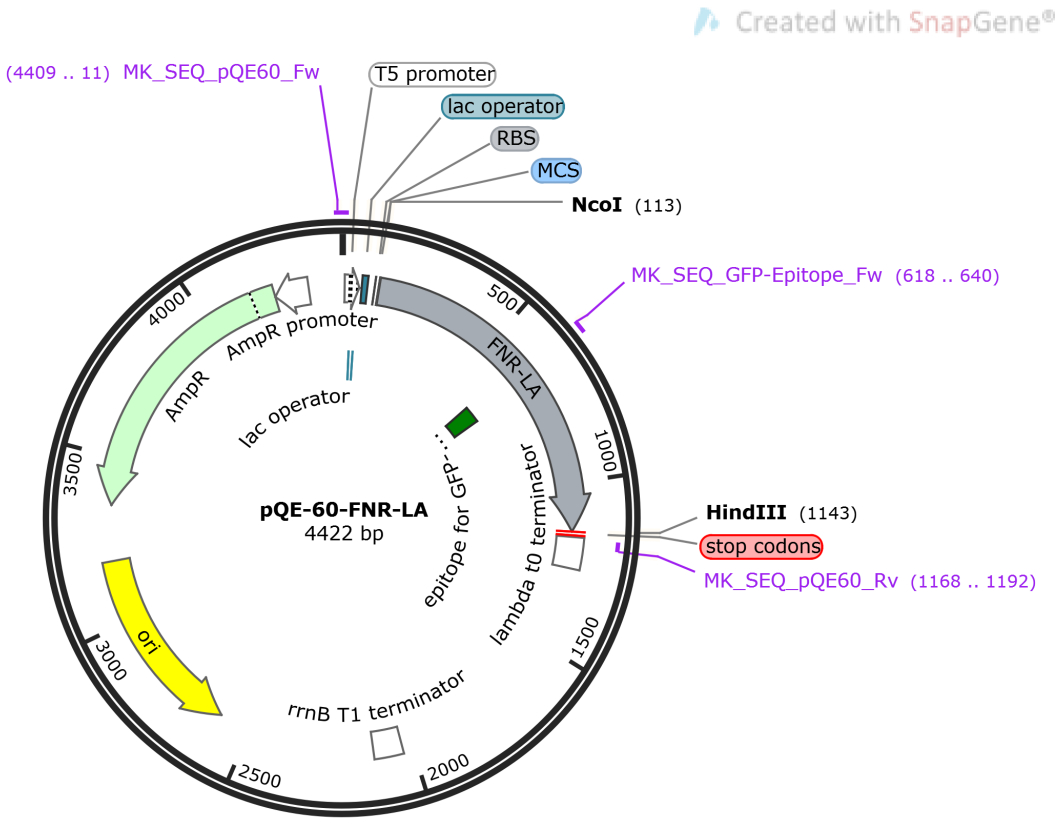

Figure 11.7: Vector map of FNR tagged in loop A in a pQE-60 expression vector.

```
MIRAQASAVEAPATAKAKKDSKKQEEGVVTNLYKPKEPYVGRCLLNTKITGDDAP    55

GETWHMVFSTEGKIPYREGQSIGVIADGVDKNGKPHKVRLYSIASSAIGDFGDSK   110

TVSLCVKRLIYTNDAGEIVKGVCSNFLCDLQPGDNVQITGPVGKEMLMPKEELLS   165

KNYHLENEVARLKKGSGSGDPNATIIMLATGTGIAPFRSFLWKMFFEKHDDYKFN   220

GLGWLFLGVPTSSSLLYKEEFGKMKERAPENFRVDYAVSREQTNAAGERMYIQTR   275

MAEYKEELWELLKKDNTYVYMCGLKGMEKGIDDIMVSLAEKDGIDWFDYKKQLKR   330

GDQWNVEVY   339
```

Figure 11.8: Sequence of the GFP-epitope loop-A tagged FNR.

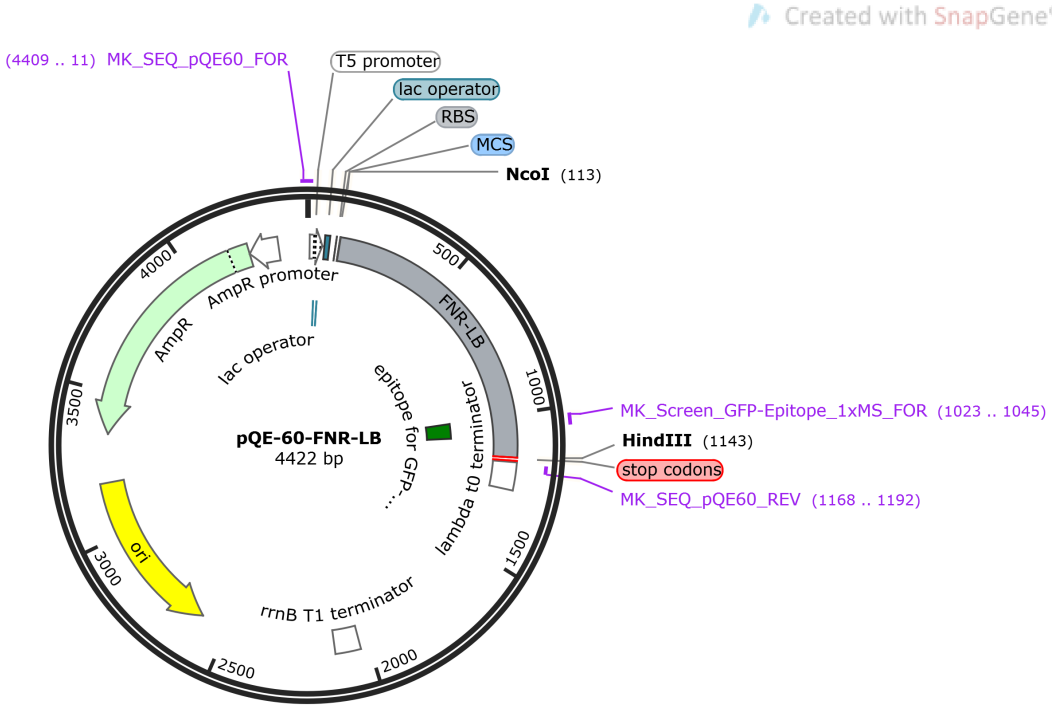

Figure 11.9: Vector map of FNR tagged in loop B in a pQE-60 expression vector.

```
MIRAQASAVEAPATAKAKKDSKKQEEGVVTNLYKPKEPYVGRCLLNTKITGDDAP    55

GETWHMVFSTEGKIPYREGQSIGVIADGVDKNGKPHKVRLYSIASSAIGDFGDSK   110

TVSLCVKRLIYTNDAGEIVKGVCSNFLCDLQPGDNVQITGPVGKEMLMPKEELLS   165

KNYHLENEVARLKKGSGSGDPNATIIMLATGTGIAPFRSFLWKMFFEKHDDYKFN   220

GLGWLFLGVPTSSSLLYKEEFGKMKERAPENFRVDYAVSREQTNAAGERMYIQTR   275

MAEYKEELWELLKKDNTYVYMCGLKGMEKGIDDIMVSLAEKDGIDWFDYKKQLKR   330

GDQWNVEVY   339
```

Figure 11.10: Sequence of the GFP-epitope loop-B tagged FNR.

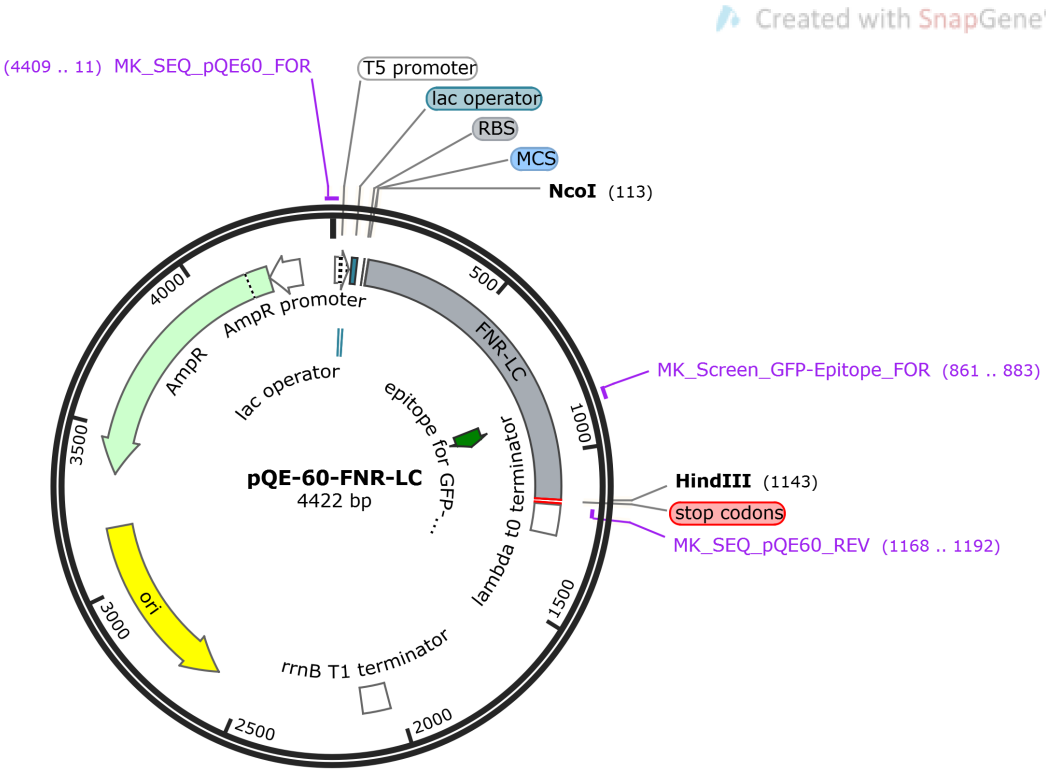

Figure 11.11: Vector map of FNR tagged in loop C in a pQE-60 expression vector.

```
MIRAQASAVEAPATAKAKKDSKKQEEGVVTNLYKPKEPYVGRCLLNTKITGDDAP    55

GETWHMVFSTEGKIPYREGQSIGVIADGVDKNGKPHKVRLYSIASSAIGDFGDSK   110

TVSLCVKRLIYTNDAGEIVKGVCSNFLCDLQPGDNVQITGPVGKEMLMPKDPNAT   165

IIMLATGTGIAPFRSFLWKMFFEKHDDYKFNGLGWLFLGVPTSSSLLYKEEFGKM   220

KERAPENFRVDYAVSREQTNAEELLSKNYHLENEVARLKKGSGSGAGERMYIQTR   275

MAEYKEELWELLKKDNTYVYMCGLKGMEKGIDDIMVSLAEKDGIDWFDYKKQLKR   330

GDQWNVEVY    339
```

Figure 11.12: Sequence of the GFP-epitope loop-C tagged FNR.